THERMODYNAMICS OF OXYGEN IN SOLID SOLUTION IN VANADIUM AND NIOBIUM-VANADIUM ALLOYS

BY

GARY LEE STECKEL
B.S., University of Missouri at Rolla, 1971
M.S., University of Illinois, 1974

THESIS

Submitted in partial fulfillment of the requirements
for the degree of Doctor of Philosophy in
Metallurgical Engineering in the Graduate College of the
University of Illinois at Urbana-Champaign, 1978

Urbana, Illinois

DISCLAIMER

THERMODYNAMICS OF OXYGEN IN SOLID SOLUTION IN VANADIUM AND NIOBIUM-VANADIUM ALLOYS

Gary Lee Steckel, Ph.D.
Department of Metallurgy and Mining Engineering
University of Illinois at Urbana-Champaign, 1978

A thermodynamic study has been made of the vanadium-oxygen and niobium-vanadium-oxygen systems utilizing the solid state galvanic cell technique. Investigations were made with a ThO_2/Y_2O_3 electrolyte over the temperature ranges 700-1200°C (973-1473 K) for the binary system and 650-1150°C (923-1423 K) for the ternary system. The activity of oxygen in vanadium obeys Henry's law for the temperatures of this investigation for concentrations up to 3.2 at. % oxygen. For higher concentrations the activity coefficient shows positive deviations from Henry's law. The oxygen activity, entropy, and enthalpy can be described over the entire composition range by interstitial solution theories when it is assumed that second nearest neighbor oxygen-oxygen interaction energies are of the same magnitude as the first nearest neighbor interactions. The terminial solubility of oxygen in vanadium was determined.

The activity of oxygen in Nb-V alloys obeys Henry's law for the temperatures of this study for oxygen concentrations less than approximately 2 at. %. For certain Nb/V ratios Henry's law is obeyed for concentrations as high as 6.5 at. % oxygen. First order entropy and enthalpy interaction coefficients have been determined to describe the effect on the oxygen activity of niobium additions to vanadium-rich alloys with dilute oxygen concentrations. Niobium causes relatively small decreases in the oxygen activity of V-rich alloys and increases the oxygen solubility limit. Vanadium additions to Nb-rich alloys also increases the oxygen solubility

and causes substantial decreases in the dilute solution oxygen activities. The change in the thermodynamic properties when molecular oxygen dissolves in vanadium and niobium-vanadium alloys and the equilibrium oxygen pressure over the binary and ternary systems were also determined.

ACKNOWLEDGMENT

The author is deeply appreciative to Professor Carl J. Altstetter for providing guidance and continued support throughout the course of his graduate study. Thanks are also due to many friends and colleagues at the University of Illinois for their valuable assistance. Last, but not least, the author wishes to thank his parents for their encouragement and support.

The support provided by the Department of Metallurgy and Mining Engineering and the Materials Research Laboratory (United States Energy Research and Developement Administration Contract AT(11-1)1198) is greatly appreciated. The assistance of the Analytical Chemistry and Microstructural Analysis groups of the Materials Research Laboratory at the University of Illinois is also acknowledged

TABLE OF CONTENTS

LIST OF TABLES

LIST OF FIGURES

1. INTRODUCTION

There is an ever increasing need for better structural metals and alloys for use in high temperature environments. Emphasis has been placed on the refractory metals, molybdenum, niobium, tantalum, tungsten, and vanadium, because of their high melting points and their strength. The group V metals, niobium, tantalum, and vanadium, are much easier to fabricate than the other refractory metals and are therefore of primary interest for many applications. Unfortuneately, these metals are, when at high temperatures, extremely reactive with the gases oxygen and nitrogen. In this connection, it has been the objective of this research program over the past several years to study the thermodynamic,[1-5] crystallographic,[6-7] and mechanical properties[7] of these metal-gas systems.

The primary purpose of the present research has been to determine the thermodynamic properties of vanadium-oxygen and niobium-vanadium-oxygen solid solutions and to determine the terminal oxygen solubilities. The EMF produced by solid state galvanic cells is used for these determinations. A secondary objective of the project is to compare the oxygen activity data with the predictions of various theoretical solution models. These comparisons are made with the hope of gaining more insight into the atomic arrangement of the various species in the solid solutions.

1.1 Solid State Galvanic Cell Technique

The galvanic cell consists of a solid oxide electrolyte between two metal-oxygen alloy electrodes. Over a range of temperature and external oxygen pressure the anionic transference number of the electrolyte is unity and it is totally ionic conducting. At a temperature high enough for

appreciable oxygen diffusion the chemical potential difference produces a flux of oxygen from the high to the low chemical potential electrode. Provided that the electrode oxygen partial pressures are within the range such that the electrolyte cannot conduct electronically, a charge is built-up on the low chemical potential electrode. This creates a flux of oxygen opposing that due to the chemical potential difference and a steady state condition is achieved. At the steady state condition there is no net flux of oxygen across the cell and an equilibrium EMF can be measured which is related to the chemical potential difference of oxygen between the two electrodes. One electrode is used as a reference with a known chemical potential so that the chemical potential of the second electrode can be determined from the measured EMF. In addition to the assumption that all charge transfer through the electrolyte is by oxygen ion migration, it is also assumed that there is only one reversible cell reaction and that there are no reactions between the electrodes and the cell atmosphere or between the electrodes and electrolyte.

Kiukkola and Wagner[8,9] first discussed and demonstrated the various applications of solid electrolytes. Since that time numerous studies have been made on the electronic and physical properties of solid oxides and many oxide electrolyte systems have been successfully developed. (see review by Etsell and Flengas[10]). The most important critera in the selection of an electrolyte for thermodynamic studies are the ionic and electronic conductivities and transport numbers over the range of oxygen pressure and temperature to be studied. The ionic transference number must be greater than 0.99 and the ionic conductivity must be sufficient for oxygen to be transfered across the cell in a relatively short period of time.

The group V metal-oxygen systems have extremely low equilibrium oxygen partial pressures, and thoria-base electrolytes with their superior thermodynamic stability are the only available electrolytes that meet the above criterea for the study of these systems. The electrolyte used in this study is a solid solution of 92 mole % ThO_2 and 8 mole % Y_2O_3 and has the fluorite structure. This mixed oxide has a 3.75 % anionic vacancy concentration set by composition which results in the desired high anionic mobility relative to the cation and electron mobilities. The total conductivity of the electrolyte as a function of oxygen pressure and temperature is shown in Figure 1.[11-15] At 1000°C (1273 K) the electrolyte exhibits p type conduction for pressures greater than 10^{-5} atm. (1.01 Pa.)[11] and n type conduction for pressures less than 10^{-30} atm. (1.01×10^{-25} Pa.).[12] Between these values the conductivity is constant and ionic in nature. Increasing the temperature increases both the ionic and electronic conductivities and reduces the useful oxygen pressure range. The minimum oxygen pressures studied in this investigation are also shown and are seen to be within the region of ionic conduction for each of the three temperatures in the figure.

1.2 Vanadium-Oxygen System

Several studies have been made of the vanadium-oxygen system to determine the terminal solubility and related thermodynamic properties. Techniques such as metallographic observation, x-ray parametric measurements, internal friction, microhardness and electrical resistivity measurements, and thermal techniques have been employed in these studies.[16-20] Some data have been reported for this system from experiments utilizing the solid state electrolytic cell technique.[21]

Early investigations of the high-vanadium region of the V-O system

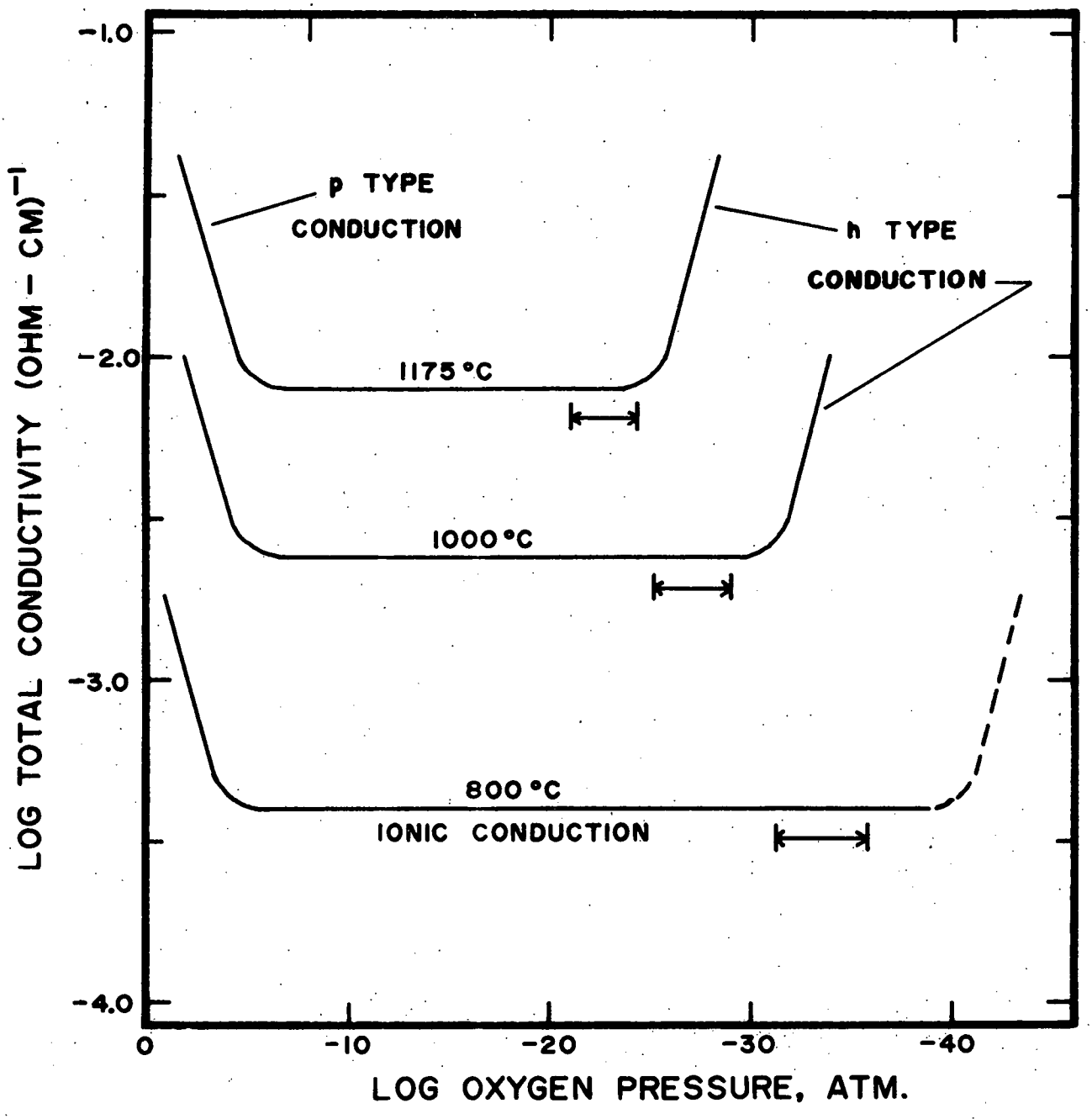

Figure 1: Logarithm of total conductivity versus logarithm of oxygen partial pressure for ThO_2/Y_2O_3 electrolyte at 800, 1000, and 1175°C. The bars under each curve represent the range of oxygen pressures studied.

were made by Seybolt and Sumsion[16] and by Rostoker and Yamamoto.[17] These studies were also included in a review by Stringer.[22] Seybolt and Sumsion established the solubility limit of oxygen in b.c.c. α vanadium as 3.2 at. % at 600°C (873 K) and 1000°C (1273 K). The phase boundary had no appreciable temperature dependence. Rostoker and Yamamoto set the terminal solubility at 3.2 at. % at 1600°C (1873 K). The solubility decreased to 0.2-0.8 at. % at temperatures below 900°C (1173 K). More recent publications by Henry et. al.[18] and by Alexander and Carlson,[19] using vanadium of higher purity than that available to the early investigators, have indicated that the solubility limit is much greater than previously reported. Henry et. al. reported that the solubility varied from 6.8 at. % at 600°C (873 K) to 10.4 at. % at 1200°C (1473 K). Alexander and Carlson reported the same value at 600°C (873 K), but found a slightly lower solubility of 9.5 at. % at 1200°C (1473 K). Henry et. al. and Alexander and Carlson also found that alloys of various oxygen contents did not retain their high temperature structure when quenched to room temperature. Alloys with an oxygen content in the range 5.7-9.2 at. % had a banded structure when quenched to room temperature. Room temperature x-ray analysis revealed the presence of a b.c.t. phase along with the b.c.c. α phase. The b.c.t. phase was interpreted as being a metastable transformation product of the quenching process. These banded structures are believed to have been single phase α at the high temperatures. High temperature x-ray parametric measurements by Henry et. al. have confirmed this interpretation. Seybolt and Sumsion and Rostoker and Yamamoto also noted the banded structure, but they interpreted the alloys to be two phase $\alpha+\beta$ at the high temperatures. This difference in microstructure interpretation and relatively low purity of the vanadium used by the earlier

investigators explains the lower solubilities reported in the earlier work.

Fromm and Kirchheim[21] determined the solubility over the temperature range of 650-1150°C (923-1423 K) by the use of the equilibrium galvanic cell technique. Their results showed excellent agreement with that of Henry et. al. and Alexander and Carlson. But more recently Smith[20] has reported a much lower value for the saturation concentration of the α phase (e.g. 3.88 at. % at 800 C (1073 K)). Smith's results are based upon internal friction analysis of quenched specimens, oxygen distribution experiments in the V-O-Na system, and gaseous oxidation experiments. In view of the conflicting values reported for the terminal solubility and the limited thermodynamic data, it seemed advisable to make a more thorough examination of vanadium-oxygen solid solutions.

1.3 Niobium-Vanadium-Oxygen System

A preliminary study of the niobium-vanadium system by Rostoker and Yamamoto[23] demonstrated that these metals alloyed to form a continuous series of solid solutions in the as-cast condition. However, alloys containing 30 and 40 at. % Nb after annealing at 900°C (1173 K) for 170 hours showed small amounts of a grain boundary precipitate. In a later, more extensive study of this system no second phases were observed after various annealing treatments.[24] It is now believed that a continuous series of solid solutions exists from the melt down to room temperature. Hobson[25] reviewed data on the effect of additions of W, Re, Ta, Mo, Hf, V, Cr, Zr, and Al on the strength, oxidation resistance, corrosion resistance, aging characteristics, and compositional stability of niobium. It was concluded that Nb-V alloy with an oxygen-scavenging third element could produce an alloy combining the best

properties of strength, ductility, corrosion resistance, and high temperature stability. Rajala and Van Thyne[26] reached a similar conclusion for their study of various V-based alloys. Therefore, these alloys show a great deal of promise as high temperature structural materials and a study of the thermodynamics of their reactions with oxygen is warranted.

From a more academic point of view, the Nb-V-O system has many favorable characteristics for the study of solutions containing both substitutional and interstitial solutes. Since the Nb-V binary consists of a complete series of solid solutions, the addition of oxygen might not result in the formation of any second phases other than the equilibrium oxides. As will be seen later, oxygen has a somewhat lower activity in vanadium than in niobium. Therefore, effects on the oxygen activity by substitutional solutes with a larger or smaller interaction with oxygen than the solvents can be determined by studying Nb or V-rich alloys, respectively. Finally, both niobium and vanadium have relatively high oxygen solubilities so the alloys should have fairly high solubilities, enabling a broad range of oxygen concentrations to be examined in the solid solution region of each Nb-V alloy.

Although very little has been reported on the Nb-V-O system, numerous studies have been made of various ternary systems containing an interstitial and substitutional solute. Zirconium and hafnium form extremely stable oxides. The addition of small quantities of these elements (less than 1 at. %) decreases the oxygen solubility of Nb to less than 250 atomic ppm at 1000-1600°C (1273-1873 K) by the formation of internal oxides of ZrO_2 and HfO_2, respectively.[27-30] Low temperature, internal friction experiments on the effect of Zr additions to Nb revealed the presence of O-Zr-O, Zr-N, and N-Zr-N clusters.[31-32] Mosher, Dollins,

and Wert[32] reported that the Zr-N and N-Zr-N clusters have binding enthalpies over 3 times as large as those reported for O-O, N-N, and C-C clusters in b.c.c. metals. Apparently Zr-N clusters are more affected by temperature than Zr-O clusters in Nb. de Lamotte et. al.[2] found that a 1500-2200°C (1773-2473 K) Zr additions of up to 1.5 at. % had little effect on the nitrogen solubility and caused a relatively small decrease in the absolute entropy of the nitrogen. Additionally, the nitrogen obeyed Sieverts' law over the entire temperature range.

Taylor and Doyle[33-35] studied the effect of small additions of Mo, W, and Hf on the solubility of nitrogen and oxygen in Nb. All three substitutional elements decreased the solubility of both nitrogen and oxygen at high temperatures. Horz and Steinheil[36,37] found the same effect for Mo additions to Nb in a study across the entire composition range of Nb-Mo-N solid solutions. However, they found that the Mo decreased the nitrogen solubility by increasing the nitrogen activity in the solid solution, whereas Taylor and Doyle[33] had concluded that the decreased solubility was due to the formation of a Mo_xN_y nitride phase. No molybdenum nitride phase was observed in the later work for Mo concentrations less than 80 at. %. For the Mo rich alloys (less than 20 at. % Nb) the Nb decreased the activity of nitrogen from its value in Mo. Sieverts' law was obeyed by the N for all of the Nb-Mo alloys.

Klueh and Devan[38,39] have determined the effect of several elements on the activity of oxygen in vanadium at 600°C (873 K) by equilibration experiments of the alloys with oxygen in liquid sodium. It was found that Cr, Mo, Fe, Ta, and Nb all increase the oxygen activity, with Nb and Ta having the smallest effect. Ti and Zr decreased the oxygen activity

and caused internal oxidation.

Numerous investigations have been made of f.c.c. and b.c.c. Fe-X-C systems from 800-1150°C (1073-1423 K) employing such substitutional elements as Co, Cr, Mn, Ni, Si, and V.[40-50] Ni, Co, and Si all increase the carbon activity, while Mn, Ni, Si, and V have the opposite effect. In general the behavior for these systems is of the same nature as the refractory metal-interstitial systems. Substitutional solutes with a higher attraction for the interstitial in the binary systems than the solvent will decrease the interstitial element activity and those with a lower attraction will increase the activity. The influence of the substitutional solute on the interstitial solubility is usually not as obvious since it is not readily apparent what phase will precipitate at saturation or how the substitutional solute will affect the activity of the precipitate phase.

1.4 Theoretical Models for Interstitial Solid Solutions

A secondary objective of this investigation is to compare the experimentally determined thermodynamic properties of oxygen in solid solution with those properties predicted by various theoretical solution models. These comparisons can yield valuable information about the interactions between the various atomic species in the solution. Before making these comparisons and discussing the results in detail it would seem pertinent to briefly review the models developed to describe the behavior of interstitial solid solutions. This review is not intended to be all-inclusive. Only those treatments which are believed to be applicable to the vanadium-oxygen and niobium-vanadium-oxygen results are presented. The more interested reader is referred to more thorough reviews by McLellan[51] and Kapoor.[52]

The normal procedure in statistical calculations is to start with a physical model for the mixed crystal, calculate the canonical partition function, and use the relation,

$$F = -kT \ln Q, \tag{1}$$

where Q is the canonical partition function, F is the Helmholtz free energy, and k and T have their usual meanings. The other thermodynamic functions can then be calculated from F, remembering that for condensed phases $F \cong G$, the Gibbs free energy. The canonical partition function is calculated by forming the sum over all the accesseible quantum states of energy, E_q, of the crystal.

$$Q = \sum_q \exp\ (-E_q/kT). \tag{2}$$

This is often written as the product,

$$Q = \Omega_c \Omega_i, \tag{3}$$

where Ω_c is the positional or configurational partition function and Ω_i is the internal partition function. Ω_i is determined by summing over the accessible vibrational and electronic states of the system. The determination of this quantity is an extremely complex problem and for most of the models considered here it is assumed that Ω_i is independent of solute concentration. This would appear to be an unreasonable assumption, but as McLellan[51] states, "most of the calculations of Ω_c involve approximations such that the corresponding thermodynamic functions involve errors of such a magnitude that assuming that the thermodynamic functions arising from Ω_i do not vary with solute concentration is a fair approximation".

By classical thermodynamics a solution is ideal if the relative partial enthalpies and volumes of its components are zero and the relative partial entropies are due only to the random distribution of the atoms in the lattice. By statistical mechanics Ω_i is defined to be unity for an ideal solution. If n_1 is the number of metal atoms, n_2 is the number of interstitial atoms, and β' is the number of interstitial sites per metal site, then the number of configurations, W, for a random binary interstitial solution is,

$$W = \frac{(\beta' n_1)!}{n_2!(\beta' n_1 - n_2)!} . \tag{4}$$

The partition function can then be represented by the equation,

$$Q^{id} = \Omega_c = W \exp(-E/kT), \tag{5}$$

where E is the energy of the one highly degenerate energy level of the ideal system. Furthermore, it can be shown that the partial molar configurational entropy of the interstitial solute, $\bar{S}_2^{c,id}$, is

$$\bar{S}_2^{c,id} = -R \ln \frac{N_2/\beta' N_1}{1-N_2/\beta' N_1} = -R \ln \frac{N_2}{\beta' - N_2(\beta'+1)}, \tag{6}$$

where N_1 and N_2 are the solvent and solute mole fraction, respectively. Thus, for the ideal interstitial solution the partial molar Gibbs free energy, $\bar{G}_2^{id}$, is

$$\bar{G}_2^{id} = G_2^o + RT \ln \frac{N_2}{\beta' - N_2(\beta'+1)}, \tag{7}$$

where G_2^o is the molar free energy of pure component 2 under a given set of

reference conditions. The activity, a_2, of the interstitial solute is defined by the relationship,

$$\bar{G}_2 - G_2^o = RT \ln a_2 \tag{8}$$

and hence for the ideal interstitial solution

$$a_2 = \frac{N_2}{\beta' - N_2(\beta'+1)} . \tag{9}$$

Real solutions are rarely ideal, however it is useful to describe real solutions relative to the ideal solution. The activity coefficient, γ, is defined for this purpose by the relation,

$$\gamma_2 = a_2 \left[\frac{N_2}{\beta' - N_2(\beta'+1)} \right]^{-1} . \tag{10}$$

By the combination of equations (7), (8), and (10) it can be shown that for a real solution

$$\bar{G}_2 = \bar{G}_2^{id} + RT \ln \gamma_2, \tag{11}$$

with $\gamma_2 = 1$ for an ideal solution.

A model closely related to the ideal solution, but which describes many real solutions, is the regular solution which was first introduced by Hildebrand[53] for substitutional solutions. The regular solution is assumed to be random, so the partial molar entropies are the same as for an ideal solution. The relative partial enthalpy is nonzero and therefore results in deviations from ideal behavior. Several variations of the regular solution have been derived. These various regular solution models differ in their description of the energetics of the solution.

The simplest of the regular solutions has been termed "quasi-regular".[54] The solute mutual interaction energies are assumed to be negligible, but a finite solvent-solute interaction energy, $\bar{E}_2$, is allowed. $\bar{E}_2$ is the energy required to insert a solute atom into the solution, measured with respect to the energy of an atom at rest in a vacuum. This model also allows for a nonconfigurational entropy term, $\bar{S}_2^{ex}$. $\bar{S}_2^{ex}$ and $\bar{E}_2$ are both assumed to be independent of solute concentration and temperature. McLellan has shown that for such a model[55]

$$\bar{G}_2 = \bar{E}_2 - T\bar{S}_2^{ex} + RT \ln \frac{N_2}{\beta' - N_2(\beta'+1)} . \qquad (12)$$

By the combination of equations (8), (10), and (12)

$$RT \ln \gamma_2 = \Delta\bar{H}_2^{\infty} - T\Delta\bar{S}_2^{\infty} \qquad (13)$$

and

$$a_2 = \frac{N_2}{\beta' - N_2(\beta'+1)} \exp \Delta\bar{H}_2^{\infty}/RT \exp -\Delta\bar{S}_2^{\infty}/R, \qquad (14)$$

where $\Delta\bar{H}_2^{\infty} = \bar{E}_2 - H_2^{o}$ and $\Delta\bar{S}_2^{\infty} = \bar{S}_2^{ex} - S_2^{o}$ are the relative partial enthalpy and nonconfigurational entropy of the solute atoms with respect to pure solute at infinite dilution. Since $\bar{E}_2$ and $\bar{S}_2^{ex}$ are independent of solute concentration, equation (13) demonstrates that γ_2 is also independent of N_2 and hence quasi-regular solutions obey Henry's law. The quasi-regular treatment has been extended to ternary solutions having a substitutional solute, component 3, in addition to the interstitial solute.[56] In the ternary model $\Delta\bar{S}_2^{\infty}$ is assumed to be the same as for the 1-2 binary system and the partial relative enthalpy, $\Delta\bar{H}_2^{T,\infty}$, is a linear sum of the

relative enthalpies, $\Delta\bar{H}_2^{1,\infty}$ and $\Delta\bar{H}_2^{3,\infty}$, determined from the 1-2 and 3-2 binaries. Thus, equations (13) and (14) are the same as for a binary system except that $\Delta\bar{H}_2^{\infty}$ is replaced by

$$\Delta\bar{H}^{T,\infty} = \frac{N_1}{N_1+N_3}\Delta\bar{H}^{1,\infty} + \frac{N_3}{N_1+N_3}\Delta\bar{H}^{3,\infty}. \qquad (15)$$

The linear sum of the partial relative enthalpies is the result of making the assumption that the bonding between components 1&2 and 3&2 are the same as for the respective binaries.

Kirkaldy and Purdy[57] have derived a regular solution model for f.c.c. lattices having a substitutional and an interstitial solute. In this model the nonconfigurational entropy is assumed to be zero and the energy of the solution is assumed to consist of pairwise interaction energies of nearest neighbor pairs. The model will be derived here for a b.c.c. structure assuming the interstitials occupy the octahedral sites ($\beta' = 3$). The total energy of the solution, E, is given by the sum of the various energy pairs,

$$E = P_{11}E_{11}+P_{12}E_{12}+P_{13}E_{13}+P_{22}E_{22}+P_{23}E_{23}+P_{33}E_{33}, \qquad (16)$$

where E_{ij} is the energy of an ij pair and P_{ij} is the number of such pairs. The subscript 1 refers to the solvent, 2 is the interstitial solute, and 3 is the substitutional solute. The P_{ij} values are calculated assuming a random solution and are related to the number of atoms by the relations,

$$P_{11} = 4\left[n_1 - n_3(1-n_3)/(n_1+n_3)\right]$$

$$P_{12} = 2n_2\left[1 - n_3/(n_1+n_3)\right]$$

$$P_{13} = 8n_3(1-n_3)/(n_1+n_3)$$
$$P_{22} = 2n_2^2/3(n_1+n_3)$$
$$P_{23} = 2n_2n_3/(n_1+n_3) \qquad (17)$$
$$P_{33} = 4n_3^2/(n_1+n_3).$$

After performing the sum of the energy pairs, differentiating with respect to n_2, and converting to mole fractions, the partial molar energy of the interstitial component can be shown to be

$$\overline{E}_2 = \frac{4N_2E_{22}}{3(1-N_2)} + \frac{2N_1E_{12}}{1-N_2} + \frac{2N_3E_{23}}{1-N_2}. \qquad (18)$$

The number of configurations for the random solution is

$$W = \frac{\left[3(n_1+n_3)\right]!}{n_2!(3n_1+3n_3-n_2)!} \times \frac{(n_1+n_3)!}{n_1!n_3!}. \qquad (19)$$

Since $S = k \ln W$, after applying Sterling's approximation, differentiating, and converting to mole fractions,

$$\overline{S}_2^c = -R \ln \frac{N_2}{3-4N_2}, \qquad (20)$$

which is the same as $\overline{S}_2^{c,id}$ for a binary interstitial solution. Since $\overline{G}_2$ is approximately equal to $\overline{E}_2 - T\overline{S}_2^c$,

$$\overline{G}_2 = \frac{4N_2E_{22}+6N_1E_{12}+6N_3E_{23}}{3(1-N_2)} + RT \ln \frac{N_2}{3-4N_2} \qquad (21)$$

and after applying equations (8) and (10),

$$RT \ln\left[\frac{a_2}{N_2}(3-4N_2)\right] = RT \ln \gamma_2 = \frac{2N_1E_{12}+2N_3E_{23}}{(1-N_2)} - G_2^o + \frac{4N_2E_{22}}{3(1-N_2)}$$

$$= J_0 + J_1 \frac{N_2}{1-N_2}, \qquad (22)$$

where $J_0 = \left[(2N_1E_{12}+2N_3E_{23})/(1-N_2) - G_2^o\right]$ and $J_1 = 4E_{22}/3$. The pairwise interaction energies are assumed to be independent of composition. Therefore, plots of RT ln γ_2 versus $N_2/(1-N_2)$ at constant temperature and metal atom ratio, N_1/N_3, are linear for solutions which obey this model. The interstitial mutual interaction energy, E_{22}, can be determined from the slope and E_{12} and E_{23} are determinable from the intercept. For a binary system equation (22) reduces to

$$RT \ln \gamma_2 = 2E_{12} - G_2^o + \frac{4N_2E_{22}}{3(1-N_2)}. \qquad (23)$$

In principle, since the interaction energies are assumed to be independent of composition, the activity of component 2 can be predicted from the application of equation (23) to the 1-2 and 2-3 binary systems. However, in practice, the interaction energy E_{23} is not assumed to be the same as that for the 2-3 binary. Instead, energies E_{12} and E_{22} are determined to be the same as for the 1-2 system and E_{23} is determined from the ternary data.[42,43]

Hoch[58] and McLellan and Chraska[56] have developed models very similar to that of Kirkaldy and Purdy. However, in these models a nonconfigurational entropy term is allowed which is assumed to be independent of temperature and composition. This quantity would appear in equations (22) and (23) as an additional intercept term. These two types of regular solution behavior have been used to describe dilute

solutions of numerous systems.[42,43,56-60] A few of these systems are: Fe-C,[60] Fe-Mn-C,[42,59] Ta-H,[58] and Ni-Cu-C.[56]

Oriani and Alcock[61] have pointed out that, strictly speaking, the regular solution model is not internally consistent. The inconsistency arises from the fact that the finite interaction energies allowed by the model necessarily imply deviations from perfect randomness of the distribution of the atomic species. The success of the regular solution, despite this inconsistency, is attributed to the fact that it is usually applied to systems for which the solute mutual interaction energies are smaller than kT.[51] Under these conditions the deviations from randomness are slight.

Speiser and Spretnak[62] developed a model which accounts for deviations from regular solution behavior by assuming that each interstitial atom blocks a number of surrounding interstitial sites, z", from being occupied. This results in a nonideal configurational entropy, which is determined to be,

$$\overline{S}_2^c = -R \ln \frac{N_2}{\beta' - N_2(\beta' + z")} . \qquad (24)$$

Combining this entropy term with the enthalpy assumptions of the quasi-regular solution yields the following equation for the solute free energy:

$$\overline{G}_2 = \overline{E}_2 - T\overline{S}_2^{ex} + RT \ln \frac{N_2}{\beta' - N_2(\beta' + z")} . \qquad (25)$$

This type of behavior has been termed "quasi-athermal".[54] The model can obviously only apply to solutions for which the interaction energy between interstitials is repulsive. Although the quasi-athermal model

has been used to describe real solutions,[40,63] it is also internally inconsistent. The concept of blocked sites infers an infinite repulsive interaction for the calculation of the configurational entropy, while this same interaction energy is regarded to be negligible for the enthalpy calculation.

The quasi-chemical model, first introduced by Guggenheim,[64] removes the internal inconsistencies of the regular and athermal treatments. As for the regular solution, the total energy of the solution is attributed to the sum of nearest neighbor pairwise interaction energies which do not vary with concentration. However, the deviations from random behavior resulting from these interactions are accounted for in the calculation of the configurational entropy. All nonconfigurational effects are assumed to be independent of composition. McLellan and Dunn[65] have derived expressions for the thermodynamic properties of the interstitial solute using the quasi-chemical method. Their expressions for the partial molar configurational entropy and enthalpy for a binary solution are

$$\bar{S}_2^c = R \ln \left[\left(\frac{\theta/\beta'}{1-\theta/\beta'} \right)^{z-1} \left(\frac{1-\theta/\beta'-\phi}{\theta/\beta'-\phi} \right)^{z/2} \right] + \frac{zE_{22}(1-2\theta/\beta')(1-\sigma)\left[(1-\theta/\beta')\theta/\beta'\right]^2}{2T(2\phi\sigma-1)(1-\theta/\beta'-\phi)(\theta/\beta'-\phi)} \qquad (26)$$

and

$$\bar{H}_2-\bar{H}_2^{\infty} = (z/2)E_{22}\left[1+\frac{(1-2\theta/\beta')(1-\sigma)\left[(1-\theta/\beta')\theta/\beta'\right]^2}{(2\phi\sigma-1)(1-\theta/\beta'-\phi)(\theta/\beta'-\phi)}\right], \qquad (27)$$

where $\bar{H}_2^{\infty}$ is the enthalpy of solution at infinite dilution, z is the

coordination number between interstitial sites, $\Theta = N_2/N_1$, $\sigma = 1\text{-exp } -E_{22}/RT$, and

$$\phi = \frac{1-\left[1-4\sigma(1-\theta/\beta')\theta/\beta'\right]^{1/2}}{2\sigma}.$$

The activity of the interstitial solute determined from equations (26) and (27) is

$$a_2 = \frac{\theta/\beta'}{1-\theta/\beta'}\left[\frac{1-\theta/\beta'-\phi}{\theta/\beta'-\phi}\left(\frac{\theta/\beta'}{1-\theta/\beta'}\right)^2\right]^{-z/2} \times \exp \Delta\bar{H}_2^{\infty}/RT \exp \Delta\bar{S}_2^{\infty}/R \exp zE_{22}/2RT, \qquad (28)$$

where $\Delta\bar{H}_2^{\infty}$ and $\Delta\bar{S}_2^{\infty}$ are the relative partial enthalpy and nonconfigurational entropy of the solute atoms with respect to pure solute at infinite dilution. Equations (26) through (28) have been used to describe the Fe-C system.[66,67] This model has also been extended to include the effect of a substitutional solute.[69,70] The resulting model satisfactorily describes the carbon activity in f.c.c. alloys in the Fe-Cr-C, Fe-Mn-C, Fe-Co-C, and Fe-Al-C systems.[68] And, perhaps more importantly, it properly describes the variation of $\bar{S}_2^c$ and $\bar{H}_2$ with composition and temperature for these systems.[68]

A quasi-chemical model first developed by Jacob and Alcock[70] has been used to describe the dissolution of oxygen and nitrogen interstitially in substitutional solutions. This treatment is somewhat more sophisticated than the previous models in that it allows the interaction energies to vary with composition. Specifically, the bonding between the interstitial atom and the metal atoms is assumed to depend upon the relative number of

atoms of types 1 and 3 surrounding the interstitial. Various interpretations of the bond energy dependence on the atomic environment have been given.[71-73] However, this model is very limited in its applicability because the solution is required to obey Sieverts' law and the nonconfigurational entropy is not allowed to vary with N_3. This investigation will indicate that the entropy of oxygen in the Nb-V-O system varies with the Nb/V ratio. Therefore, the model can not be applied to this system and will not be considered further.

The "central atoms" model, introduced independently by Lupis and Elliott[74] and Mathieu et. al.,[75] differs from the previous models in that it considers as the basic units the atoms instead of their interaction energies. This offers the advantage of describing the energy of the central atom by any suitable function of the arrangement of the atomic species in the nearest neighbor shells. Additionally, variations in the vibrational modes of the central atom can be accounted for. It is conceivable that the free energy of the central atom can be calculated for all possible configurations of the atoms in the nearest neighbor substitutional and interstitial sites by application of the proper energy function. Unfortunately, in practice the mathematics of the model are extremely complex and in order to reduce the number of parameters it is usually assumed that the energy of the central atom is linearly dependent on the surroundings. This approach is equivalent to that of the previous models in which the energy of the solution is described by the sum of pairwise interaction energies. Making use of this assumption, Foo and Lupis[76,77] have arrived at the following equations for the interstitial activity in binary (equation (29)) and ternary solutions (equation (30)):

$$\ln a_{2,B} = \ln y_2 + \Delta\bar{H}_2^{\infty}/RT - \Delta\bar{S}_2^{\infty}/R$$

$$-2z \ln \frac{(1-y_2) + \left[(1-y_2)^2 + 4y_2 \exp -\Delta g_2^{(2)}\right]^{1/2}}{2} \qquad (29)$$

$$\ln a_{2,T} = \ln a_{2,B} - 2Z \ln \left\{\left[(1+y_3)(1-y_2) + \lambda_{32}(y_2-y_3)\right]\right.$$

$$+ \left\langle \left[(1+y_3)(1-y_2) + \lambda_{32}(y_2-y_3)\right]^2 \right.$$

$$\left.\left. + 4(1-\lambda_{32})y_2(1+y_3)^2 \right\rangle^{1/2} \right\} + 2Z \ln 2(1+y_3). \qquad (30)$$

In these equations $y_2 = N_2/\left[\beta' - N_2(\beta'+1)\right] = (\Theta/\beta')/(1-\Theta/\beta')$, $y_3 = N_3/(N_1+N_3)$, Z is the number of substitutional nearest neighbors to an intersititial site, $\lambda_{32} = 1-\exp -(\Delta g_3^{(2)} - \Delta g_1^{(2)})$, and $\Delta g_i^{(2)}$ are parameters which analyze the bonding between the i^{th} species and the interstitial central atom. These parameters may be related to the interaction energies for dilute interstitial concentrations by the expression,

$$E_{2i} = 2RT\Delta g_i^{(2)}. \qquad (31)$$

The $\Delta g_i^{(2)}$ parameters are presumed to be proportional to reciprocal temperature with a nonzero intercept term indicating that the vibrational frequency of the interstitial atom is altered by the presence of an i atom nearest neighbor. Positive values for $\Delta g_2^{(2)}$ are indicative of a repulsion between interstitial atoms, while positive values for λ_{32} indicate that the interstitial is more attracted to the solvent than the substitutional solute.

Most theoretical solution models are derived under constant volume

conditions. This is the case for all of the models presented except the central atoms model which was derived at constant pressure. Most experimental measurements, including those of this study, are made under constant pressure conditions. Therefore, it is important to consider the magnitude of the consequent corrections required. Wagner[78] and Lupis[79] have addressed this problem. It was concluded that the substitution of a constant pressure condition for that of a constant volume condition affects very markedly the composition dependence of the chemical potential, but only slightly that of the activity and activity coefficient. The applicability of the models presented to the V-O and Nb-V-O systems will usually be tested by comparing the theoretical and experimental variations of the activity coefficient. It is therefore assumed that no corrections for constant pressure are required and that the comparisons will give a true test of the relevance of the models to these systems.

1.5 Thermodynamics of Substitutional Solutions

By following the same procedure as that used for interstitial solutions it can be shown that the partial molar configurational entropy of the i^{th} species of an ideal substitutional solution is

$$\bar{S}_i^{id} = -R \ln N_i. \tag{32}$$

Thus, from the definition of an ideal solution,

$$\bar{G}_i^{id} = G_i^{o} + RT \ln N_i. \tag{33}$$

From the definition of the activity, equation (8), it follows that for an ideal substitutional solution $a_i = N_i$ and the activity coefficient, γ_{N_i}, is therefore defined by the relationship,

$$\gamma_{N_i} = a_i/N_i \tag{34}$$

where the subscript N_i denotes that the activity coefficient of the i^{th} species is being defined by the substitutional formalism. As for interstitial solutions, the activity coefficient describes real solutions relative to the ideal solution. For a real solution

$$\bar{G}_i = \bar{G}_i^{id} + RT \ln \gamma_{N_i} \tag{35}$$

with $\gamma_{N_i} = 1$ for the ideal solution. Another means of discussing solution thermodynamics is by the excess partial molar quantities. Using the Gibbs free energy as an example, the excess quantities are defined by expressions of the form

$$\bar{G}_i^{xs} = \bar{G}_i - \bar{G}_i^{id} \tag{36}$$

and it follows that

$$\bar{G}_i^{xs} = \bar{H}_i^{xs} - T\bar{S}_i^{xs} = RT \ln \gamma_{N_i}. \tag{3 }$$

Wagner[80] has described the thermodynamic behavior of multicomponent systems by using a Taylor series expansion for the excess partial molar free energy or the logarithm of the activity coefficient. Following this procedure the activity coefficient for component 2 of a ternary system can be written

$$\bar{G}_2^{xs}/RT = \ln \gamma_{N_2} = \ln \gamma^{\infty}_{N_2} + N_2 \left(\frac{\partial \ln \gamma_{N_2}}{\partial N_2}\right) + N_3 \left(\frac{\partial \ln \gamma_{N_2}}{\partial N_3}\right) +$$

$$\frac{N_2^2}{2}\left(\frac{\partial^2 \ln \gamma_{N_2}}{\partial^2 N_2}\right) + N_2 N_3 \left(\frac{\partial^2 \ln \gamma_{N_2}}{\partial N_2 \partial N_3}\right) + \frac{N_3^2}{2}\left(\frac{\partial^2 \ln \gamma_{N_2}}{\partial^2 N_3}\right) + \ldots \tag{38}$$

where $\gamma^{\infty}_{N_2}$ is the activity coefficient at infinite dilution in the 1-2 binary. If terms involving second and higher order derivatives are disregarded, the logarithm of the activity coefficient becomes a linear function of the mole fractions of the solutes,

$$\bar{G}_2^{xs}/RT = \ln \gamma_{N_2} = \ln \gamma^{\infty}_{N_2} + N_2\epsilon_2^{(2)} + N_3\epsilon_2^{(3)}, \tag{39}$$

where the coefficients $\epsilon_2^{(2)}$ and $\epsilon_2^{(3)}$ are defined by the expressions,

$$\epsilon_2^{(2)} = \left(\frac{\partial \ln \gamma_{N_2}}{\partial N_2}\right)_{N_1 \to 1}$$

$$\epsilon_2^{(3)} = \left(\frac{\partial \ln \gamma_{N_2}}{\partial N_3}\right)_{N_1 \to 1}. \tag{40}$$

These quantities have been termed first order free energy interaction coefficients.[80] The Taylor series expansion may also be applied to the excess enthalpy and entropy.[81] Disregarding second and higher order derivatives these are

$$\bar{H}_2^{xs} = \bar{H}_2^{xs^{\infty}} + N_2\left(\frac{\partial \bar{H}_2^{xs}}{\partial N_2}\right) + N_3\left(\frac{\partial \bar{H}_2^{xs}}{\partial N_3}\right)$$

and

$$\bar{S}_2^{xs} = \bar{S}_2^{xs^{\infty}} + N_2\left(\frac{\partial \bar{S}_2^{xs}}{\partial N_2}\right) + N_3\left(\frac{\partial \bar{S}_2^{xs}}{\partial N_3}\right).$$

First order enthalpy and entropy interaction coefficients may then be defined by the relations,

$$\eta_2^{(2)} = \left(\frac{\partial \bar{H}_2^{xs}}{\partial N_2}\right)_{N_1 \to 1} \qquad \eta_2^{(3)} = \left(\frac{\partial \bar{H}_2^{xs}}{\partial N_3}\right)_{N_1 \to 1} \tag{43}$$

and

$$\sigma_2^{(2)} = \left(\frac{\partial \bar{S}_2^{xs}}{\partial N_2}\right)_{N_1 \to 1} \qquad \sigma_2^{(3)} = \left(\frac{\partial \bar{S}_2^{xs}}{\partial N_3}\right)_{N_1 \to 1}. \tag{44}$$

Since $\bar{G}_2^{xs} = \bar{H}_2^{xs} - T\bar{S}_2^{xs}$ it can be determined from equations (39)-(44) that

$$RT \ln \gamma_{N_2}^{\infty} = \bar{H}_2^{xs^{\infty}} - T\bar{S}_2^{xs^{\infty}} \tag{45}$$

and

$$RT \ln \gamma_{N_2} = \bar{H}_2^{xs^{\infty}} - T\bar{S}_2^{xs^{\infty}} + N_2\left[\eta_2^{(2)} - T\sigma_2^{(2)}\right] + N_3\left[\eta_2^{(3)} - T\sigma_2^{(3)}\right]. \tag{46}$$

By definition, the activity coefficient is not a function of N_2 for solutions which obey Henry's law. Therefore, if Henry's law is obeyed over the entire temperature range, $\eta_2^{(2)}$, $\sigma_2^{(2)}$, and $\epsilon_2^{(2)}$ are all zero and equation (46) reduces to

$$RT \ln \gamma_{N_2} = \bar{H}_2^{xs^{\infty}} - T\bar{S}_2^{xs^{\infty}} + N_3\left[\eta_2^{(3)} - T\sigma_2^{(3)}\right]. \tag{47}$$

By the combination of equations (34) and (47) the activity may be described by the expression,

$$a_2 = N_2 \exp\left[-\frac{\bar{S}_2^{xs^{\infty}} + \sigma_2^{(3)} N_3}{R}\right] \exp\left[\frac{\bar{H}_2^{xs^{\infty}} + \eta_2^{(3)} N_3}{RT}\right]. \tag{48}$$

Expressions (32)-(48) have been derived for substitutional solutes. However, in practice these expressions are often used to describe the thermodynamics of interstitial elements in metallic solutions. This is

particularly true for the dissolution of the diatomic gases oxygen and nitrogen into solid solution. For the reaction oxygen (or nitrogen) gas going into solid solution Sieverts' law is frequently obeyed. That is, the oxygen mole fraction is proportional to the square root of the equilibrium oxygen pressure. If the P_{O_2} = 1 atm. (1.01×10^5 Pa.) is selected as a standard state for both the gas phase and the oxygen in solution, the oxygen activity is defined to be $(P_{O_2})^{1/2}$ and the preceding expressions for substitutional solutions are applicable. Equation (48) is then a statement of both Henry's and Sieverts' laws and $\overline{H}_2^{xs}$ and $\overline{S}_2^{xs}$ are the enthalpy and entropy changes for oxygen going from the gas phase into a solution with $N_2 = 1$. This represents a nonphysical reference state since a second phase usually precipitates at values of $N_2 \ll 1$. It is therefore often preferable to define 1 at. % oxygen in solution as the standard state. This allows the activity of the oxygen to be conveniently described relative to both the gas phase and the oxide phase. As will be shown later, the terminal oxygen solubility for a binary system can be readily determined using this standard state. The equilibrium oxygen pressure is related to the at. % oxygen in solution, X, by the expression,

$$(P_{O_2})^{1/2} = \gamma' X \exp -\Delta\overline{S}^{\circ}/R \exp \Delta\overline{H}^{\circ}/RT \qquad (49)$$

where the activity coefficient, γ', equals a/X and $\Delta\overline{S}^{\circ}$ and $\Delta\overline{H}^{\circ}$ are the standard enthalpy and entropy of oxygen in solution, respectively. When Henry's and Sieverts' laws are obeyed γ' is one and equation (49) is of the same form as equation (48) for a binary system. Since $X = 100N_2$ and $a_2 = (P_{O_2})^{1/2}$ it can be readily determined that

$$\Delta\bar{S}^{o} = \bar{S}_2^{xs^{\infty}} + R \ln 100 \tag{50}$$

and

$$\Delta\bar{H}^{o} = \bar{H}_2^{xs^{\infty}}. \tag{51}$$

When there are deviations from Henry's or Sieverts' law these equations are no longer valid. However, the activity coefficients for the different standard states may be compared over the entire composition range by the expression,

$$\ln \gamma' = \ln \gamma_{N_2} - \ln 100 + \Delta\bar{S}^{o}/R - \Delta\bar{H}^{o}/RT \tag{52}$$

Substitutional solution theory provides expressions for the thermodynamic properties which are somewhat less mathematically complex than those of interstitial theory. Furthermore, substitutional theory allows for the description of the oxygen in solution by Sieverts' law. There is no equivalent statement of this convenient law by interstitial theory. Therefore, although oxygen is located in interstitial positions in vanadium and niobium-vanadium alloys, its behavior will be described in substitutional solution terms. However, interstitial theory must be used to properly interpret the physical significance of the results. Equations have therefore been derived which enable one to convert the substitutional properties, γ_N, $\bar{H}^{xs^{\infty}}$, and $\bar{S}^{xs^{\infty}}$, to the interstitial properties, , $\Delta\bar{H}^{\infty}$, and $\Delta\bar{S}^{\infty}$. If it is assumed that the oxygen occupies octahedral interstitial positions in the b.c.c. lattice, the relationship between the activity coefficients of the two solution theories is

$$\ln \gamma = \ln \gamma_N + \ln (3\text{-}4N). \tag{53}$$

Equation (53) is valid over the entire composition range of the solid

solution. This equation demonstrates that, strictly speaking, a solution which obeys Henry's law by substitutional solution theory can not obey the interstitial statement of Henry's law. However, for dilute solutions ln (3-4N) can be approximated by ln 3 and the solution can be described by Henry's law for both treatments. Expressions (14) and (48) for the activity can then be equated resulting in the following:

$$\Delta\bar{H}^{\infty} \cong \bar{H}^{xs^{\infty}} \tag{54}$$

$$\Delta\bar{S}^{\infty} \cong \bar{S}^{xs^{\infty}} - R \ln 3. \tag{55}$$

In this study the above approximation is within the limits of experimental accuracy for concentrations up to around 5 at. % oxygen. The interstitial solution theory properties may be determined from those based upon the 1 at. % oxygen standard state by the combination of equations (50)-(55). The subscript denoting the atomic species has been omitted from equations (53)-(55), as it will be throughout the remainder of the thesis, since these quantities will always be describing the properties of the oxygen.

2. EXPERIMENTAL PROCEDURE

2.1 Preparation of Electrolytes

The electrolytes employed in this investigation were either purchased commercially or pressed and sintered in our laboratory.* The minimum purities of the thoria and yttria used for the production of electrolytes were 99.9 % and 99.99 %, respectively. The mean volume diameter of the thoria powder was 5-15 microns. Although the particle size of the yttria was not reported by the supplier, it was observed to be somewhat finer than that of the thoria.

The electrolytes were pressed and sintered by a procedure similar to that employed by Alcock and Steele.[14] 2.79 grams of ThO_2 and 0.21 grams of Y_2O_3 were mixed and ground together with 3 drops of H_2O. The water was the only additive used and was employed to prevent the pellet from cracking upon removal from the die after pressing. The pellets were pressed to 42 metric toms/mm^2, giving an as-pressed pellet with the approximate dimensions 4 mm thick x 16 mm diameter. The pellets were then dried in air a 110°C (383 K) for 10-12 hours. The sintering treatment was carried out at 2100°C (2373 K) for 3 hours in a vacuum furnace which maintained a pressure in the low 10^{-6} torr (10^{-4} Pa.) range. The pellets were heated to the sintering temperature over a period of 8 hours and cooled to room temperature over a period of 2 hours to prevent cracking due to thermal shock. The vacuum sintering resulted in highly reduced, black pellets. The original oxygen/metal ratio was restored by annealing the pellets at 1375°C (1648 K) in air

*The commercial electrolytes were purchased from the Zirconium Corp. of America and the ThO_2 and Y_2O_3 powders were purchased from the Rare Earth Division of American Potash and Chemical Corp.

for 30 hours. Once again the heating and cooling rates were minimized. This treatment yielded brown, translucent electrolytes. All of the above heat treatments were carried out with the pellets resting on thoria discs to minimize contamination.

The electrolytes were ground and polished through 0.25 micron diamond paste. The final dimensions were 2 mm thick x 14 mm diameter, as compared to the commercial electrolyte dimensions 3 mm thick x 12.5 mm diameter. Optical microscopy revealed that the structure and porosity of our electrolytes compared favorably with those of the commercial electrolytes. A few of our electrolytes were tested by repeating the EMF measurements of various cells which had previously been made using commercial electrolytes. The EMFs were reproducible within ±5 mV (±230 cal./mole), which is within the limits of experimental error of the technique. It was therefore assumed that the properties of these electrolytes were adequate for experimental use and no further tests were conducted.

2.2 Preparation of Niobium-Vanadium Alloys

The niobium-vanadium alloys for the study of the Nb-V-O ternary system were prepared by conventional arc melting techniques. The niobium was purchased* in rod form and was the same stock as used by Nickerson.[5] The vanadium was donated by the U.S. Bureau of Mines in the form of as-cast bars of approximately 11.5 x 6.5 x 1.2 cm. The chemical analyses of these materials are given in Table I.

The arc melting was carried out in a furnace having a copper crucible with a tungsten electrode and an argon atmosphere. In order to facilitate homogenization of the alloys the niobium and vanadium pieces were distributed in the crucible as evenly as possible. The more dilute element was rolled

*Purchased from Wah Chang Albany Corp.

TABLE I

Analysis of Starting Material (Atomic ppm)

	Niobium			Vanadium			
				Ternary Study		Binary Study	
	A	B	C	D	E	F	E
H	278	---	---	<50	---	50	---
C	332	---	---	<40	488	425	640
N	318	---	800	<35	141	550	620
O	539	---	1040	96	210	640	1910
Na	---	<20 *	---	---	---	---	---
Al	---	50-200 *	---	---	---	95	---
Si	---	200	---	<27	---	910	---
K	---	<20	---	---	---	---	---
Ca	---	<20	---	---	---	---	---
Ti	78	---	---	---	---	55	---
V	---	30	---	matrix	---	**	---
Cr	---	30	---	---	---	100	---
Fe	83	30	---	---	---	90	---
Ni	---	---	---	5	---	---	---
Cu	---	50	---	<8	---	---	---
Zr	275	400	---	---	---	---	---
Nb	***	matrix	---	---	---	---	---
Mo	---	40	---	---	---	30	---
Hf	42	12	---	---	---	---	---
Ta	297	100	---	---	---	---	---
W	106	30	---	---	---	---	---

A Lot analysis.
B Materials Research Laboratory, University of Illinois (mass spectrographic analysis).
C Oregon Metallurgical Corporation, Albany, Oregon (vacuum fusion analysis).
D Lot analysis (all other elements were below detection limits of emission spectrography).
E Leco Corporation, St. Joseph, Michigan (vacuum fusion analysis).
F Supplier's typical ingot analysis, values are maximum content.
* Al seemed to be inhomogeneous.
** 99.85 wt. %.
*** 99.76 wt. %.

into very thin strips, 0.2 mm thick, thus maximizing its surface area and facilitating the uniform mixing of the two metals. A zirconium button was melted in a separate compartment of the crucible prior to melting the alloy. It acted as a getter for impurities in the argon atmosphere. Each alloy was melted four times. Both buttons were etched to remove any oxide layer picked up during cooling and turned over between melts. The final weight of the alloys was within ±0.20 wt. % of the initial weight.

The as-cast alloys were approximately 12 mm in diameter and 12-30 mm long, depending upon the weight and Nb/V ratio. Generally the buttons weighed 25-30 grams with some weighing as little as 15 grams. These buttons were swaged to a 3.1 mm diameter rod and cold rolled into strips 0.6 mm thick. The width of the strips depended upon the deformation characteristics of the various alloys and varied from 5.6 to 7.0 mm. Each strip had a uniform width over the length of the strip. No intermediate annealing was required at any stage of the deformation process.

Microprobe analyses performed on sections taken from various areas of the swaged rods or rolled strips indicated that the alloys were homogeneous over their cross-section and length. The niobium and vanadium concentrations of the alloys were checked by titrimetric and spectrophotometric methods. Substitutional impurity levels were determined by mass spectrographic analyses and the presence of interstitial elements O, C, and N was determined by vacuum fusion analyses. All of these chemical analyses are given in Table II.

2.3 Electrode Preparation

The vanadium used for the study of the vanadium-oxygen system was purchased in rod form.* The chemical analysis of this material is given

*Purchased from Wah Chang Albany Corp.

TABLE II

Analysis of Niobium-Vanadium Alloys (Atomic ppm)

V* / Nb*	85.2 / 14.8	70.7 / 29.3	50.5 / 49.5	35.1 / 64.9	20.7 / 79.3	19.9 / 80.1	5.1 / 94.9
C	519	---	239	---	---	380	---
N	---	181	---	---	610	---	---
O	1303	989	775	1742	1036	908	726
F	---	0.3	<0.3	0.4	0.4	2	<0.3
Na	<1	<1	<1	<1	≤1	≤1	<1
Mg	≤0.2	≤0.05	≤0.05	≤0.1	≤0.05	<2	≤0.1
Al	2	3	2	2	5	8	6
Si	≤3	2	≤2	10	6	10	6
K	<0.5	<0.5	<0.5	<0.5	<0.5	<0.5	<0.5
Ca	≤0.2	1	≤0.08	≤0.3	≤0.04	≤2	0.3
Ti	<0.6	<0.1	<0.5	≤0.2	≤0.1	≤1	≤0.1
Cr	30	30	20	20	10	20	5
Mn	≤0.4	1	10	5	2	100	0.4
Fe	20	7	7	10	6	10	2
Co	<0.03	<0.03	<0.03	≤0.03	≤0.03	≤0.03	≤0.03
Ni	≤0.2	≤0.04	0.1	≤0.1	≤0.2	≤0.5	≤0.2
Cu	4	10	20	9	8	100	4
Zn	≤0.06	<0.06	<0.06	<0.06	<0.06	<0.06	<0.06
Zr	30	0.6	200	2	≤0.06	400	0.8
Mo	≤2	0.3	≤0.4	<0.6	0.4	1	1
Hf	≤0.2	<0.08	1	<0.08	<0.08	4	<0.08
Ta	≤10	2	6	5	5	10	20
W	10	1	200	0.5	0.3	50	4

*Vanadium and niobium concentrations are in at. %. These were determined at the Materials Research Laboratory, University of Illinois (titrimetric and spectrophotometric analyses).
Carbon, nitrogen, and oxygen were determined at Leco Corporation, St. Joseph, Michigan (vacuum fusion analysis).
All other elements were determined at the Materials Research Laboratory, University of Illinois (mass spectrographic analysis).

in Table I. The vanadium-oxygen and niobium-vanadium-oxygen alloys were prepared by doping the metal strips with known quantities of oxygen in a high vacuum Sieverts' apparatus. A detailed description of this apparatus is given elsewhere.[82] The vanadium strips were outgassed and doped at 1300°C (1573 K) with the pressure in the low 10^{-7} torr (10^{-5} Pa.) range. The niobium-vanadium alloys were outgassed and doped at temperatures varying from 1150-1350°C (1423-1623 K). Since vanadium has a much higher vapor pressure than niobium the lower temperatures were used for the vanadium-rich alloys to limit vanadium losses. Following the outgassing treatment the vacuum pumps were closed to the specimen chamber and the oxygen was introduced step-wise to prevent the formation of a surface oxide layer. The strips were annealed 0.5 hour after doping and before the vacuum pumps were reopened to the chamber to insure that all of the oxygen had been absorbed. The strips were then given an homogenization anneal for 0.5 to 3 hours at the doping temperature with the pressure in the mid 10^{-7} torr (10^{-5} Pa.) range. The length of this ammeal varied directly with the quantity of oxygen added to the strips. Following the anneal, the strips were slowly cooled to 900-1000°C (1173-1273 K) and radiation cooled to room temperature. The oxygen concentrations of the alloys were checked by vacuum fusion analysis and compared to the expected values.* The vanadium alloys were doped with oxygen between 0.6 and 10.0 at. % and the niobium-vanadium alloys were doped with oxygen between 0.3 and 10.8 at. %.

Rectangular electrodes were cut from the doped strips and had the dimensions 13 x 7 x 0.7 mm for the vanadium alloys and 13 x 5.6-7.0 x 0.6 mm for the niobium-vanadium alloys. The electrode surfaces were

*The vacuum fusion analyses were performed by Leco Corporation.

ground and attack polished through 0.05 micron alumina in a chromic acid slurry.[18] This resulted in highly planar electrode surfaces with parallel faces. The vanadium-oxygen electrodes were slightly etched in a solution consisting of equal parts of HF, HNO_3, and H_2O. The niobium-vanadium-oxygen electrodes were etched in a solution of H_2O, HF, HNO_3, and H_2SO_4 in the ratio 10:2:1:1. Platinum EMF leads and platinum/platinum + 13 % rhodium thermocouples were spot welded to each electrode.

2.4 Experimental Apparatus and Technique

A schematic cross-section of the experimental apparatus is given in Figure 2. The cell was supported between two vertical, high density alumina rods in a vacuum furnace. Rings made of 0.5 mm diameter platinum were placed between the support tubes and the electrodes. These rings underwent creep at the operating temperatures under the load of a 1.4 kg. stainless steel weight placed on the upper support tube. This helped to insure good physical contact between the electrolyte and electrodes. Thoriated tungsten resistance elements surrounded the cell and were used for heating with a.c. current. The temperature was controlled with a proportional controller using the upper electrode thermocouple. The vertical position of the support tubes and the cell could be varied relative to the furnace elements to maintain the temperature gradient between the electrodes at less than $3^{o}C$. Cylindrical niobium sheets placed between the cell and furnace elements acted as electrical shielding and as a getter for gas impurities. A high impedance (10^{12} ohm) vibrating reed electrometer was used as a buffer between the cell and a digital recorder. Several radiation shields around the furnace elements reduced the heat loss and helped maintain a uniform cell temperature. The ambient pressure was maintained in the 10^{-8} to low 10^{-7} torr (10^{-6} to low 10^{-5} Pa.)

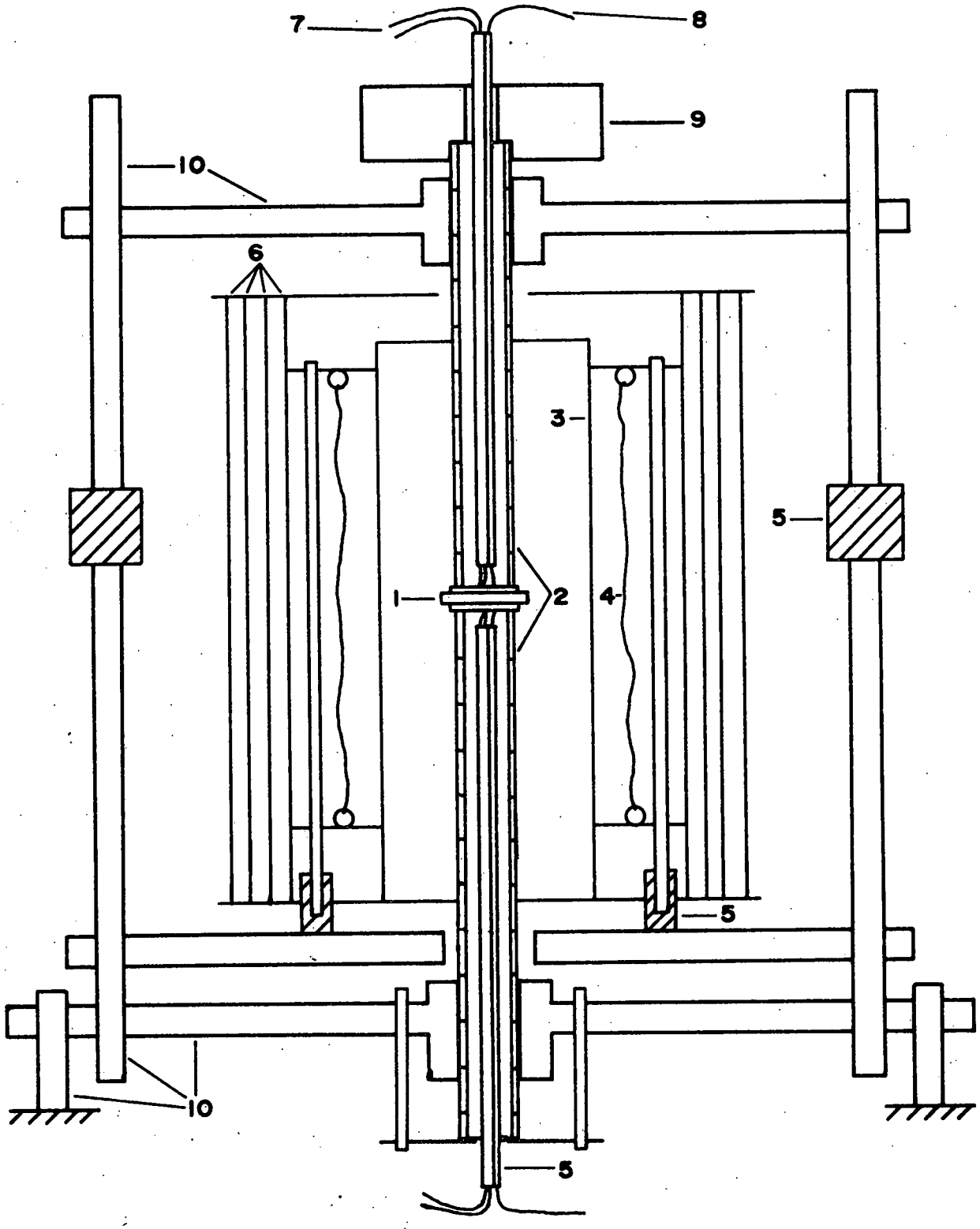

Figure 2: Schematic cross-section of the experimental apparatus.

1. cell
2. lucalox tube
3. Nb shield
4. furnace winding
5. ceramic insulator
6. heat shields
7. thermocouples
8. EMF leads
9. stainless steel weight
10. stainless steel frame

range to slow down contamination from the environment.

For accurate EMF measurements it was essential that care was taken in the electrical isolation of the cell. Since measurements were made with one electrode grounded, it was required that the other electrode have a high impedance to ground. The top support was therefore isolated from the lower support by alumina spacers at room temperature. Since one electrode was grounded it was possible to construct a double cell configuration. This assembly consisted of three electrodes with two electrolytes sandwiched between the electrodes. The middle electrode was grounded and was the reference electrode for the other two. Equilibrium EMF measurements were made between the reference electrode and each of the other electrodes independently. Since the electrometer could not monitor the EMFs across both cells simultaneously, one cell was always left at open circuit while measurements were made on the other cell. In order to maintain a temperature gradient of less than $3^{o}C$ only the thinner electrolytes were used for the double cells. To insure that there was no electrical interaction between the two cells one set of electrodes was tested using both the single and double cell arrangements. The EMF was reproducible within ± 6 mV for both cells.

Once the EMF and thermocouple leads were attached to the electrodes the cell was assembled and aligned between the support tubes. The weight was placed on the upper support tube, radiation shields installed, and the lead wires were spot welded to the vacuum feedthrough terminals. The system was then evacuated to the low 10^{-7} torr (10^{-5} Pa.) range prior to heating. The temperature was gradually increased to $1000^{o}C$ (1273 K) over a space of 6 to 8 hours, maintaining vacuum. This temperature was maintained until the cell EMF (or both cell EMFs) reached a constant value.

Equilibrium was generally reached after 4-5 hours for the vanadium-oxygen system and 8-12 hours for the niobium-vanadium-oxygen system. The electrode temperatures and cell EMF (or EMFs) were then recorded. This procedure was repeated at 1100°C (1373 K), 900°C (1173 K), 800°C (1073 K), etc., down to 600°C (873 K). Data points were then taken midway between the above mentioned temperatures on rising tempearture up to 1200°C (1473 K). This procedure was followed to determine whether the EMF depended upon the direction of temperature change prior to reaching equilibrium. EMF measurements at temperatures above 1100°C (1373 K) were always taken last since electronic conduction through the electrolyte causing oxygen transfer across the cell often occurred at these temperature. After the high temperature measurements were made the EMF was checked at a lower temperature to determine the extent of oxygen transfer. The long times to equilibrium at the low temperatures and the electronic conduction at high temperatures limited the temperature interval of these investigations to 650-1200°C (923-1473 K) for the vanadium-oxygen system and 650-1150°C (923-1423 K) for the niobium-vanadium-oxygen system.

2.5 Galvanic Cells for the Vanadium-Oxygen System

For the study of the vanadium-oxygen system only single cells were utilized. Equilibrium EMF measurements were made on the following cell:

I	V + 10.0 at. % O ($\alpha+\beta$ phases)	electrolyte (ThO_2/Y_2O_3)	V-O solid solution (α phase)

The reaction for cell I is

$$[O]_{\text{Two Phase}} \longrightarrow [O]_{\text{Single Phase}}. \qquad (56)$$

The equilibrium EMF, E, for the cell reaction is related to the difference

in free energy of oxygen between the saturated and unsaturated solutions by

$$\Delta\bar{G}_I = -nFE = \Delta\bar{G}_I^{\circ} + RT \ln \gamma' X, \tag{57}$$

where n is the ionic charge, F is the Faraday constant, $\Delta\bar{G}_I^{\circ}$ is the standard free energy change, γ' is the activity coefficient of the single phase electrode, and X is the oxygen concentration of the single phase electrode in at. %. The standard states are the 1 at. % solution for the unsaturated electrode and the saturated solution (equilibrium between the α and β phases) for the two phase electrode. At the terminal solubility the EMF will be zero and from equation (57)

$$\Delta\bar{G}_I^{\circ} = -nFE^{\circ} = -RT \ln \gamma' X_s, \tag{58}$$

where X_s is the terminal solubility in at. %. Cell I is thus used to explore the behavior of oxygen in solid solution in vanadium.

For niobium-oxygen and tantalum-oxygen solid solutions thermodynamic information for the reaction oxygen going from the gas phase into the solid solution,

$$1/2\ O_2(g) \longrightarrow [O], \tag{59}$$

can be deduced from the terminal solubility of the α phase and free energy of formation values of the equilibrium oxides.[3-5] A similar calculation is not possible for V-O solid solutions, as no data are available for the adjacent β phase. However, thermodynamic information for reaction (59) can be determined from the EMF of a second cell with a Nb-O solid solution as a reference. A similar procedure was used by Fromm and Kirchheim[21] to determine the oxygen equilibrium pressure over

V-O solid solutions. The following cell was utilized for these determinations:

II Nb + 0.45 at. % O | electrolyte (ThO_2/Y_2O_3) | V + 3.21 at. % O.

The EMF produced by cell II is related to the oxygen equilibrium pressure of the V-O electrode, $P_{O_2,V}$, and the oxygen equilibrium pressure of the Nb-O electrode, $P_{O_2,Nb}$, by the relation,

$$E = (RT/4F) \ln (P_{O_2,Nb})/(P_{O_2,V}). \quad (60)$$

The standard free energy change for equation (59) is related to the equilibrium oxygen pressure, P_{O_2}, at any oxygen composition of the solid solution by equation (49). Therefore, by the combination of equations (49) and (60) the standard heat of solution, $\Delta\overline{H}^o$, and the standard entropy of solution, $\Delta\overline{S}^o$, for oxygen gas in the V-O solid solutions can be determined from the EMF of cell II and known values of the equilibrium oxygen pressure of the Nb-O electrode.[3] Cell II is thus used to determine the change in the thermodynamic functions when molecular oxygen dissolves in vanadium.

2.6 Galvanic Cells for the Niobium-Vanadium-Oxygen System

For the study of the Nb-V-O system both single and double cells were used. Equilibrium EMF measurements were made on the following double cell:

III Nb-V-O (T_1) | electrolyte (ThO_2/Y_2O_3) | Reference V-O Binary (B) | electrolyte (ThO_2/Y_2O_3) | Nb-V-O (T_2)

and the single cell

IV Nb-V-O (T_3) | electrolyte (ThO_2/Y_2O_3) | Reference V-O Binary (B).

For double cell III the ternary electrodes, T_1 and T_2, had different oxygen concentrations and/or Nb/V ratios so that two unequal and independent EMFs were generated relative to the binary reference electrode. The only difference between double cell III and cell IV was that the utilization of the double cell enabled twice as much data to be collected in a given period of time. The V-O reference electrodes had oxygen concentrations such that they were either α solid solutions or two phase over the entire temperature interval. For most measurements single phase reference electrodes containing 3 to 4 at. % oxygen were used since these electrodes were easier to grind and polish than the more brittle, harder two phase electrodes.

The reaction for each cell of double cell III and for cell IV is

$$[O]_{T_i} \longrightarrow [O]_B. \tag{61}$$

The EMF, E_i, for reaction (61) is related to the oxygen equilibrium pressure of the binary electrode, $P_{O_2,B}$, and the oxygen equilibrium pressure of the ternary electrode, P_{O_2,T_i}, by the relation,

$$E_i = (RT/4F) \ln (P_{O_2,T_i})/(P_{O_2,B}). \tag{62}$$

For the ternary electrodes the P_{O_2} = 1 atm. (1.01×10^5 Pa.) was used as the standard state rather than the 1 at. % oxygen standard state. The gas phase standard state was more convenient because it enabled all of the alloys to have the same reference state regardless of the Nb/V ratio. As previously stated, with this standard state the activity, a, is defined a as the $(P_{O_2})^{1/2}$. The activity of oxygen in the ternary electrodes can therefore be determined directly from the EMF measurements on cells III & IV by using equation (62) and the results of the vanadium-oxygen system.

3. RESULTS

3.1 Vanadium-Oxygen System

The raw EMF data for cell I are presented in Figure 3 as a function of temperature. Straight lines were fitted to the data by least squares analysis. The EMF equations resulting from this analysis are listed in Table III. Equation (57) can be used to interpolate compositions to find E°, the EMF for a 1 at. % solution. The data for different oxygen concentrations can be normalized by substituting equation (58) into equation (57) to give:

$$nF(E - E^{\circ})/RT = -\ln \gamma' - \ln X \qquad (63)$$

The validity of Henry's law was tested by plotting $nF(E - E^{\circ})/RT$ versus $\ln X$ for temperatures from 700-1200°C (973-1473 K). This plot (Figure 4) is linear with a slope of -1.03 for concentrations up to 3.2 at. % oxygen over the entire temperature interval, but deviates from linearity for higher concentrations. Least squares analysis of the data for the individual temperatures and the three lowest oxygen concentrations gives calculated slopes varying from -1.08 for 700°C (973 K) to -1.00 for 1200°C (1473 K). Therefore, Henry's law is fairly well obeyed for compositions up to about 3 at. %, but is not obeyed for higher concentrations. By our choice of standard states γ' is defined to be 1 over the region in which Henry's law is obeyed. By use of equation (57) and the plots exemplified by Figure 4, γ' can be calculated for the compositions which do not obey Henry's law. It will be shown later that γ' can be analytically represented as a function of temperature and composition over the entire composition

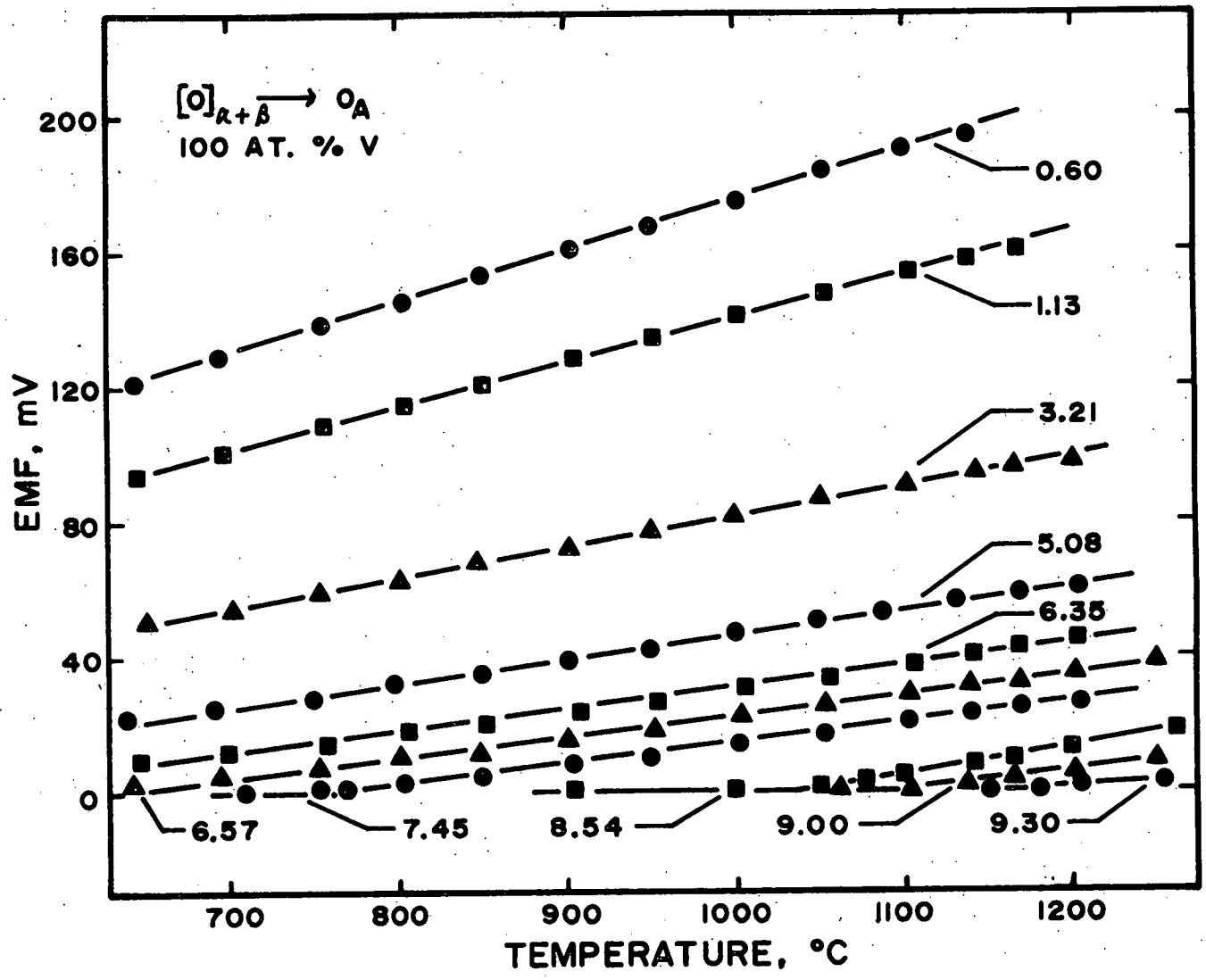

Figure 3: EMF versus temperature for the vanadium-oxygen system. The oxygen concentration of each single phase electrode is indicated in at. % O.

TABLE III

EMF versus Temperature Equations for the Vanadium-Oxygen System

At. % O	Slope	EMF Intercept	Temperature, °C
0.60	0.150	25.4	646-1139
1.13	0.130	10.2	647-1168
3.21	0.090	-8.8	652-1200
5.08	0.071	-24.6	640-1203
6.35	0.066	-34.8	649-1203
6.57	0.063	-40.7	650-1249
7.45	0.064	-49.5	778-1204
8.54	0.076	-78.2	1030-1262
9.00	0.060	-65.7	1100-1249
9.30	0.037	-43.9	1190-1254
9.75*	0.018	-21.7	1220-1262

*The data for the 9.75 at. % oxygen electrode are not shown in Figure 3. The results of this electrode were only used to determine the point on the solvus line at 1220°C.

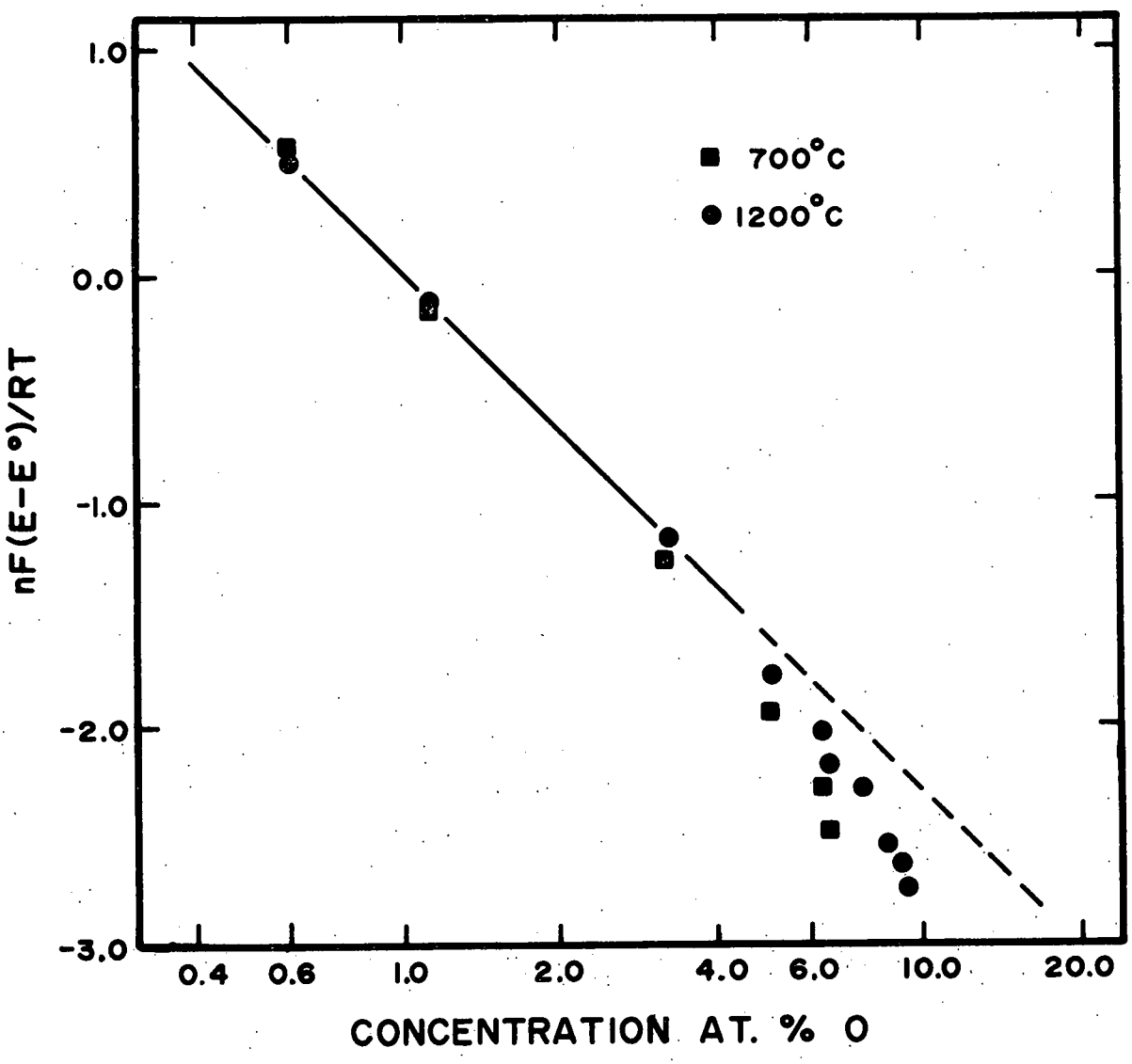

Figure 4: EMF versus logarithm of oxygen concentration for cell I.

range of the α phase.

Values of E° were substituted into equation (58) to calculate $\Delta\overline{G}_I^\circ$. From the temperature dependence of $\Delta\overline{G}_I^\circ$ the standard enthalpy and entropy changes for reaction (56) over the temperature range 700-1200°C (973-1473 K) were determined to be 1010 ± 100 cal/mole and 6.11 ± 0.15 cal/mole, K, respectively.

The EMF of cell II is presented in Figure 5 and can be described as a function of temperature by the equation

$$E = -0.113T + 202.8 \pm 0.6 \text{ mV}. \qquad (64)$$

From these data and the known equilibrium oxygen pressure of the Nb + 0.45 at. % oxygen electrode,[3,5]

$$P_{O_2,Nb} = 1.01 \times 10^5 X^2 \exp (2/R)\left[13.3 \pm 0.4 - (91,370 \pm 300)/T\right] \text{ Pa.}, \qquad (65)$$

the equilibrium pressure of the V + 3.21 at. % oxygen electrode can be calculated from equation (60). Since the 3.21 at. % oxygen alloy has been shown to obey Henry's law ($\gamma' = 1$), the standard enthalpy, $\Delta\overline{H}^\circ$, and entropy, $\Delta\overline{S}^\circ$, of solution have been determined from equation (49) to be -100,720 ± 330 cal/mole and -14.6 ± 0.6 cal/mole, K, respectively. These values are in good agreement with those reported by Fromm and Kirchheim[21] ($\Delta\overline{H}^\circ$ = -100,970 cal/mole and $\Delta\overline{S}^\circ$ = -14.9 cal/mole, K). From the values of $\Delta\overline{H}^\circ$ and $\Delta\overline{S}^\circ$ the equilibrium oxygen pressure over α solid solutions having X % dissolved oxygen is

$$P_{O_2,V} = 1.01 \times 10^5 (\gamma' X)^2 \exp (2/R)\left[14.6 \pm 0.6 - (100,720 \pm 330)/T\right] \text{Pa.} \qquad (66)$$

The terminal solubility can be determined by solving equation (58) for X_s, but γ' must be known as a function of concentration and temperature

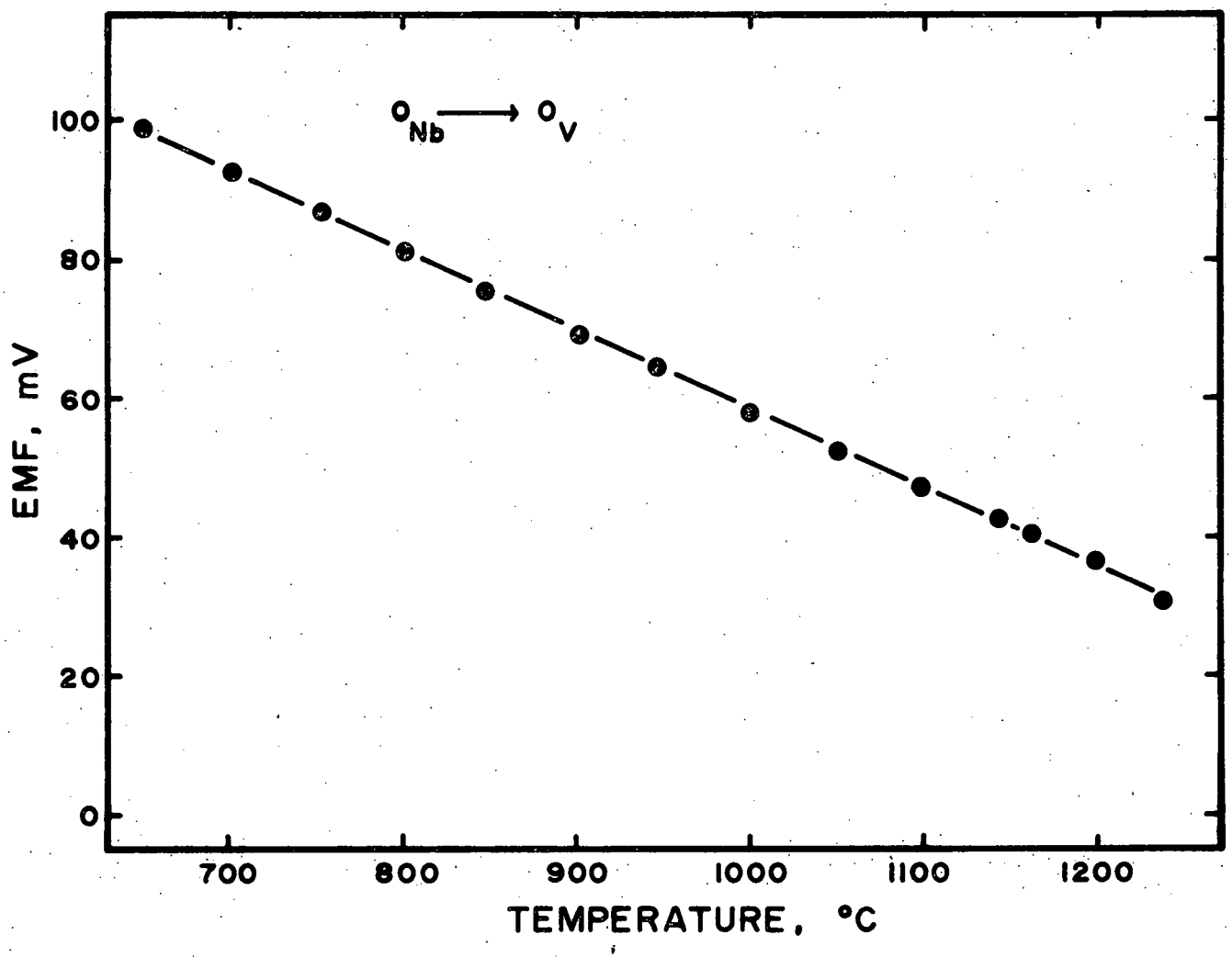

Figure 5: EMF versus temperature for cell II.

in order to solve this equation. It was found that a convenient functional relationship for γ' could be determined by converting from the 1 at. % O standard state to the P_{O_2} = 1 atmosphere (1.01×10^5 Pa.) standard state. Since by this standard state the activity equals $(P_{O_2})^{1/2}$, it follows from equation (34) that

$$1/2 \ln P_{O_2} = \ln \gamma_N + \ln N. \tag{67}$$

Values of the activity coefficient, γ_N, were then calculated for the raw EMF data from equations (66) and (67) using values of γ' determined from equation (63). Following Darken and Gurry,[83] the function, $\ln \gamma_N/(1-N)^2$, was plotted as a function of the oxygen mole fraction at the temperatures indicated in Figure 6. Straight lines fitted to these plots by least squares analysis enabled the activity coefficient to be described as a function of temperature and concentration as follows:

$$\ln \gamma_N = \left[(19.98 - 96,470/T)N + 12.00 - 50,770/T\right](1-N)^2. \tag{68}$$

The activity coefficient, γ', for the 1 at. % standard state can then be determined from equations (52) and (68) and is,

$$\ln \gamma' = \left[(0.20 - 964.70/T)X + 12.00 - 50,770/T\right](1-X/100)^2 - 11.96 + 50,690/T. \tag{69}$$

Equation (69) is valid over the entire composition range of the α phase from 700-1200°C (973-1473 K). However, since Henry's law is obeyed for solutions up to 3 at. % oxygen it is not necessary to use equation (69) unless the oxygen content exceeds this value. Equation (69) is a better representation of the data for temperatures above 1000°C (1273 K) than for the lower temperatures. This is a consequence of the fact that fewer data

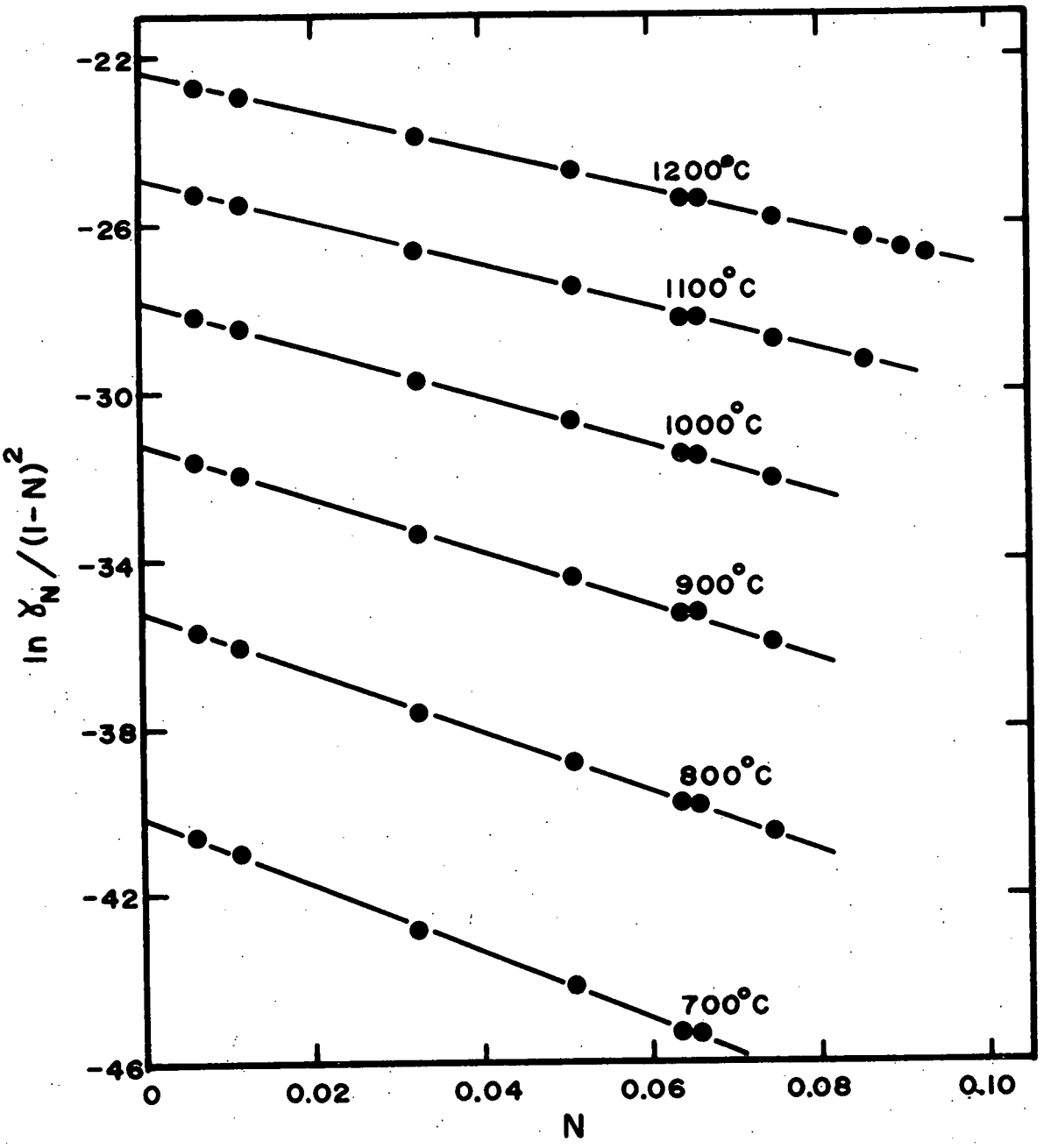

Figure 6: Concentration dependence of oxygen activity coefficient in α vanadium.

points were available at the lower temperatures.

Equations (58) and (69) can be used to calculate the terminal solubility at any temperature from 700-1200°C (973-1473 K). The calculated solubility is presented in Figure 7. Also plotted in Figure 7are solubility points determined from EMF measurements on cell I by observing the temperature at which the EMF falls to zero or rises from zero on falling or increasing temperature, respectively. The agreement between the two determinations is excellent. The results of other recent investigations are also shown in Figure 7 with the reference numbers indicated on the figure. The terminal solubility presented in the present study shows good agreement with the results of Henry et. al.,[18] Alexander and Carlson,[19] and Fromm and Kirchheim.[21] The results of Smith[20] show a considerably lower value for the solubility. Smith's results are based upon specimens prepared by oxygen distribution experiments in the V-O-Na system and by gaseous oxidation experiments. The solubility limit was determined by the formation of an oxide layer on the surface of single phase specimens. It is possible that the temperatures used, 800°C (1073 K) and less, were too low for the solid solution to dissolve a nonequilibrium oxide layer, resulting in lower estimates of the solubility limit.

Optical microscopy revealed the presence of the same structures as noted by Henry et. al.[18] and Alexander and Carlson.[19] Alloys with oxygen concentrations less than approximately 6 at. % had typical solid solution structures when quenched from high temperatures. Alloys having greater than 6 at. % oxygen, when quenched from the solid solution region, had banded martensitic structures of transformed α (Figure 8). As mentioned previously, this phase is a metastable transformation product of the quenching process. Figure 9 shows the structures that resulted when the

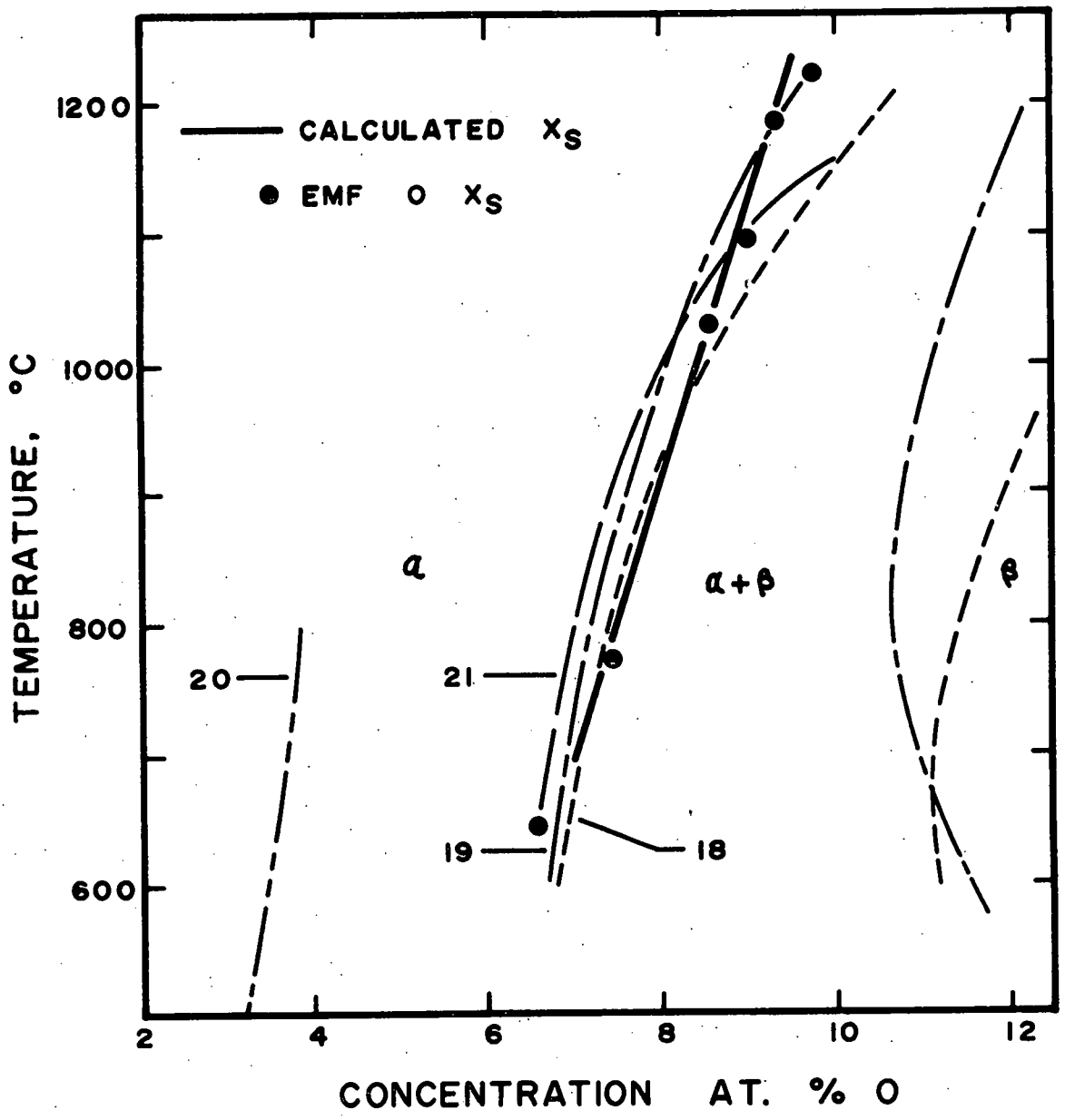

Figure 7: Oxygen solubility in vanadium.

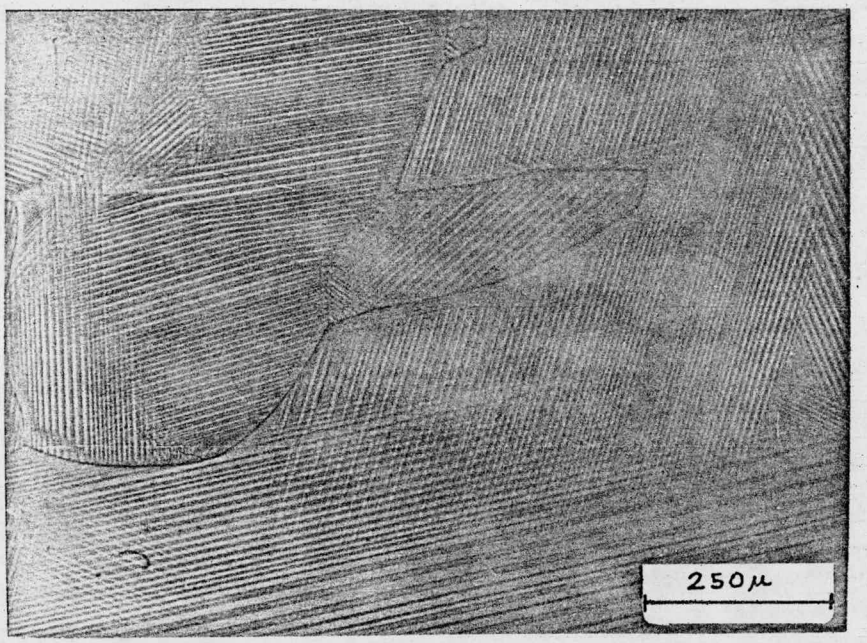

Figure 8: V + 6.35 at. % O alloy vacuum quenched from 1000°C. Martensitic structure of transformed α.

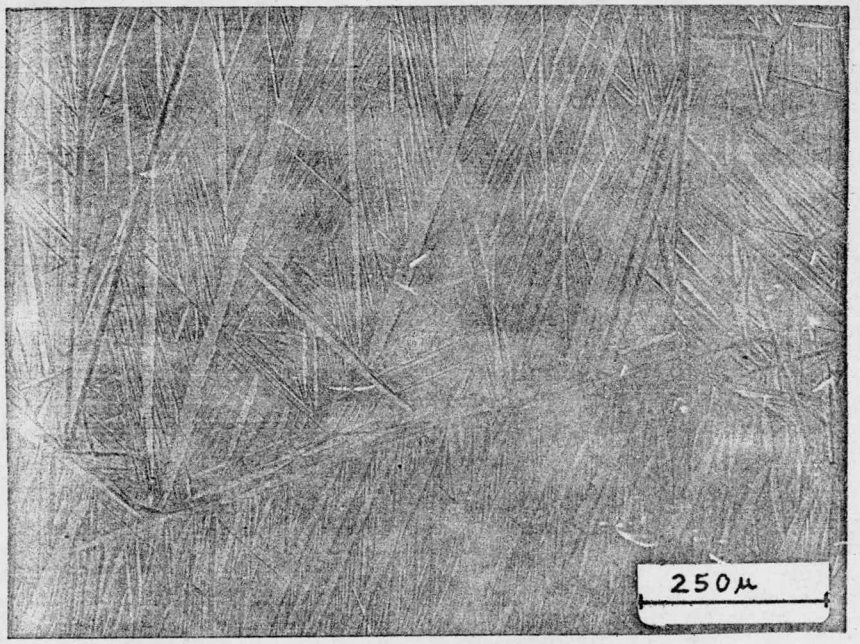

Figure 9: V + 7.45 at. % O vacuum quenched from 800°C. Striated platelets of β embedded in a matrix of transformed α.

higher oxygen content alloys were quenched from the two phase region. Striated platelets of β were embedded in a matrix of transformed α.

3.2 Niobium-Vanadium-Oxygen System

3.2.1 Results of the EMF Measurements

The EMF data for cells III & IV are presented in Figures 10-15 as a function of temperature. The vanadium concentrations indicated are for the alloys prior to the addition of oxygen.* Although several different V-O reference electrodes were used, all the data are presented relative to the V-O two phase electrode. The EMF for the reaction oxygen going from the $\alpha+\beta$ mixture to NbO is also presented in the figures. This allows the ternary data to be readily compared to the oxide phases of both binary systems. Straight lines were fitted to the data by least squares analysis and the resulting EMF equations are given in Table IV. For several runs when the EMF was greater than approximately 160 mV and the temperature exceeded 950°C (1123 K), the data points fell below the straight lines at the higher temperatures (Figures 10-13). This was assumed to be due to electronic conduction through the electrolyte at the high temperatures. The least squares analysis was performed only on the low temperature data for these runs and this line was extended over the entire temperature range.

By the combination of equation (62), the results of the V-O system, and the EMF equations in Table IV, the equilibrium oxygen partial pressure can be calculated for each Nb-V-O alloy as a function of temperature. With the P_{O_2} = 1 atm. (1.01×10^5 Pa.) standard state the activity coefficient relative to the oxygen mole fraction is defined by equation (67)

*The 20.3 at. % V value is the average composition for the 19.9 and 20.7 at. % V alloys.

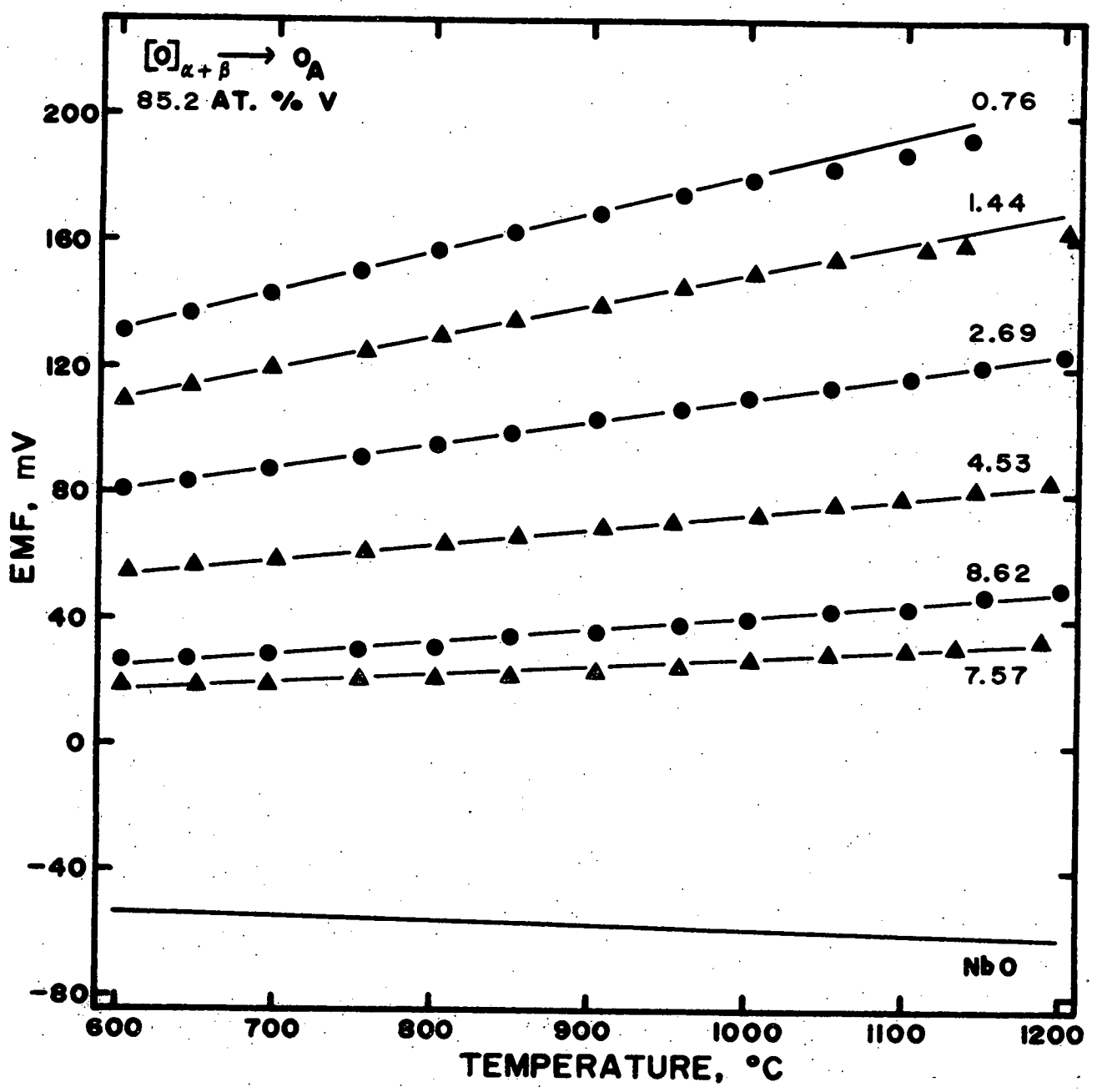

Figure 10: EMF versus temperature for the 85.2 at. % V alloy. The oxygen concentration of each ternary electrode is indicated in at. % O.

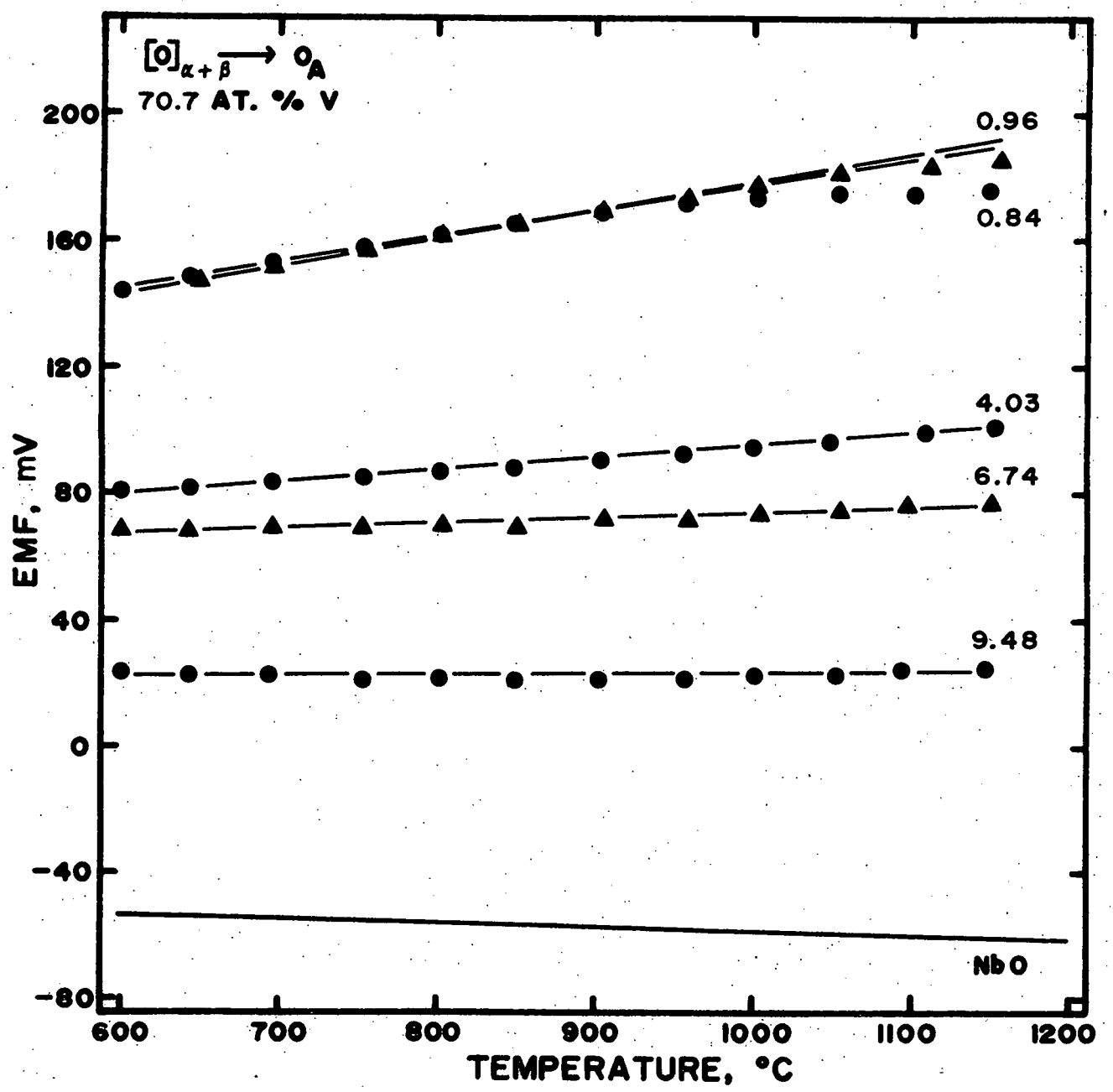

Figure 11: EMF versus temperature for the 70.7 at. % V alloy. The oxygen concentration of each ternary electrode is indicated in at. % O.

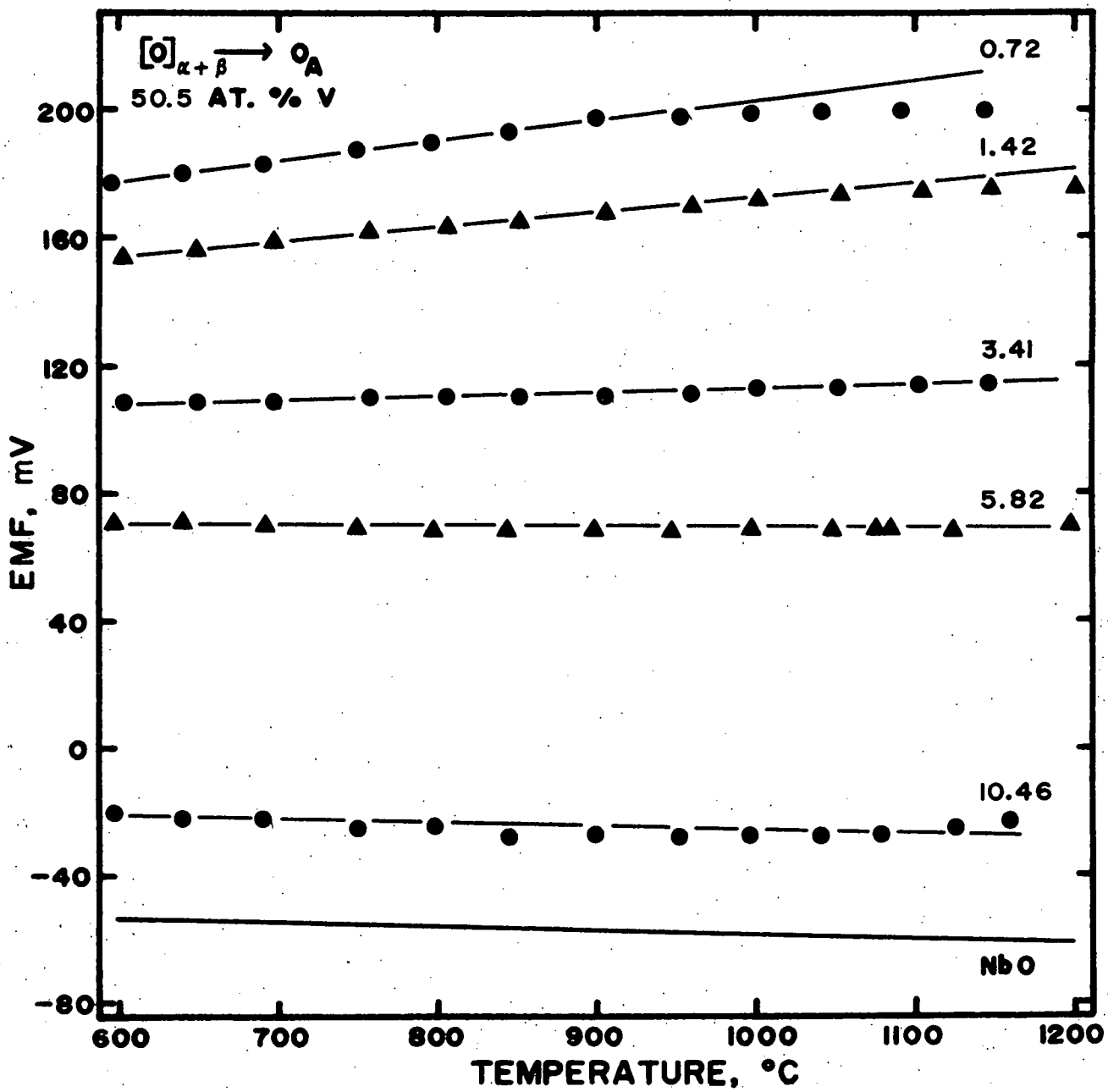

Figure 12: EMF versus temperature for the 50.5 at. % V alloy. The oxygen concentration of each ternary electrode is indicated in at. % O.

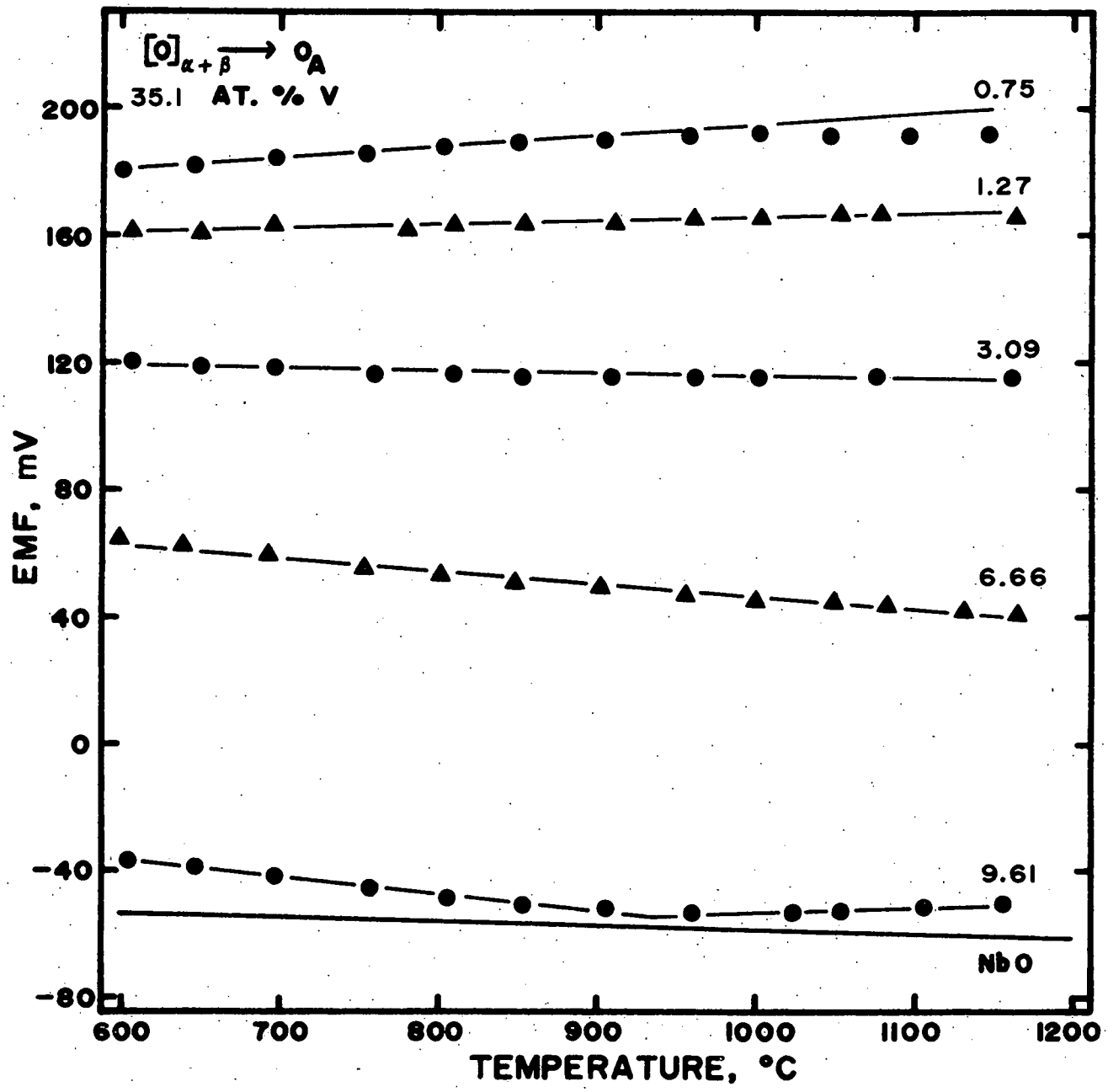

Figure 13: EMF versus temperature for the 35.1 at. % V alloy. The oxygen concentration of each ternary electrode is indicated in at. % O.

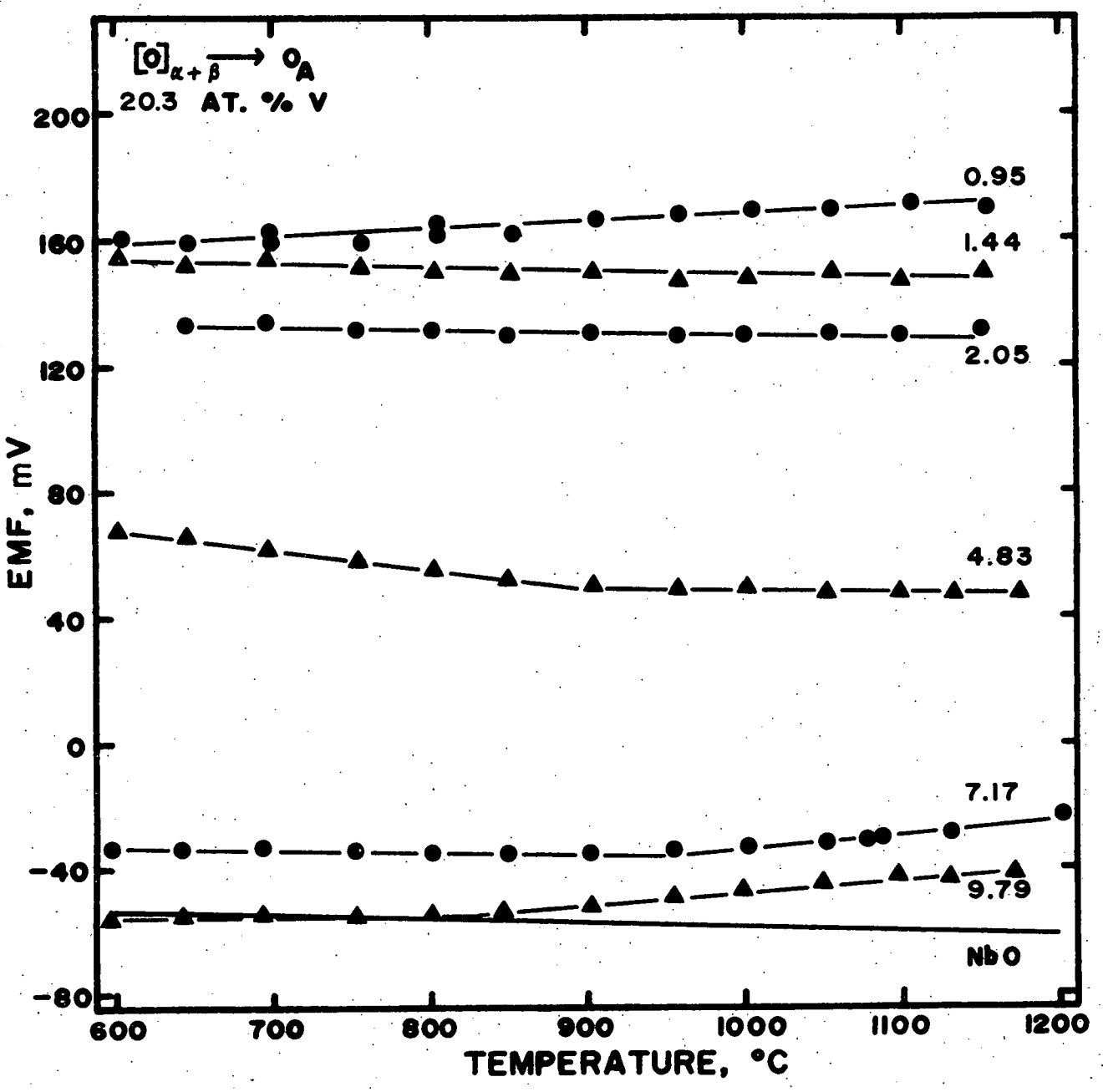

Figure 14: EMF versus temperature for the 19.9 and 20.7 at. % V alloys. The 1.44, 2.05, and 7.17 at. % O samples were prepared from the 19.9 at. % V alloy. The 0.95, 4.83, and 9.79 at. % O samples were prepared from the 20.7 at. % V alloy.

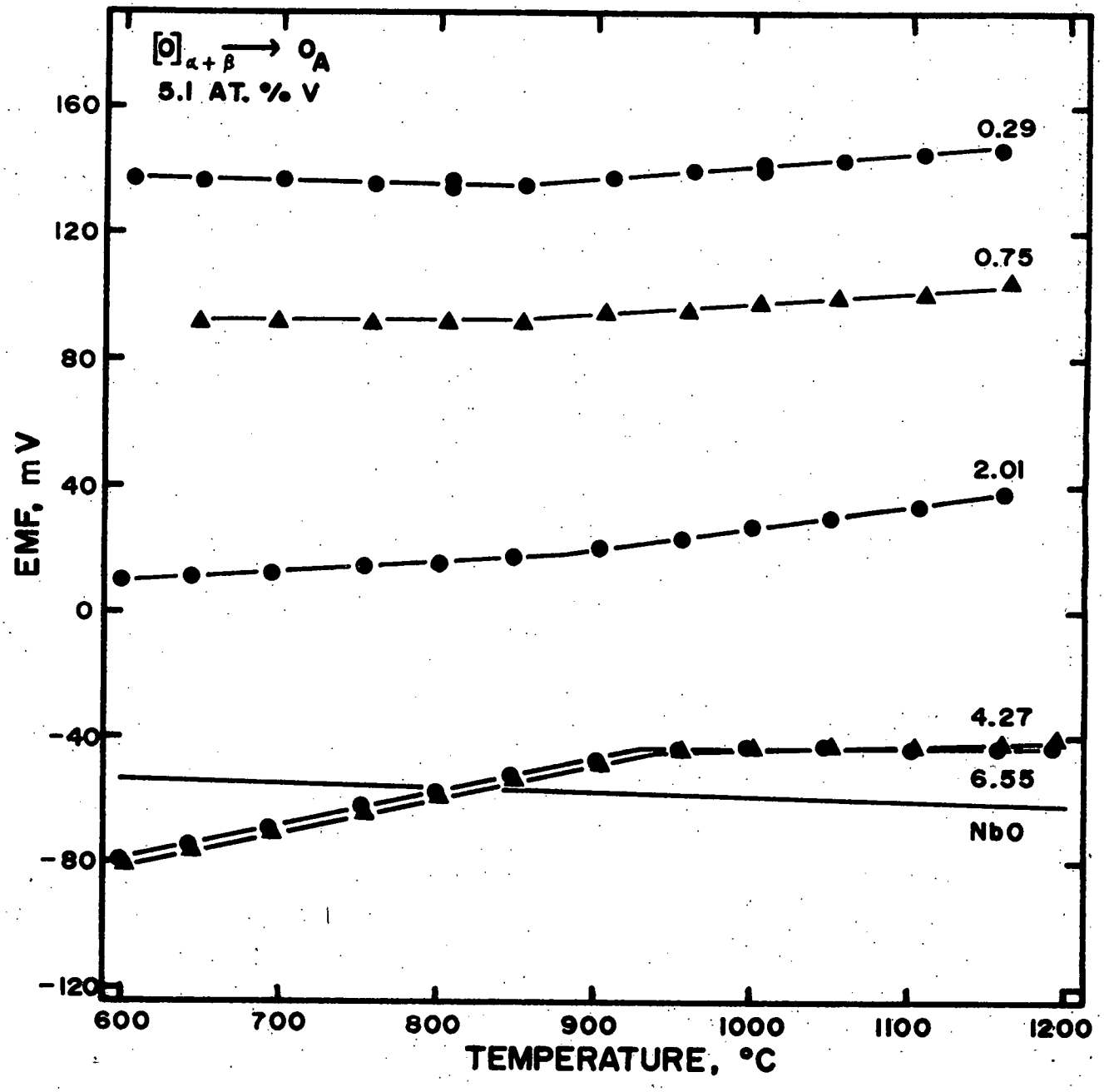

Figure 15: EMF versus temperature for the 5.1 at. % V alloy. The oxygen concentration of each ternary electrode is indicated in at. % O.

TABLE IV

EMF versus Temperature Equations for the Niobium-Vanadium-Oxygen System

At. % V	At. % O	Slope	EMF Intercept	Temperature, °C
85.2	0.76	0.125	56.2	604-957 (1140)*
"	1.44	0.100	49.6	604-1003 (1203)*
"	2.69	0.073	36.8	602-1200
"	4.53	0.051	24.2	603-1198
"	7.57	0.027	0.2	604-1187
"	8.62	0.040	1.0	603-1199
70.7	0.84	0.082	95.3	602- 904 (1148)*
"	0.96	0.087	90.8	647- 959 (1155)*
"	4.03	0.038	57.1	602-1152
"	6.74	0.016	57.0	602-1150
"	9.48	0.003	20.4	602-1147
50.5	0.72	0.064	139.2	599- 917 (1142)*
"	1.40	0.045	127.2	606-1002 (1202)*
"	3.41	0.010	101.9	606-1199
"	5.82	-0.003	72.6	599-1199
"	10.46	-0.009	-17.0	600-1160
35.1	0.75	0.034	160.2	602- 904 (1145)*
"	1.27	0.011	154.0	608-1163
"	3.09	-0.008	123.2	608-1160
"	6.66	-0.041	87.0	600-1163
"	9.61	-0.053	-5.1	605- 933
"	"	0.018	-71.6	933-1155
20.7	0.95	0.024	143.6	606-1154
19.9	1.44	-0.011	159.4	604-1152
"	2.05	-0.008	137.2	646-1150
20.7	4.83	-0.063	105.2	603- 891
"	"	-0.010	58.5	891-1174
19.9	7.17	-0.007	-28.9	599- 956
"	"	0.045	-79.0	956-1201
20.7	9.79	0.006	-59.6	600- 829
"	"	0.040	-87.8	829-1171
5.1	0.29	-0.009	142.6	607- 850
"	"	0.040	101.3	850-1157
"	0.75	-0.001	93.0	648- 853
"	"	0.037	59.8	853-1164
"	2.01	0.030	-8.1	600- 873
"	"	0.069	-41.8	873-1160
"	4.27	0.110	-147.9	602- 940
"	"	0.012	-55.6	940-1195
"	6.55	0.106	-142.4	600- 933
"	"	-0.001	-42.1	933-1192

*The least squares analysis was performed over the temperature range indicated. The linear relationship was extended up to the temperature in parentheses, which is the highest temperature for which EMF measurements were made.

and $\ln \gamma_N$ can also be determined as a temperature function. Isothermal plots of $\ln \gamma_N$ versus N for each Nb-V alloy indicated that the activity coefficient is essentially constant for low oxygen concentrations and increases in a nonlinear fashion for higher values of N.

Over the composition range in which the activity coefficient is constant Henry's and Sieverts' laws are obeyed. Average activity coefficients were calculated and are represented as a function of temperature by equations of the form,

$$\ln \gamma_N^o = A + B/T \tag{70}$$

where γ_N^o is the activity coefficient of oxygen at infinite dilution in the particular Nb-V alloy. The comparison of equations (70) and (37) indicates that $A = -\bar{S}^{xs^o}/R$ and $B = \bar{H}^{xs^o}/R$, where $\bar{S}^{xs^o}$ and $\bar{H}^{xs^o}$ are the excess entropy and enthalpy of the oxygen at infinite dilution in the particular Nb-V alloy. Since Sieverts' law is obeyed, the oxygen pressure is related to concentration and temperature by the equation,

$$P_{O_2} = 1.01 \times 10^5 N^2 \exp\left[(2/R)(-\bar{S}^{xs^o} + \bar{H}^{xs^o}/T)\right] \text{Pa.} \tag{71}$$

The calculated values of $\bar{H}^{xs^o}$ and $\bar{S}^{xs^o}$ are presented in Table V along with the values for the Nb-O[3] and V-O systems. The excess quantities for the binaries were calculated using equations (50) and (51). The concentration ranges over which Sieverts' law is obeyed are also indicated as a function of temperature.

The quantities in Table V are plotted as a function of alloy concentration in Figure 16. $\bar{H}^{xs^o}$ and $\bar{S}^{xs^o}$ are a linear function of the niobium mole fraction, N_{Nb}, for the vanadium-rich alloys. Therefore, Wagner interaction coefficients can be determined from the slope of these plots and the

activity, $(P_{O_2})^{1/2}$, can be represented by equation (48) for dilute oxygen concentrations with N_{Nb} less than 0.65. The values of the interactions coefficients and excess quantities at infinite dilution in V as determined by least squares analysis are given in Table VI. The agreement between the values of $\overline{H}^{xs\infty}$ and $\overline{S}^{xs\infty}$ in Table VI with those in Table V for the V-O analysis is indicative of the excellent fit of this analysis to the ternary data. Values are also given in Table VI for the interaction between V and O in Nb-rich alloys. These values are determined from only two data points, N_V = 0.000 and 0.051, and are therefore not necessarily indicative of intermediate compositions. They are useful, however, for comparing interactions between Nb and O with those between V and O.

At the higher oxygen concentrations the activity coefficients were a function of the oxygen content of the alloy and it was found that γ_N could be fit to a polynomial of the form,

$$\ln \gamma_N = A_0 + A_1 N + A_2 N^2. \tag{72}$$

The curve fitting was done isothermally at 50 degree intervals from 650-1150°C (923-1423 K) over the entire oxygen composition range. The resulting values of A_0, A_1, and A_2 were then determined to be linear functions of reciprocal temperature and can be written,

$$A_i = a_i + b_i/T \tag{73}$$

Thus, by the combination of equations (37), (72), and (73),

$$\begin{aligned} \overline{H}^{xs} &= R(b_0 + b_1 N + b_2 N^2) \\ \overline{S}^{xs} &= -R(a_0 + a_1 N + a_2 N^2). \end{aligned} \tag{74}$$

The equilibrium oxygen pressure can then be determined as a function of

TABLE V

$\bar{S}^{xs^o}$ and $\bar{H}^{xs^o}$ from Sieverts' Law Analysis

N_V	$\bar{S}^{xs^o}$, cal/mole, K	$\bar{H}^{xs^o}$, cal/mole	Max. N_O^*	T, K
1.0	-23.75	-100,720	0.0321	973-1473
0.852	-24.56	-102,670	0.0269	923-1423
0.707	-25.65	-104,380	0.0674	923-1423
0.505	-27.72	-107,600	0.0140	923-1223
0.505	"	"	0.0341	1223-1423
0.351	-28.49	-108,250	0.0309	923-1423
0.203	-29.07	-108,490	0.0205	923-1423
0.051	-30.74	-106,480	0.0075	923-1273
0.051	"	"	0.0201	1273-1423
Nb	-22.45	-91,370	N_s	1123-1548

*Max. N_O represents the maximum oxygen concentration for which Sieverts' law is obeyed. N_s is the terminal oxygen solubility limit.

TABLE VI

First Order Atomic Fraction Interaction Coefficients of Enthalpy, $\eta_O^{(i)}$, and Entropy, $\sigma_O^{(i)}$

Interaction Coefficient	Concentration Range	Excess Quantity at ∞
$\eta_O^{(Nb)}$ = -12,180 cal/mole	$N_{Nb} \leq 0.649$	$\bar{H}^{xs^\infty}$ = -100,860 cal/mole
$\sigma_O^{(Nb)}$ = -7.31 cal/mole, K	$N_{Nb} \leq 0.949$	$\bar{S}^{xs^\infty}$ = -23.66 cal/mole, K
$\eta_O^{(V)}$ = -296,270 cal/mole	$N_V \leq 0.051$	$\bar{H}^{xs^\infty}$ = -91,370 cal/mole
$\sigma_O^{(V)}$ = -162.6 cal/mole, K	$N_V \leq 0.051$	$\bar{S}^{xs^\infty}$ = -22.45 cal/mole, K

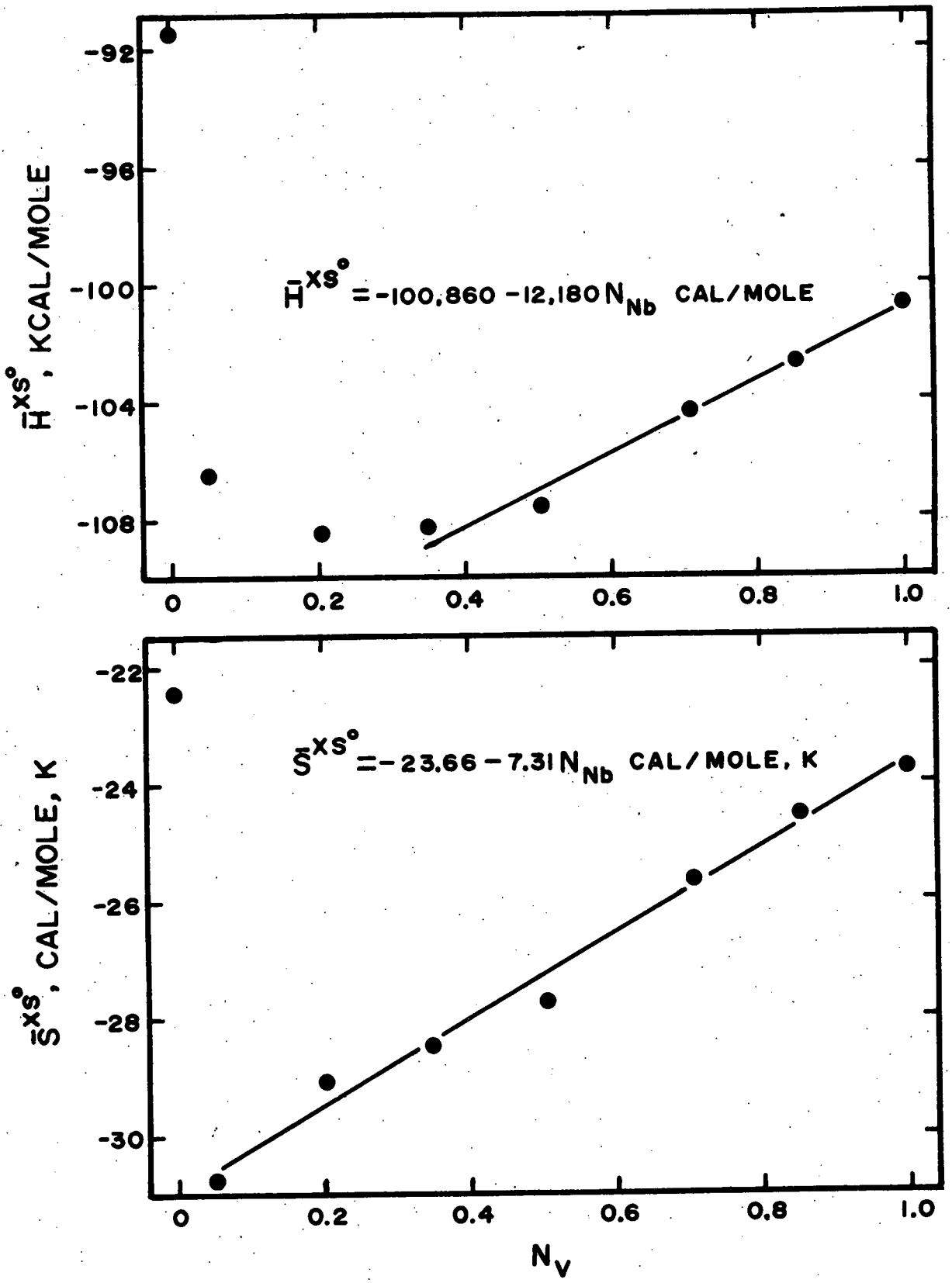

Figure 16: Excess oxygen quantities at infinite dilution in the Nb-V-O alloys as a function of the vanadium atom fraction.

temperature and oxygen composition for each Nb-V alloy by equation (71) with the quantities $\overline{H}^{xs}$ and $\overline{S}^{xs}$ replacing $\overline{H}^{xs^o}$ and $\overline{S}^{xs^o}$, respectively. The polynomial coefficients are given in Table VII. The curve fitting technique was also applied to the V-O system and the results of that analysis are also given in the table. The coefficients for the 20.3 and 5.1 at. % V alloys are broken down into two temperature ranges. This is due to the slope changes in the EMF curves for these alloys (see Figures 14 and 15).

As an example of the fitting procedure, the equilibrium oxygen pressure is plotted as a function of temperature and oxygen concentration for the 35.1 at. % V alloy in Figure 17. The data points represent the oxygen pressures calculated from the EMF equations in Table IV. The dashed lines through the data points were calculated from equation (71) and the data in Table V for concentrations up to 3.09 at. % O and from equations (71) and (74) along with the data of Table VII for the higher oxygen concentrations. It is apparent that the fitting procedures describe the data well and the two analyses are quite compatible with each other. The calculated oxygen pressures for the Nb-O and V-O binary systems are also shown at the three temperatures for comparison with the ternary alloys. The figure readily demonstrates that the addition of 35 % vanadium to niobium significantly decreases the activity of oxygen in solid solution. No second phases were precipitated in any of the Nb-35.1 % V-O alloys. Therefore, it would appear that adding V to Nb substantially increases the oxygen solubility limit. It is seen that these effects of the alloying were diminished as the temperature was increased. The trends shown by this alloy were representative of those exhibited by all of the alloys. The results Nb-rich and V-rich alloys at 1000°C (1273 K) are plotted in Figures 18 & 19.

TABLE VII

Polynomial Curve Fit Coefficients

N_V	a_0	b_0	a_1	b_1	a_2	b_2	T,K
1.0	11.86	-50,580	10.24	-14,860	-223.6	409,390	973-1473
0.852	12.38	-51,840	0.83	9,350	-42.28	6,750	923-1423
0.707	13.17	-52,670	-12.08	-470	78.9	108,040	923-1423
0.505	13.85	-54,050	-7.93	7,200	-14.7	222,200	923-1423
0.351	14.47	-54,440	-1.92	-22,140	-101.3	623,360	923-1423
0.203	13.76	-53,440	82.2	-116,600	-1250	2.181×10^6	923-1173
0.203	14.61	-54,440	8.2	-29,650	-568.1	1.385×10^6	1173-1423
0.051	16.85	-55,270	-210.1	270,000	1798	-1.899×10^6	923-1223
0.051	16.11	-54,410	-272.2	346,100	4825	-5.571×10^6	1223-1423

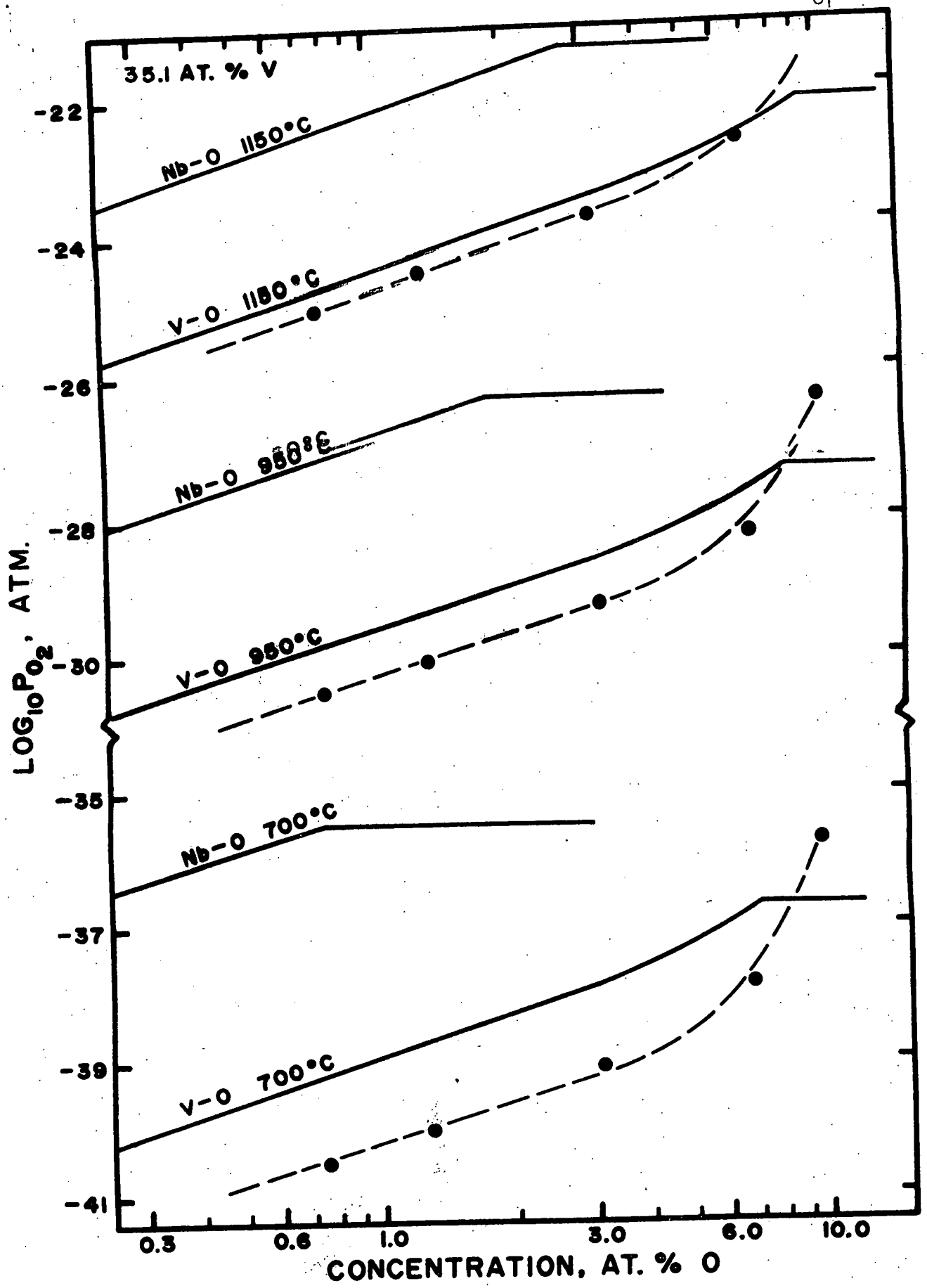

Figure 17: Equilibrium oxygen partial pressure as a function of the oxygen concentration for the 35.1 at. % V alloy at 700, 950, and 1150°C.

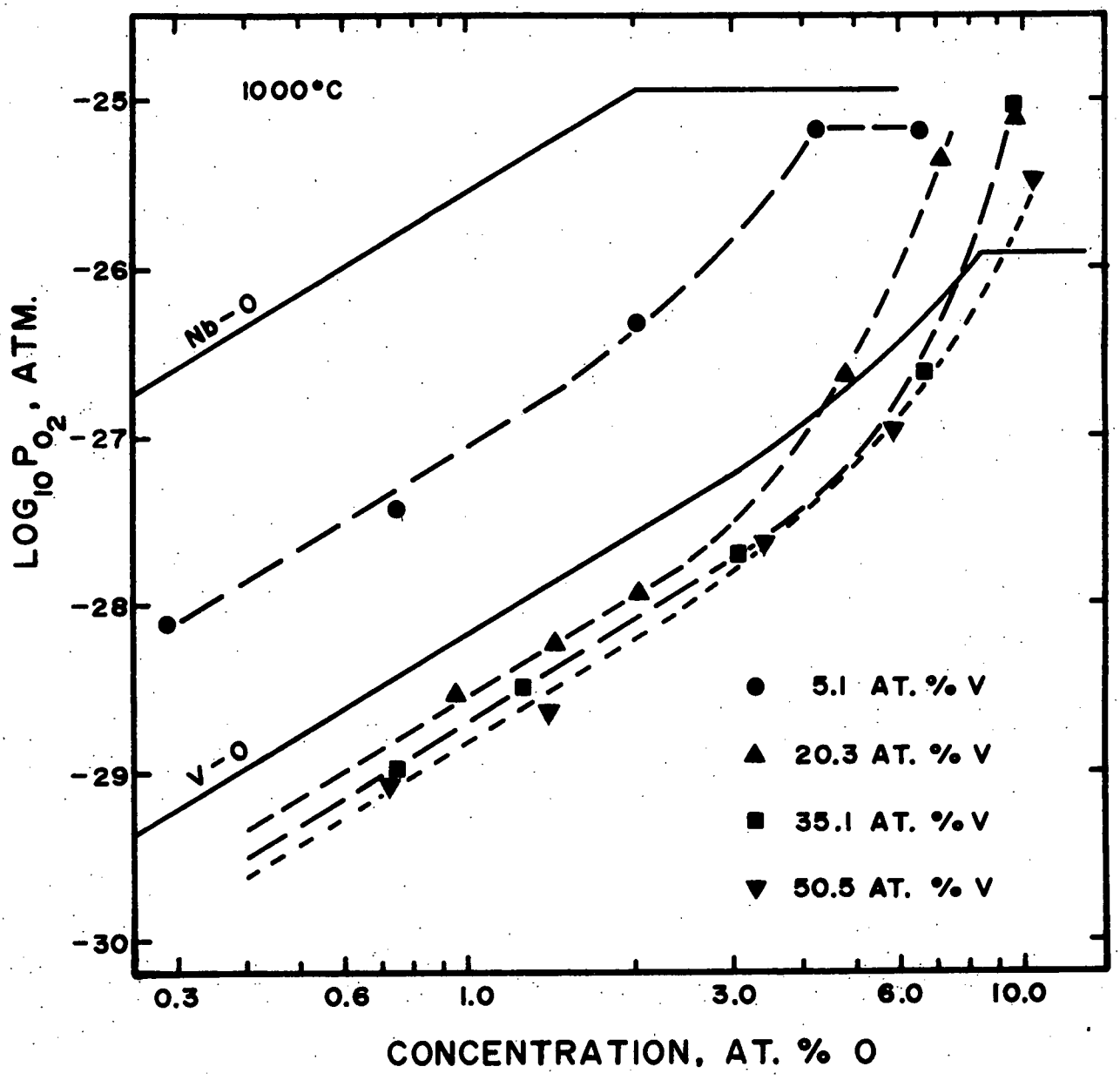

Figure 18: Equilibrium oxygen partial pressure as a function of the oxygen concentration for the niobium-rich alloys at 1000°C.

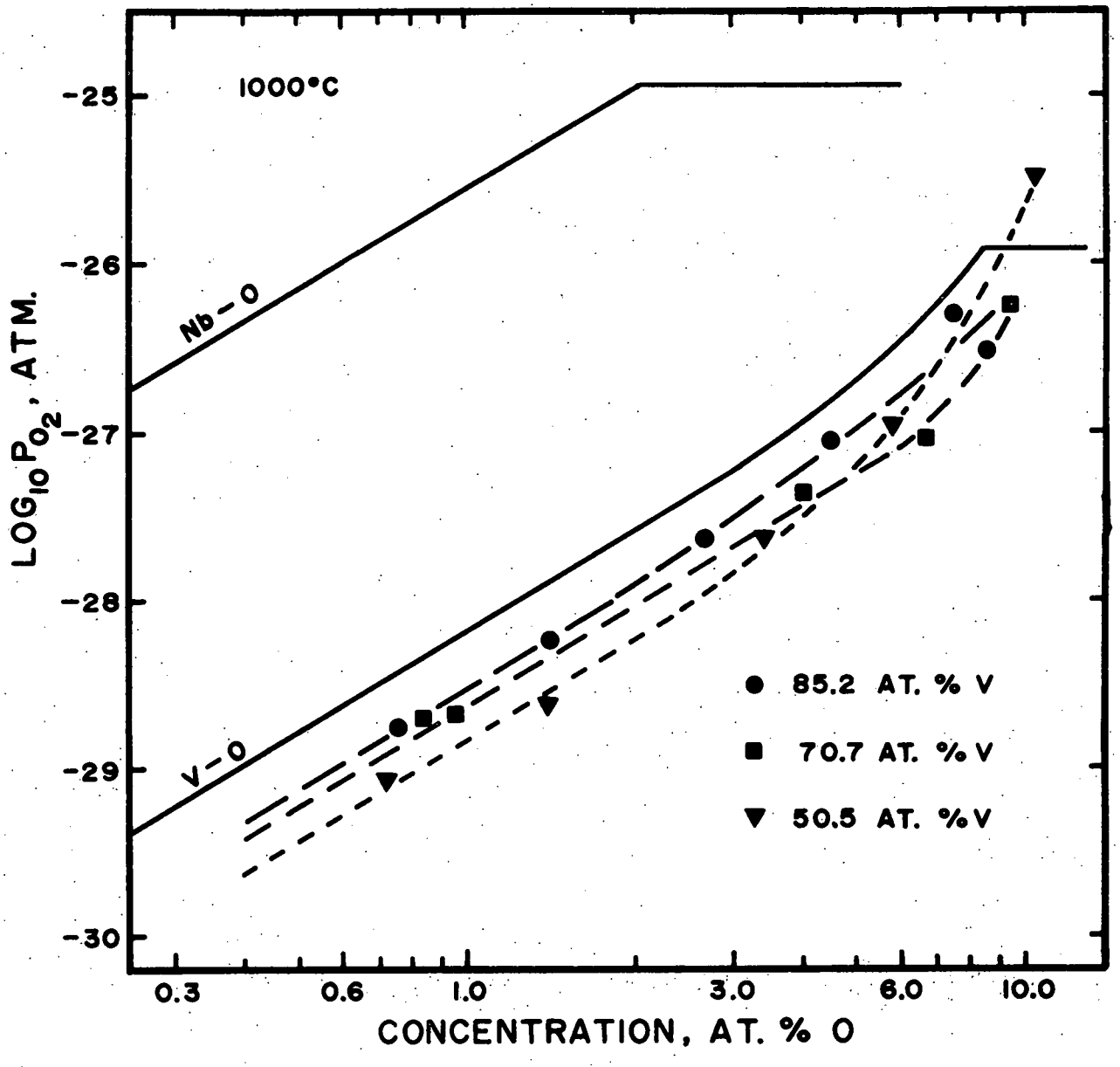

Figure 19: Equilibrium oxygen partial pressure as a function of the oxygen concentration for the vanadium-rich alloys at 1000°C.

The 50.5 at. % V and Nb-O and V-O curves are included in both figures to aid in comparisons between the figures. For the Nb-rich alloys the equilibrium oxygen partial pressures progressively decreased at a given oxygen content as the amount of vanadium in solution was increased. However, the effect of vanadium additions greater than approximately 20 % was slight. In fact, for any given oxygen concentration less than roughly 5 at. %, the oxygen pressure varied less than an order of magnitude for variations in the V content from 20 to 100 %. Furthermore, these figures indicate that the deviations from Sieverts' law were also a function of the Nb/V ratio. The V-rich alloys deviated only slightly from Sieverts' law for oxygen concentrations up to 7 at. %, whereas, the 5.1-50.5 at. % V alloys showed substantial deviations for oxygen concentrations in excess of only 3 %.

3.2.2 Microscopy and Auger Electron Spectroscopy

The results of the EMF measurements indicated the possibility of oxide phase precipitation for certain oxygen concentrations of the Nb-rich alloys. The EMF for the 5.1 at. % V alloy was roughly the same for the 4.27 and 6.55 % O concentrations (see Figure 15). This suggests the probable formation of an oxide phase above approximately 4.2 at. % oxygen. The 9.79 % O sample for the 20.3 % V alloy did not follow the functional relationship between oxygen partial pressure and oxygen concentration exhibited by the other samples (Figure 18). This also suggests the precipitation of an oxide phase. Therefore, optical and transmission electron microscopy were performed on the high oxygen concentration samples for each Nb-V alloy.

Optical microscopy indicated that the 85.2, 70.7, 50.5, and 35.1 % V alloys had solid solution structures for all of the oxygen compositions studied. However, the 7.57 and 8.62 % O samples for the 85.2 % V alloy,

when vacuum quenched from around 1000°C (1273 K), had the same martensitic structure (Figure 8) as the high oxygen V-O alloys. As for the V-O system this phase was interpreted as being a metastable transformation product formed during the quenching process. This phase was not seen in the 4.53 % oxygen sample or in any of the lower vanadium alloys.

A grain boundary precipitate was present in the 20.7 at. % V-9.79 at. % O alloy after water quenching from 700 and 1000°C (973 & 1273 K). The amount of this phase, which is shown in Figure 20, did not appear to be a function of temperature. The precipitate did not appear in any of the lower oxygen concentrations of the 20.7 or 19.9 % V alloys. A similar grain boundary phase was observed in the 5.1 % V alloy with 4.27 and 6.55 % O (Figure 21). The volume fraction of this phase was also independent of the quenching temperature. However, the 4.27 % O alloy had a very low fraction of the precipitate and it is assumed that this oxygen concentration is very near the minimum concentration for which this phase forms. Since the precipitates in Figures 20 & 21 are fairly large, up to 25 microns, it was possible to determine their structure by electron diffraction. Both precipitates have the same structure as NbO, which is related to the NaCl structure, except with three molecules per unit cell. Lattice parameters were calculated for the precipitates and are 4.20 Å for the 20.7 % V-9.79 % O alloy and 4.22 Å for the 5.1 % V-6.55 % O alloy. These values may be compared to the published lattice parameter of NbO which is 4.210 Å.[84]

Analytical electron microscopy, AEM, and Auger electron spectroscopy, AES, were also employed to further characterize the grain boundary phases. In the AEM work energy dispersive x-ray analysis, EDEX, was utilized in an attempt to compare the Nb/V ratios between the matrix and precipitate for the 5.1 % V-6.55 % O alloy. This analysis indicated that the Nb/V ratios

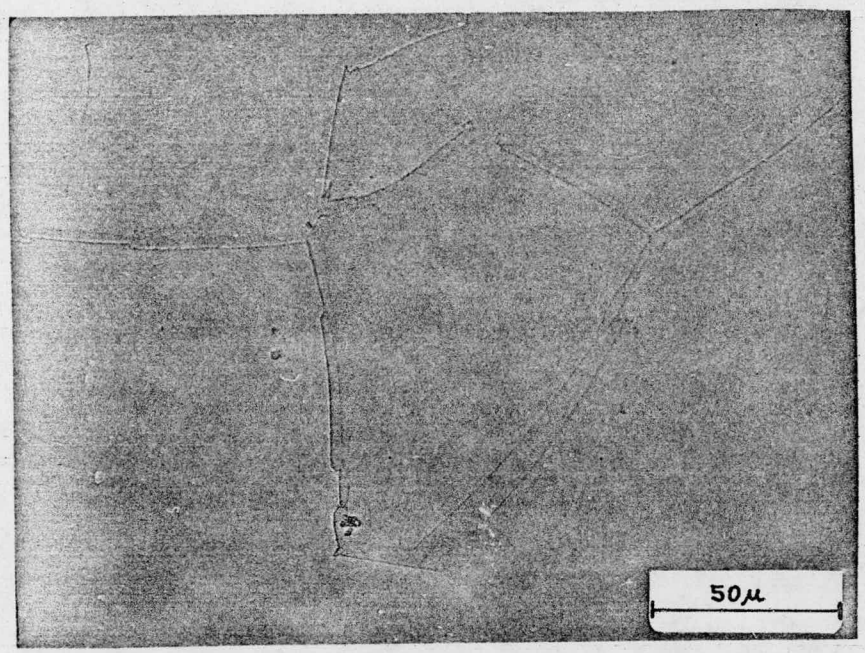

Figure 20: 20.7 at. % V-9.79 at. % O alloy vacuum quenched from 1000°C. Solid solution matrix with grain boundary precipitate. Mechanically polished.

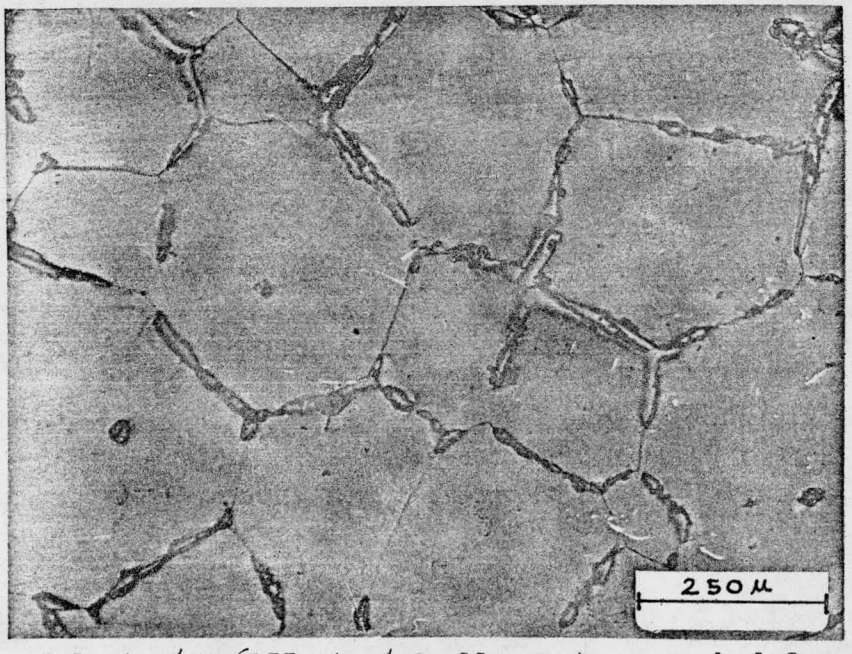

Figure 21: 5.1 at. % V-6155 at. % O alloy water quenched from 800°C. Solid solution matrix with grain boundary precipitate. Electropolished.

were qualitatively the same for the precipitate as for the matrix. The AES study was made on the 5.1 % V-6.55 % O and 20.7 % V-9.79 % O alloys. This analysis also indicated that the Nb/V ratios were qualitatively the same in the precipitates as in the matrix. AES was also used to determine variations in the oxygen content within these alloys. Figure 22 shows an AES scan of the 510 eV oxygen peak across a sample of the 20.7 % V-9.79 % O alloy. The horizontal line across the electron image designates the location of the line scan across the sample. The second line plots the variation in the oxygen concentration. Substantial increases in the oxygen concentration are noted at grain boundaries which contain precipitates. Unprecipitated grain boundaries and the matrix showed little variation in the oxygen signal. The general curvature of the oxygen scan across the sample is believed to be due to geometrical effects and does not reflect changes in the oxygen concentration. Similar plots were obtained for the 5.1 % V-6.55 % O alloy. These results demonstrate that precipitates are oxygen-rich phases.

It is concluded from the electron diffraction, AEM, and AES analyses that the precipitates formed are isostructural with NbO with vanadium in solution on the niobium lattice. This suggests a certain range of solubility of NbO in the Nb-V-O system. However, this suggestion cannot be definitely concluded from the results. Since the highest temperature employed in this investigation is less than half the melting point of the alloys, the redistribution of Nb and V would be very slow. Therefore, the precipitates formed may not be at equilibrium.

Electron microscopy was also used to determine if any second phases were formed for the higher oxygen compositions of the other Nb-V alloys. For the 70.7 and 35.1 % V alloys no second phases were observed. The only

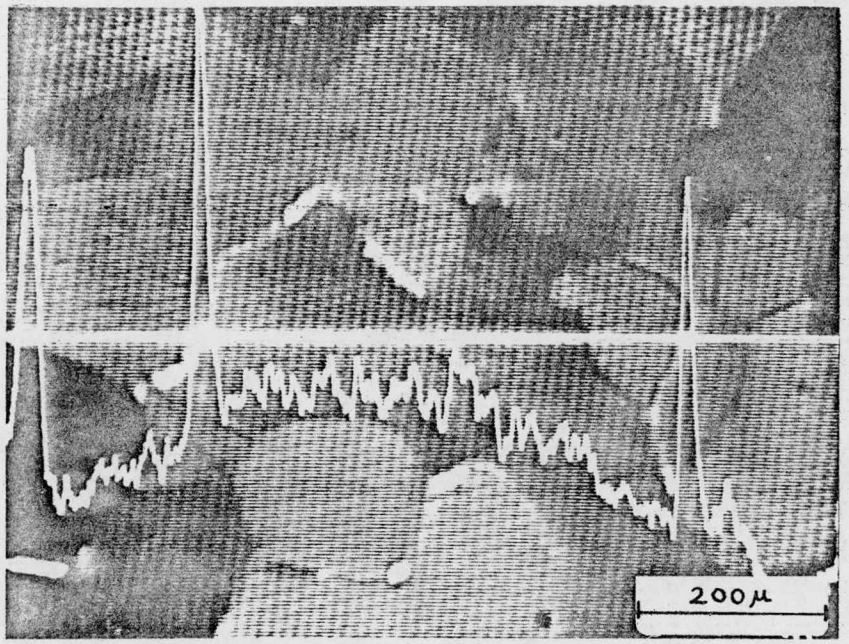

Figure 22: 20.7 at. % V-9.79 at. % O alloy water quenched from 800°C. AES absorbed electron current image with superimposed oxygen line scan. Horizontal line indicates the line scanned.

second phase noted in the 85.2 % V alloys was the martensitic phase noted optically. For the 50.5 % V-10.46 % O and 19.9 % V-7.17 % O alloys there was evidence of very small precipitates in samples water quenched from 700 and 1100°C (973 & 1373 K). An example of the type of contrast observed is shown in Figure 23 for four different orientations of the same area. It is believed that the contrast was caused by sperically symmetric strains around coherent precipitates. A description of the various contrast effects for this type of precipitate has been given by Phillips and Livingston[85] and Ashby and Brown[86] for the kinematical and dynamical theories of diffraction, respectively. When only one strong reflection is operating, the contrast appears as a pair of lobes which are summetrically placed about a line of no contrast. This line of no contrast is perpendicular to the reciprocal lattice vector, $\bar{g}$, used to form the image. These diffraction contrast effects are exemplified by the precipitates in Figure 23. The length of the line of no contrast is approximately equal to the particle diameter. Thus, the precipitates shown were in the 250-400 Å size range. It was noted that the precipitates formed inhomogenously within the matrix and were often found near grain boundaries and on dislocations. The size and density distributions were not rigorously determined. However, these distributions appeared to be the same for the two annealing temperatures. In view of the above observations it was assumed that these precipitates were formed during the quenching process and were not present at the higher temperatures. To test this hypothesis a set of samples which had been annealed at 800°C (1073 K) and water quenched, were subsequently aged at 350°C (623 K) for 50 hours. The ageing treatment resulted in an increase in the precipitate size by a factor of 2-3 times. This is demonstrated by Figure 24 in which the aged and unaged precipitates are shown for the same

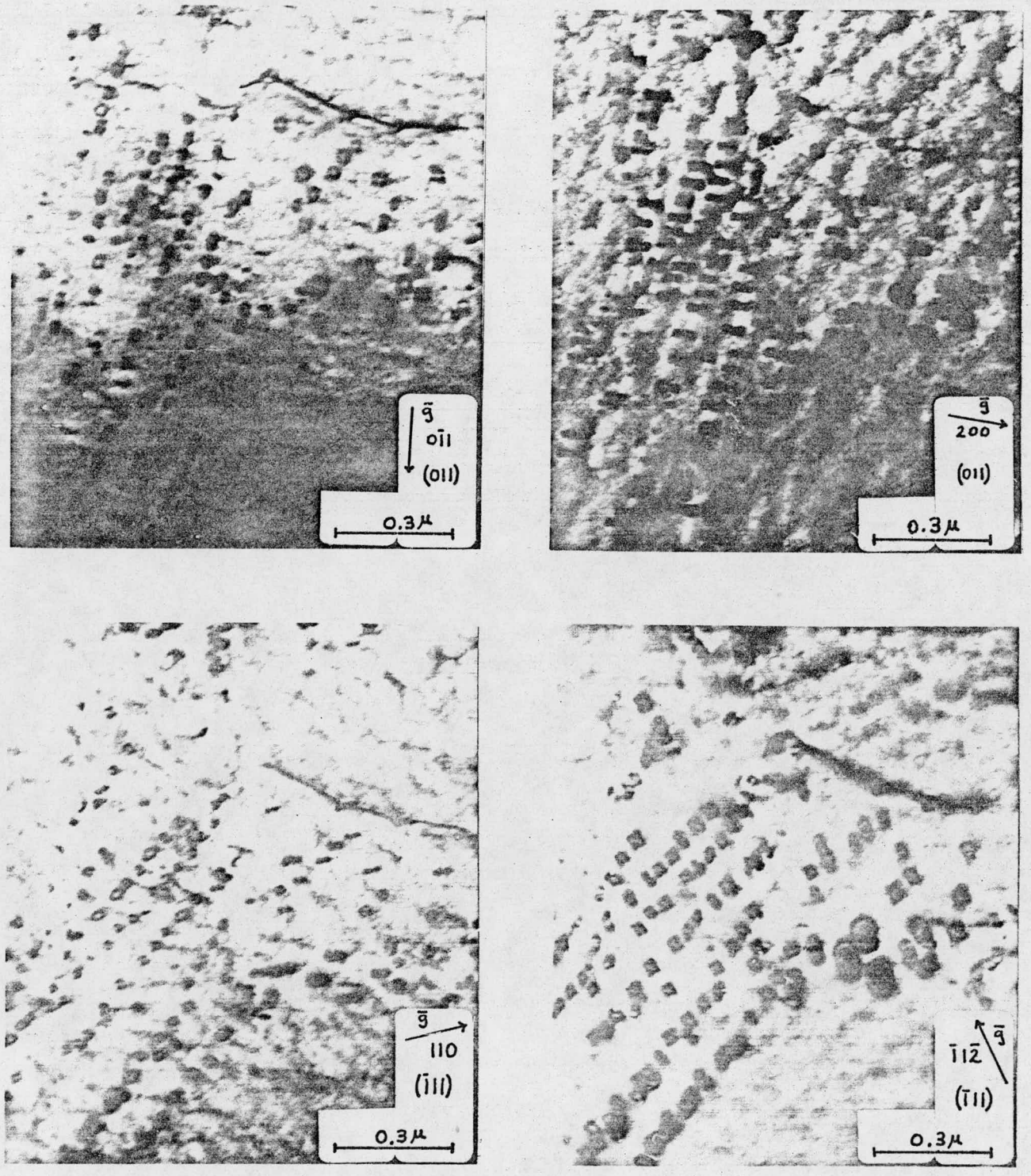

Figure 23: 19.9 at. % V-7.17 at. % O alloy water quenched from 700°C. Four orientations of the same area showing relationship between strain field contrast and the operating reciprocal lattice vector.

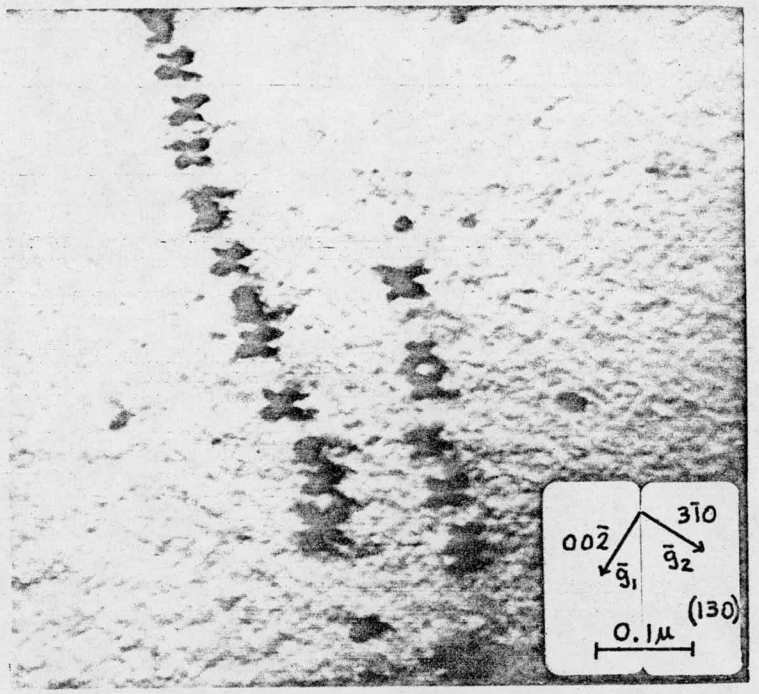

a.

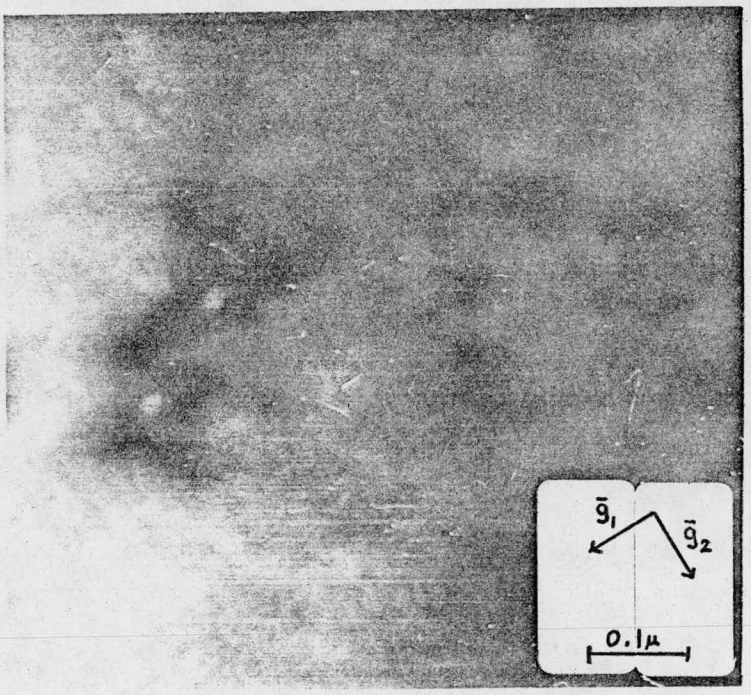

b.

Figure 24: 50.5 at. % V-10.46 at. % O alloy.
a. Water quenched from 700°C.
b. Water quenched from 700°C and aged 50 hours at 350°C.

alloy. The "cloverleaf" contrast shown in this figure is the result of two strong reflections operating with the reciprocal lattice vectors perpendicular to one another. The precipitate diameter is proportional to the region of no contrast in the center of the cloverleaf. Therefore, the particle size was increased significantly as a result of the ageing. Since the precipitates grew at 350°C (623 K), but had the same size when quenched from 700 and 1100°C (973 & 1373 K), it is concluded that they were formed upon cooling from the quench temperatures and were not present within the temperature range of the EMF measurements.

A second type of precipitate, which was present for all three oxygen compositions of the 19.9 at. % V alloy, is shown in Figure 25. This precipitate was not observed in any of the 20.7 % V alloys. Since the 19.9 % V alloy had a relatively high zirconium concentration (400 at. ppm), and since ZrO_2 has a lower free energy of formation than that for oxygen in solution, this precipitate was suspected to be ZrO_2. The x-ray energy spectrum was determined for the foil area containing the precipitate and compared to that for the matrix. The results of that analysis are shown in Figure 26. The two spectrums are identical except for the small peak at approximately 15.7 keV. This is the zirconium K_α peak, and the presence of Zr in the precipitate was thus verified. Although the 50.5 % V alloy also had a fairly high concentration of Zr, no precipitates were noted in any samples for that alloy. The precipitates were extremely inhomogeneously distributed in the 19.9 % V alloy and it is assumed that they were present in the 50.5 % V alloys, but did not happen to be in the thin regions of the TEM samples.

The presence of zirconium in these alloys removes a quantity of oxygen from solution equal to two times the Zr concentration in the formation of

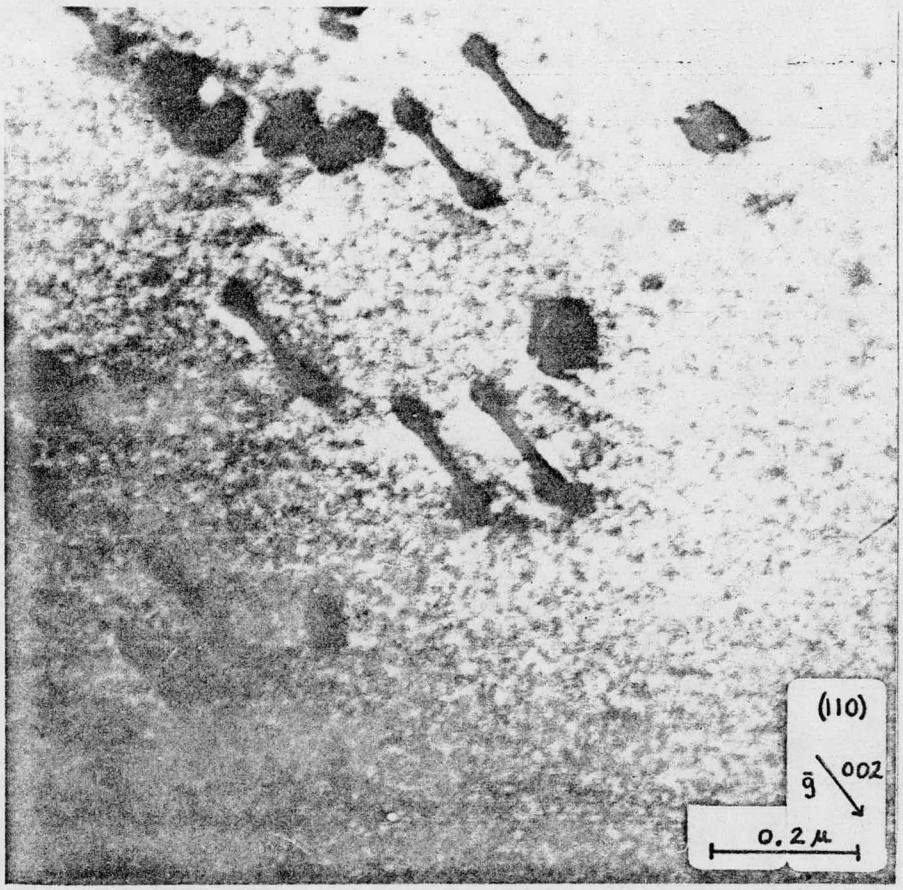

Figure 25: 19.9 at. % V-1.44 at. % O alloy vacuum quenched from 1000°C showing ZrO_2 precipitates.

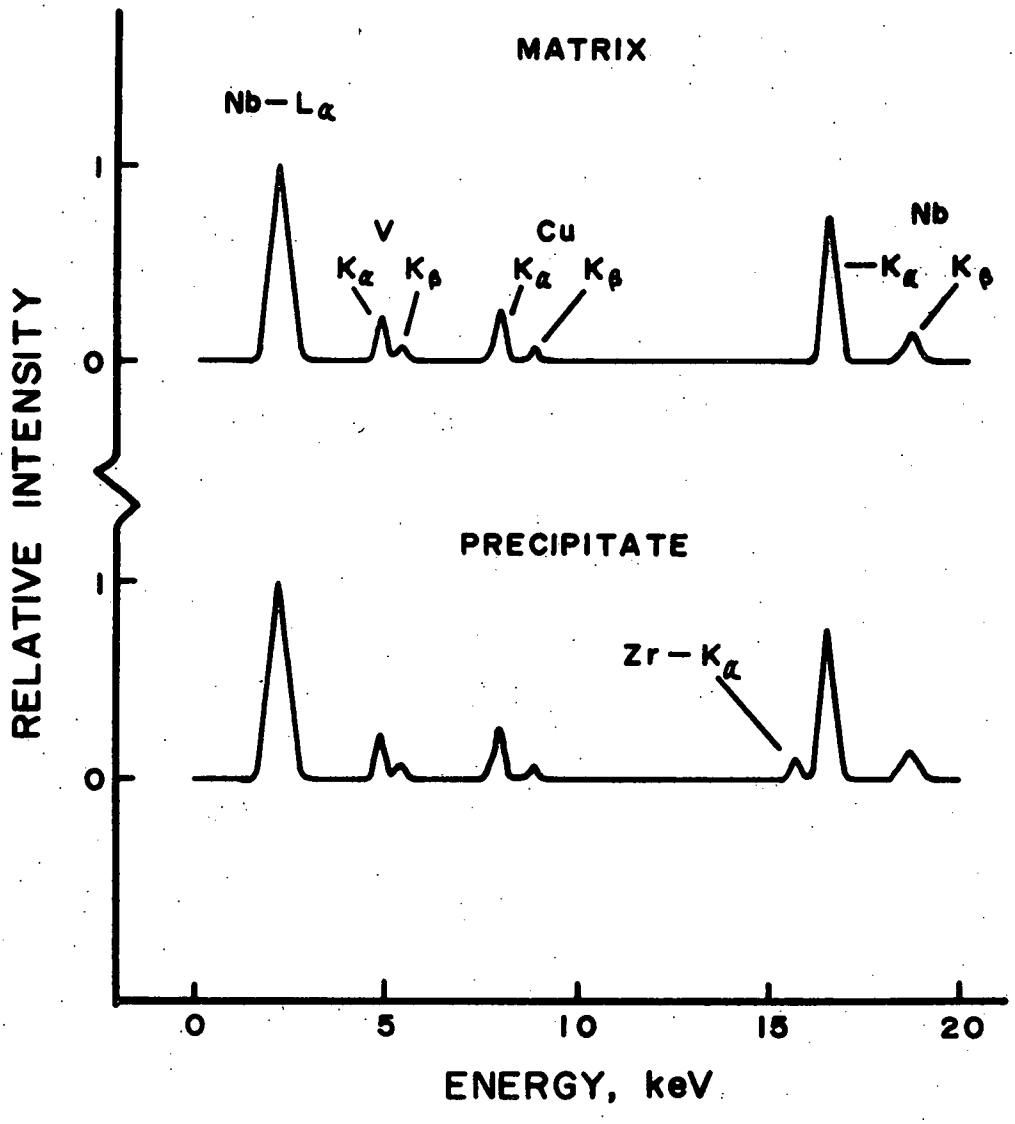

Figure 26: X-ray energy spectrum for 19.9 at. % V-1.44 at. % O alloy. Spectrums are compared for the matrix and the precipitates shown in Figure 25. The Cu peak is from the sample holder.

the internal oxides. This would be only 800 and 400 at. ppm for the 19.9 and 50.5 % V alloys, respectively. This is a relatively insignificant amount relative to the total quantity of oxygen in solution. It is therefore concluded that the zirconium does not significantly influence the thermodynamic data. This conclusion is supported by the agreement of the data in Figures 14 and 18 for the high Zr, 19.9 % V alloy and the much lower Zr, 20.7 % V alloy.

4. DISCUSSION

4.1 Application of Theoretical Solution Models to the Vanadium-Oxygen and Niobium-Vanadium-Oxygen Systems

In order to apply interstitial solution models to real systems some assumption must be made regarding the location of the interstitial atoms in the solution. For the case of b.c.c. metals, oxygen, nitrogen, and carbon are usually assumed to occupy octahedral (0, 0, 1/2) interstices. This assumption has been based upon the results of internal friction studies in which the presence of a Snoek peak could best be explained by octahedral site occupancy.[87] However, it has been argued that occupancy of the tetrahedral (0, 1/2, 1/4) positions can also cause Snoek peaks.[88,89] Attempts have been made to determine the more energetically favorable site by elasticity calculations. These calculations have also left the issue unresolved, particularly for the case of oxygen in vanadium. Beshers[88] has predicted octahedral occupancy for oxygen in V, while Shatalov and Khachaturyan[89] have proposed tetrahedral site occupancy for any of the interstitial elements in V. However, recent neutron diffraction experiments on V-O, V-N, and V-C solid solutions have indicated that all three interstitial elements occupy the octahedral positions.[90] For the V-O system the experiments were performed on samples quenched from 500°C (773 K) containing roughly 3 at. % O. The composition and temperature of these experiments were similar to those of this investigation. Therefore, on the basis of the neutron diffraction measurements, octahedral site occupancy will be assumed throughout this section.

Befor testing the applicability of the interstitial solution models

it will be advantageous to calculate the functions, $\Delta\overline{S}^{ex}$ and $\overline{H} - \overline{H}^{\infty,V}$. $\Delta\overline{S}^{ex}$ is the nonconfigurational entropy change for the reaction oxygen gas going into solution. It is related to the total oxygen entropy change for the reaction, $\Delta\overline{S}$, and the absolute entropy of gaseous oxygen, S^{o}, by the relations,

$$\begin{aligned} \Delta\overline{S}^{ex} &= \Delta\overline{S} - \overline{S}^{c,id} \\ \Delta\overline{S}^{ex} &= \overline{S}^{ex} - S^{o}, \end{aligned} \tag{75}$$

where $\overline{S}^{ex}$ is defined by equation (37) with γ substituted for γ_N. $\overline{H} - \overline{H}^{\infty,V}$ is determined from the relation,

$$\begin{aligned} \overline{H} - \overline{H}^{\infty,V} &= \Delta\overline{H} - \Delta\overline{H}^{\infty,V} \\ \overline{H} - \overline{H}^{\infty,V} &= (\overline{H} - H^{o}) - (\overline{H}^{\infty,V} - H^{o}), \end{aligned} \tag{76}$$

where $\overline{H}$ is the absolute enthalpy of oxygen in solution and the superscript ∞,V refers to the infinitely dilute oxygen solution in vanadium. $\Delta\overline{S}^{ex}$ and $\overline{H} - \overline{H}^{\infty,V}$ have been calculated from equations (6) and (68) for the V-O system and equations (6) and (71) and the data in Table VII for the ternary alloys and are presented in Figure 27. The curves for the 5.1 and 20.3 at. % V alloys were calculated from the higher temperature coefficients in the table. $\Delta\overline{S}^{ex}$ and $\overline{H} - \overline{H}^{\infty,V}$ are independent of temperature for all the other alloys.

4.1.1 Regular Solution Models

Regular solutions are assumed to be random and the configurational entropy is thus given by equation (6) with $\beta' = 3$. Furthermore, $\overline{S}^{ex}$ is assumed to be constant. Therefore, $\Delta\overline{S}^{ex}$ can not vary with oxygen content when regular solution behavior is obeyed. All of the $\Delta\overline{S}^{ex}$ plots in Figure 27 vary with oxygen composition and so none of the alloys strictly obey regular

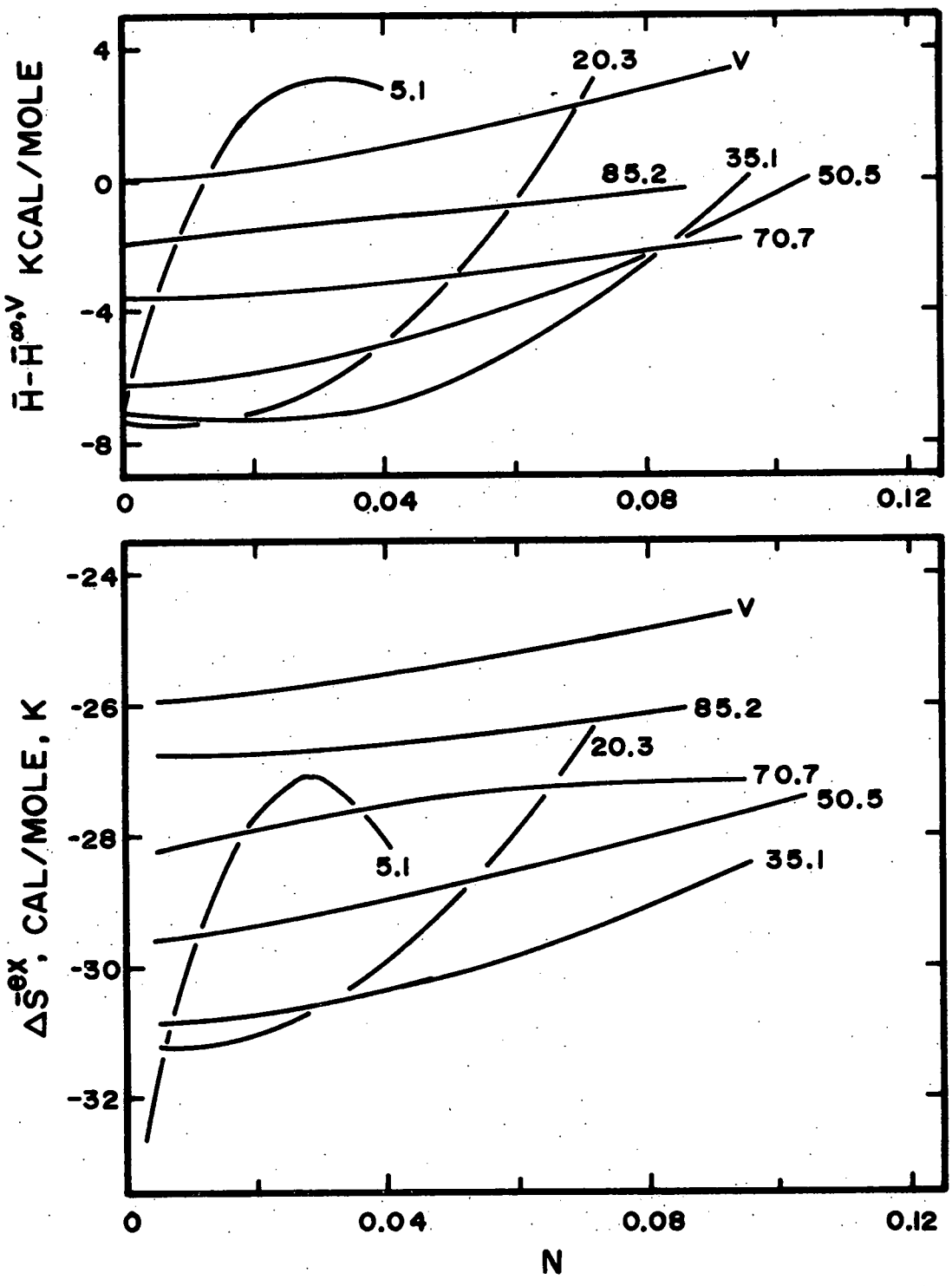

Figure 27: Variation of $\Delta\bar{S}^{ex}$ and $\bar{H}-\bar{H}^{\infty,V}$ with oxygen concentration for all of the Nb-V-O alloys and the V-O alloys.

solution behavior. However, for dilute solutions it has been shown that Henry's law is obeyed by all the alloys and average values for the entropy and enthalpy of solution have been calculated (Table V). The vanadium-oxygen system therefore obeys quasi-regular behavior for solutions having up to approximately 3.2 at. % oxygen. The values of $\Delta\overline{S}^{\infty}$ and $\Delta\overline{H}^{\infty}$ given in equations (13) and (14) can be approximated using equations (54) and (55) and the values of $\overline{S}^{xs^o}$ and $\overline{H}^{xs^o}$ given in Table V. The calculated values of $\Delta\overline{S}^{\infty}$ and $\Delta\overline{H}^{\infty}$ are -25.93 cal/mole, K and -100,720 cal/mole, respectively. $\overline{S}^{ex}$ and $\overline{E}$ may then be calculated from published values of S^o and H^o.[91] At 1000°C (1273 K) $\overline{S}^{ex}$ = 4.18 e.u. and $\overline{E}$ = -95,860 cal/mole. These values may be compared to those of the Nb-O system for which $\overline{S}^{ex}$ = 5.48 e.u. and $\overline{E}$ = -86,510 cal/mole.[3] Thus, assuming both solutions are random at low oxygen concentrations, the lower chemical potential of oxygen in vanadium is primarily the result of a lower energy of solution as opposed to a higher entropy. Since $\overline{E}$ is actually an enthalpy term its more negative value for vanadium than niobium may be due to either a stronger bond with the oxygen or could also be due to less distortion of the vanadium lattice upon insertion of the oxygen.

Although the ternary alloys obey Henry's law for dilute solutions, they do not obey quasi-regular behavior. For quasi-regular behavior to be obeyed $\overline{S}^{ex}$ in the ternary is required to equal $\overline{S}^{ex}$ in the solvent-oxygen binary and $\Delta\overline{H}^{\infty,T}$ must be a linear sum of $\Delta\overline{H}^{\infty,V}$ and $\Delta\overline{H}^{\infty,Nb}$ (equation (15)). Inspection of the data in Table V demonstrates that neigher of these requirements is met. $\Delta\overline{H}^{\infty,T}$ is much more negative than the model predicts and $\overline{S}^{ex}$ is lower than the values for either binary system. A possible reason for $\Delta\overline{H}^{\infty,T}$ not following equation (15) is that bonding between the Nb & O or V & O atoms, or both, is not the same in the ternary

system as it is in the respective binaries. Another possible explanation may be in the strain energy term. Since there is a considerable size difference between the Nb and V atoms, the size of the interstitial holes is probably significantly different for different Nb/V ratios. Also, the elastic constants would be expected to be a function of the Nb/V ratio. Thus, the $\Delta\bar{H}^{strain}$ term would be expected to vary with the Nb/V ratio. The results in Table V imply that either the bonds are stronger or the strain energy is less positive in the ternary system. A change in either the bond energies or strain energy would be expected to be accompanied by a change in the oxygen vibrational frequency, thus changing $\bar{S}^{ex}$. Alternately, the low values of $\bar{S}^{ex}$ in the ternary alloys relative to the binaries may be due to nonideal configurational entropies in the ternaries. Since the V-O interaction is stronger than that between Nb and O the oxygen atoms would be expected to cluster around the vanadium atoms, thus decreasing the configurational entropy. The values of $\Delta\bar{S}^{ex}$ and $\bar{S}^{ex}$ would therefore be more positive than those calculated by assuming a random solution and would more closely approach the values for the binary systems.

The last of the regular solution models to be considered is that of Kirkaldy and Purdy,[57] equations (22) and (23). In the derivation of the model the nonconfigurational entropy was assumed to be zero. If this restriction is removed and a nonconfigurational entropy term independent of composition is allowed, equation (23) may be rewritten,

$$RT \ln \frac{a_2}{N_2}(3-4N_2) = 2E_{12} - H_2^o - T\Delta\bar{S}_2^{ex} + \frac{4N_2E_{22}}{3(1-N_2)}. \qquad (77)$$

The interaction energies and $\Delta\bar{S}^{ex}$ are assumed to be independent of concentration. Therefore, if the model applies, a plot of the left side of equation

(77) versus $N_2/(1-N_2)$ should be linear with the slope proportional to the solute mutual interaction energy, E_{22}. Figure 28 shows plots for the V-O system at the temperatures indicated. These plots would seem to indicate that the model describes the data with the oxygen-oxygen interaction energy varying from 10,750 cal/mole at 700°C (973 K) to 8,520 cal/mole at 1200°C (1473 K). However it has previously been determined from Figure 27 that $\Delta\overline{S}^{ex}$ varies with oxygen concentration and thus one of the basic assumptions of the model is not met. The fit of the data to equation (77) must therefore be fortuitous. This conclusion is verified by Figure 29. In the upper portion of the figure the experimentally determined oxygen enthalpy in vanadium relative to infinite dilution is compared to that predicted by the model at 1000°C (1273 K) using the value of E_{22} determined by the plot in Figure 28. In the lower portion of the figure the absolute entropy of oxygen in vanaduum is compared to the absolute oxygen entropy predicted by the model at 1000°C (1273 K). The subscript 2 in these plots represents the properties predicted by the model and the experimental values have no subscript. At a given value of $N/(1-N)$ it can be shown that

$$T(\overline{S} - \overline{S}_2) = (\overline{H} - \overline{H}^{\infty,V}) - (\overline{H}_2 - \overline{H}_2^{\infty}).$$

Therefore, the errors in the entropy and enthalpy terms deduced from the model cancel each other and hence the fit of the data to equation (77) is meaningless. The model does not describe the system and the values of the interaction energies determined by the plots in Figure 28 have no physical significance. The failure of the model to describe the system despite the fit of the data to equation (77) demonstrates the importance of properly testing the assumptions of the statistical models when applying them to real systems. The variations of $\Delta\overline{S}^{ex}$ with oxygen composition for the ternary

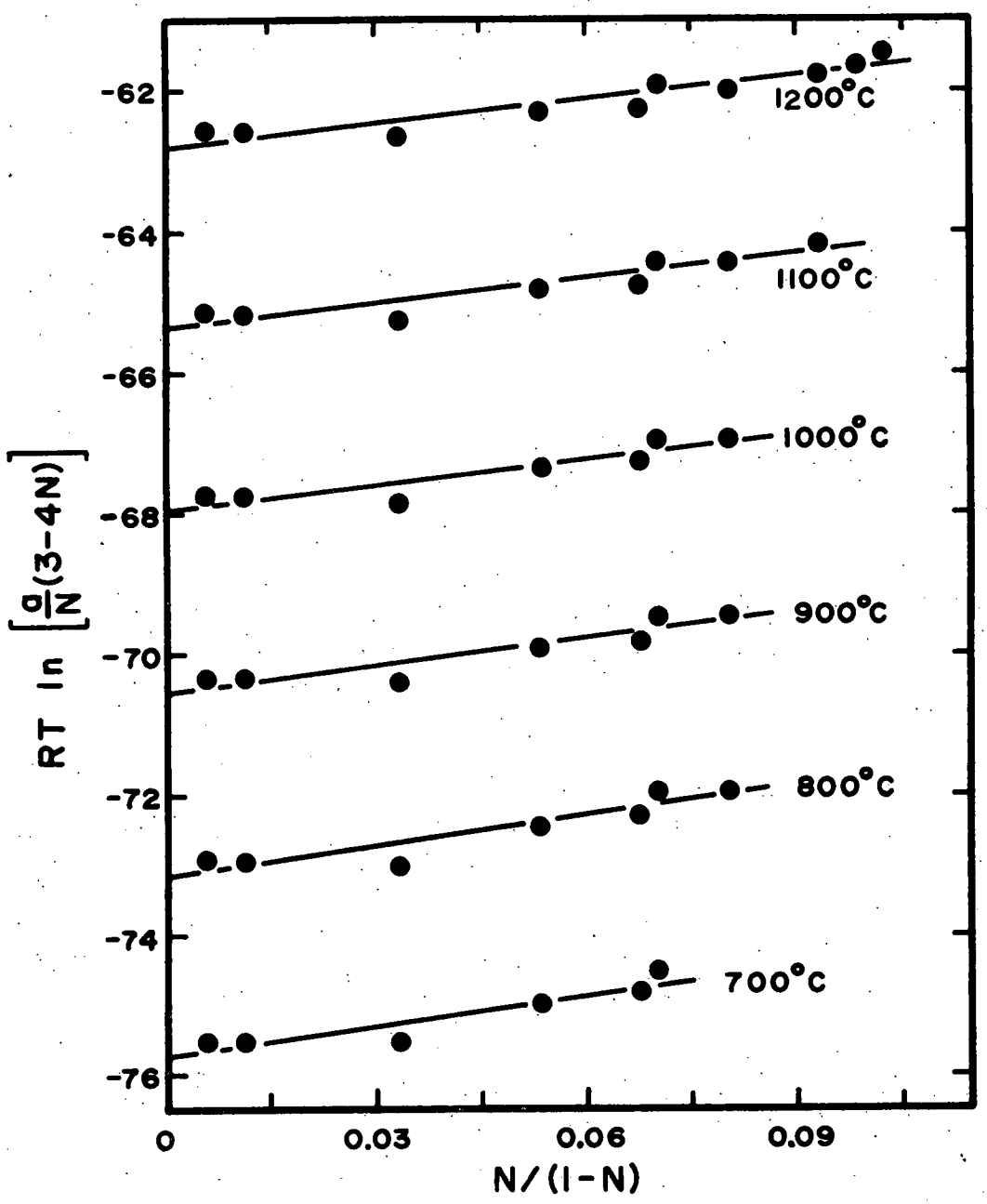

Figure 28: Application of equation (77) to the experimental data for the vanadium-oxygen system at the temperatures indicated in the figure.

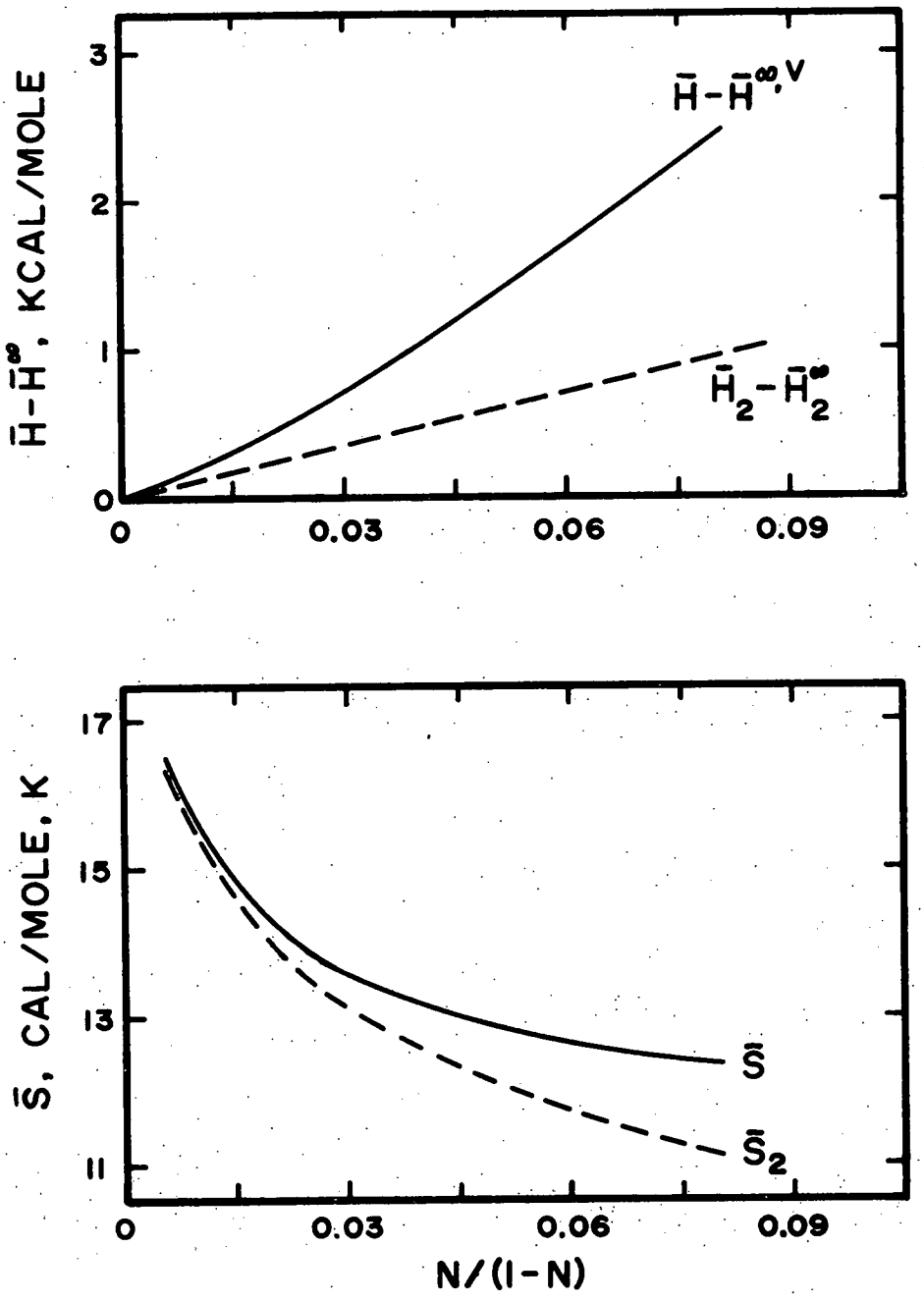

Figure 29: Comparison of the experimentally determined enthalpy and entropy (continuous lines) with those deduced from the plots in Figure 28 (dashed lines) for the vanadium-oxygen system at 1000°C.

alloys (Figure 27) clearly indicates that the model also can not apply to the Nb-V-O system.

4.1.2 Quasi-Athermal Model

If the assumption that the nonconfigurational entropy does not vary with interstitial composition is accepted, then for the V-O and Nb-V-O systems the configurational entropy can not be ideal. The positive deviations from Henry's law exhibited by these alloys at high oxygen contents are characteristic of repulsive interactions between the oxygen atoms. Consequently, it was felt that the concept of blocked sites, which results in a nonideal configurational entropy due to repulsive interactions, might describe the oxygen entropy in these solutions. However, Figure 30 demonstrates that this model is also incapable of describing the variation of the entropy with oxygen composition. The configurational entropy is plotted for the ideal interstitial solution and for three values of z" (equation (24)). The nonconfigurational entropy is the difference between these curves and the curve representing the absolute entropy of oxygen in vanadium at 1000°C (1273 K). As the number of blocked sites is increased the configurational entropy decreases with the magnitude of the decrease being greatest for high oxygen contents. The resulting nonconfigurational entropy varies with oxygen composition even more than that determined by assuming a random solution. Therefore, the blocked sites model also does not apply to the V-O system. By similar plots it has also been determined that this model does not apply to the ternary data.

4.1.3 Quasi-Chemical Model

The binary quasi-chemical model of McLellan and Dunn[65] can be tested by calculating the activity, $(P_{O_2})^{1/2}$, from equation (28) for various values

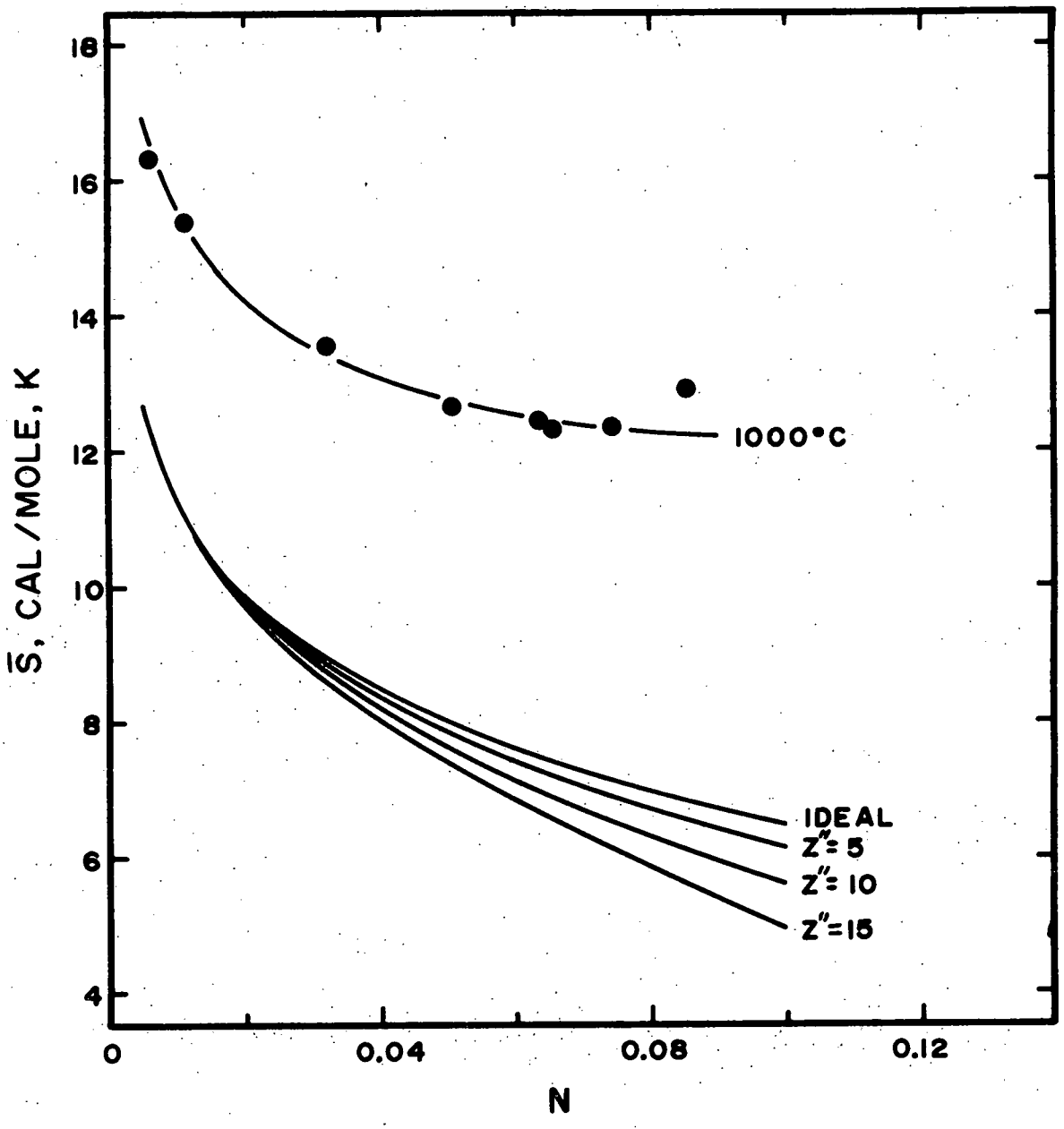

Figure 30: Comparison of the absolute oxygen entropy in vanadium at 1000°C with the ideal configurational entropy and the configurational entropy calculated assuming z" oxygen sites are blocked by each oxygen atom.

of E_{22} and oxygen composition and then comparing the calculated values to those for the V-O system. The values of $\Delta\bar{H}^{\infty}$ and $\Delta\bar{S}^{\infty}$ given in equation (28) were determined from the Henry's law region of the V-O system by plotting $(P_{O_2})^{1/2}$ versus N/(3-4N) at various temperatures. They are -101,120 cal/mole for $\Delta\bar{H}^{\infty}$ and -26.15 cal/mole, K for $\Delta\bar{S}^{\infty}$.* The coordination number for nearest neighbor interstitial sites is 4. The calculated values of $(P_{O_2})^{1/2}$ are presented in Figure 31 for several values of E_{22} at 1000°C (1273 K) and can be compared to the curve for the V-O system calculated from equations (67) and (68). The dashed line for E_{22} equals zero is an extension of the dilute solution Henry's law line. For high oxygen concentrations positive values of E_{22} (repulsive interactions) cause positive deviations from Henry's law and negative values cause negative deviations. E_{22} must be positive to describe the V-O activity curve. As E_{22} is increased the deviations from Henry's law are increased and the theoretical curve is seen to approach that for the oxygen activity in vanadium. However, values of E_{22} greater than around 10 kcal/mole do not result in further increases in the activity and the model is incapable of describing deviations from Henry's law as large as those for the V-O system. Values of E_{22} greater than 25 kcal/mole result in unrealistic activity values at low concentrations, but do not increase the activity at high concentrations above that for 10 kcal/mole.

The configurational entropy predicted by the model can be calculated using equation (26). The model assumes that the nonconfigurational entropy is invarient with composition. Therefore, a plot of the absolute oxygen entropy in vanadium minus $\bar{S}_2^c$ should not vary with oxygen concentration. Plots of $\bar{S} - \bar{S}_2^c$ for several values of E_{22} are shown in the lower portion of

*The values given previously of -100,720 cal/mole and -25.93 e.u. were approximated from equations (54) and (55). Thus the approximated values are seen to be quite accurate.

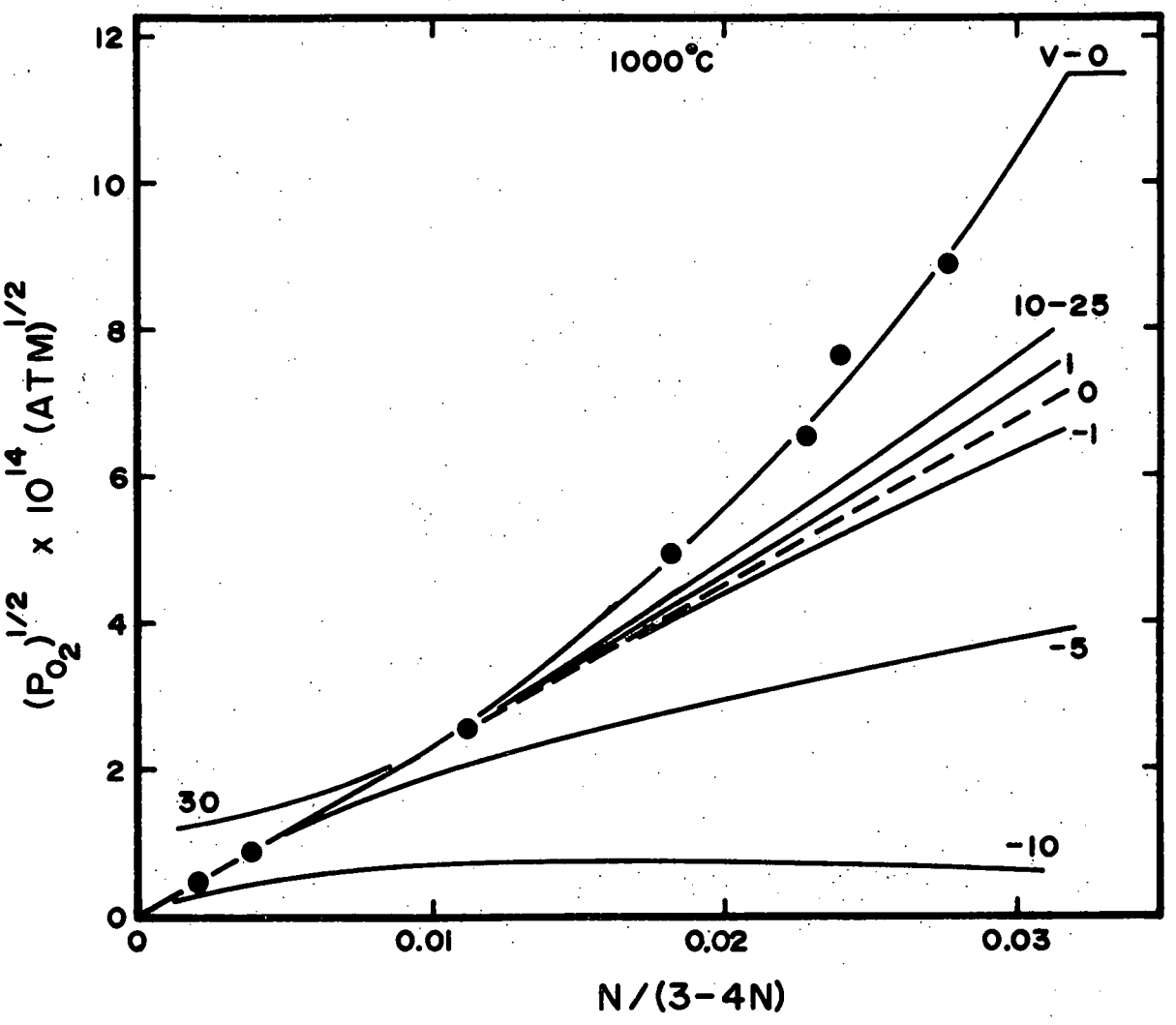

Figure 31: Comparison of the activity calculated by the quasi-chemical model for various values of the ineraction energy, E_{22}, with the oxygen activity in vanadium at 1000°C.

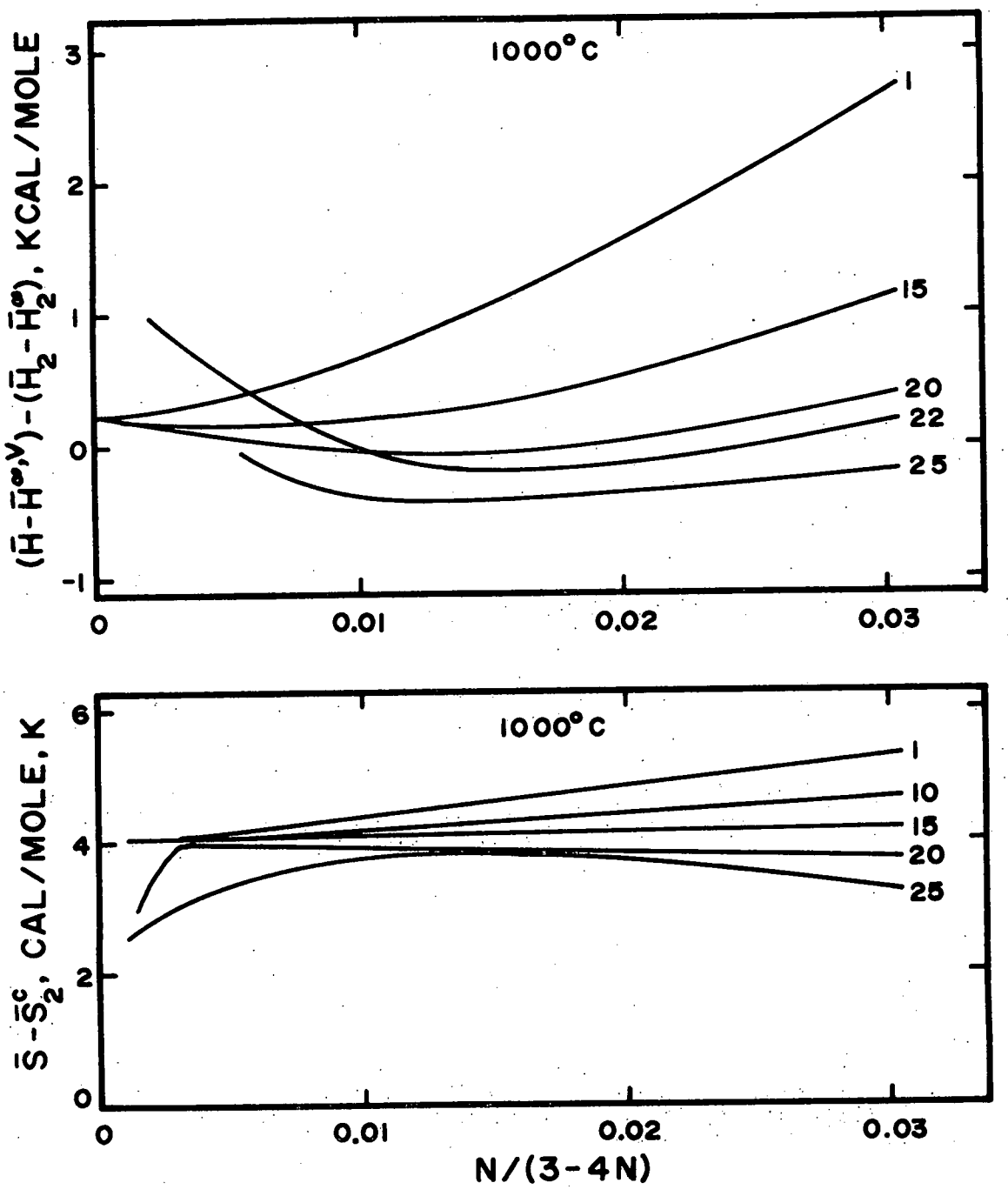

Figure 32: Comparison of the configurational entropy and enthalpy calculated by the quasi-chemical model for various values of the interaction energy, E_{22}, with the oxygen entropy and enthalpy in vanadium at 1000°C.

Figure 32 at 1000°C (1273 K). For E_{22} = 15 kcal/mole the nonconfigurational entropy is roughly 4.1 e.u. across the entire composition range. The nonconfigurational entropy at infinite oxygen dilution can be calculated from $\Delta\bar{S}^{\infty}$ and is 3.96 e.u. The model can therefore describe the configurational entropy of oxygen in vanadium assuming that the nonconfigurational entropy is constant. The enthalpy relative to infinite dilution is calculated by using equation (27). The enthalpy difference between oxygen in vanadium and that calculated by equation (27) is shown in the upper plots of Figure 32. These plots should be zero across the entire composition range for values of E_{22} which describe the oxygen enthalpy. A value of 20 kcal/mole describes the enthalpy variation fairly well. At 1200°C (1473 K) the variation of the entropy and enthalpy with oxygen composition was best described by the model by values of E_{22} equal to 20 and 24 kcal/mole, respectively. However, in order for the model to apply to the experimental results the same value of E_{22} should describe the configurational entropy and enthalpy. The inability of the model to describe these functions by the same E_{22} value results in the poor fit for the activity. The values of E_{22} used to describe the enthalpy and entropy composition variations are unrealistically high. For example, the model was found to describe the f.c.c. Fe-C system from 900-1400°C (1173-1673 K) with an E_{22} value of 1.97 kcal/mole.[67] The physical significance of the interaction energies used to describe the entropy and enthalpy is therefore regarded as questionable. It is, however, evident that repulsive interactions between oxygen atoms are quite high. This implies that second and possibly third nearest neighbor interactions, both of which are ignored by the model, may be significant. For the Fe-C system it was found that interactions outside the nearest neighbor shell could be ignored.[92,93] For octahedral sites in an f.c.c.

lattice there are 12 nearest neighbor interstitials to an interstitial at a distance of 0.707 times the lattice parameter, a_0. The 6 second nearest neighbors are at a distance of a_0 and have a metal atom situated directly between the two interstitials. For b.c.c. lattices the 4 nearest neighbors are separated from the interstitial by the distance $a_0/2$ and the second and third nearest neighbors, of which there 8 of each, are at the distances $0.707a_0$ and $0.866a_0$, respectively. Furthermore, no metal atoms are located directly between the oxygen atom and the first, second, or third neighbors. Thus, for b.c.c. lattices there are fewer nearest neighbors and the second and third nearest neighbors are much closer than for f.c.c. lattices. The second and third nearest neighbors are also not as effectively "screened" from the central interstitial by metal atoms as in an f.c.c. lattice. Therefore, it is suggested that the second and third nearest neighbor interactions would be more likely to influence the thermodynamic properties of the interstitial atoms in a b.c.c. lattice than in an f.c.c. lattice.

In order to assess the significance of the second nearest neighbor interactions it was assumed that these interactions are the same magnitude as the nearest neighbor interactions and that the third nearest neighbor interactions could be ignored. This is equivalent to regarding the second nearest neighbors as being 8 additional first nearest neighbors. Thus, the value of z in equations (26)-(28) was changed from 4 to 12. It was then found that the oxygen activity, enthalpy, and entropy at 700, 1000, and 1200°C (973, 1273, & 1473 K) could be described by the quasi-chemical model with the oxygen-oxygen interaction energies given in Table VIII. Also given in the table are E_{22} values for z = 20. This value of z is the result of assuming that the third nearest neighbors have the same interaction energy as the first and second nearest neighbors. The E_{22} values given in

TABLE VIII

Oxygen-Oxygen Interaction Energies

	E_{22}, kcal/mole	
T, K	z = 12	z = 20
973	6.75	4.20
1273	7.20	4.30
1473	7.50	4.25

the table are those which gave the best simultaneous fit with the experimental enthalpy and entropy oxygen concentration variations. They are only approximate since no elaborate curve fitting techniques were employed. The calculated enthalpy and entropy for z = 12, using the interaction energies given in Table VIII, are compared with the experimental values in Figure 33. The continuous lines represent the calculated quantities and the points are the experimental values determined directly from the slope and intercept of the EMF curves. The calculated absolute entropy curves were determined by the addition of $\overline{S}_2^c$, calculated from equation (26), and $\overline{S}^{ex}$, determined from the experimental value of $\Delta\overline{S}^{\infty}$. The lower curve for the absolute entropy at 700°C (973 K) is the sum of the ideal configurational entropy and $\overline{S}^{ex}$. Comparison of the two entropy curves for 700°C (973 K) indicates that the model predicts a configurational entropy somewhat higher than that for an ideal solution. The maximum possible configurational entropy is that for an ideal solution. Therefore, the configurational entropies calculated by the model are somewhat too high. Since the calculated entropies fit the experimental data, the error must be in the assumption that the non-configurational entropy does not vary with oxygen concentration. $\overline{S}^{ex}$ should increase as the oxygen concentration is increased in order to explain the experimental entropy variation. An alternate explanation

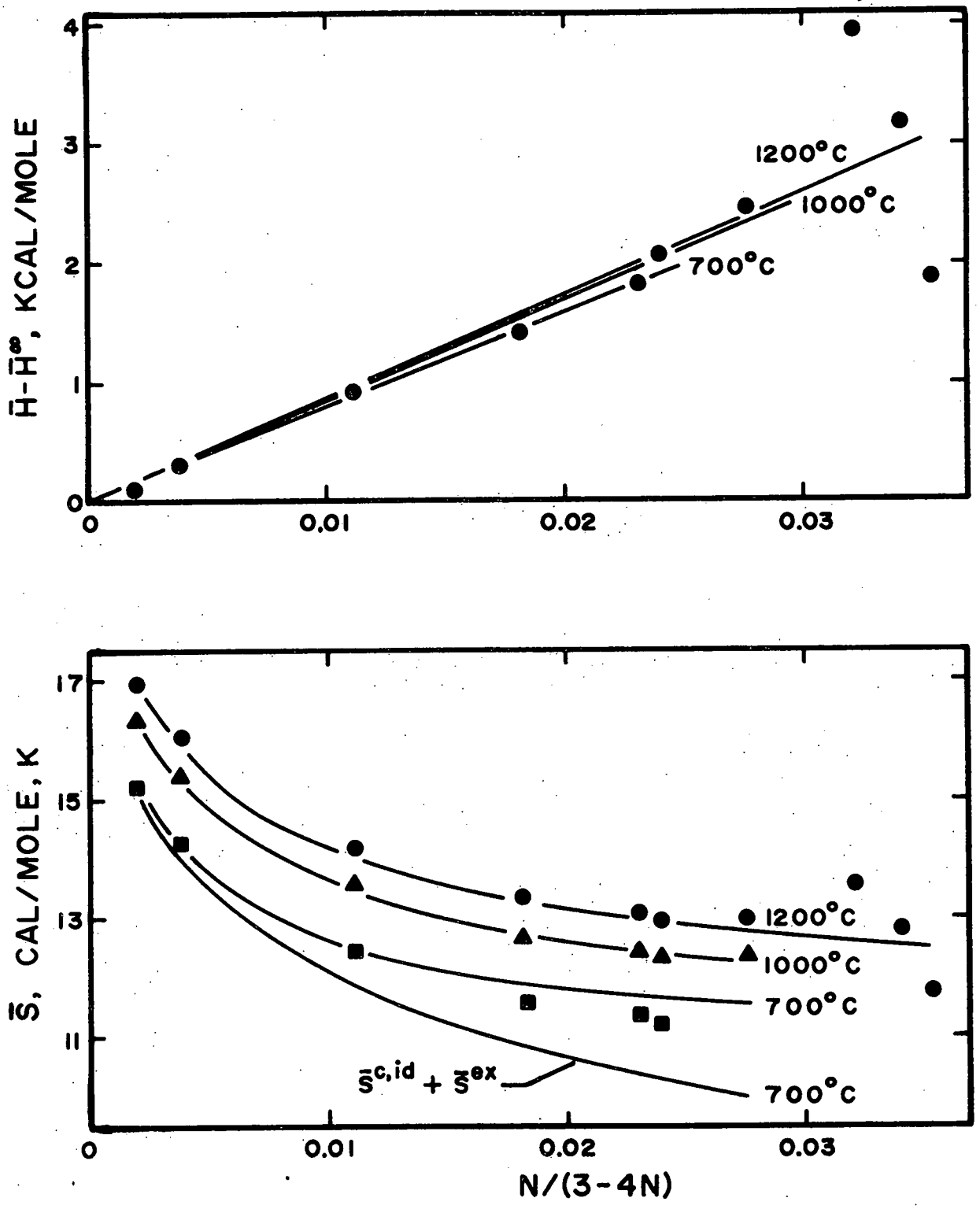

Figure 33: Comparison of the absolute entropy and enthalpy calculated by the quasi-chemical model for z = 12 (solid lines) with the absolute entropy and enthalpy of oxygen in vanadium at 700, 1000, and 1200°C (data points). The lower entropy line at 700°C represents the calculated absolute entropy for an ideal configurational entropy.

would be that at the higher oxygen concentrations some of the oxygen atoms occupy the tetrahedral interstices. This would allow for a higher configurational entropy at the higher concentrations than that given by the ideal solution curve. Despite this error in the model's description of the configurational entropy, the good fit of the model to the data is considered to be significant since the magnitude of the error is relatively small and the error does no affect the enthalpy.

The curves for the activity calculated using the interaction energies in Table VIII are plotted in Figures 34 and 35 and are compared to the experimental oxygen activity (data points.) Also included in these figures are the maximum allowable activities by the model for z = 4 ($E_{22} \geq 10$ kcal per mole). At 700°C (973 K) the curve for z = 20 best fit the experimental activity, while at 1000 and 1200°C (1273 & 1473 K) the curves for z = 12 gave the best match with the data. For all three temperatures the curve for z = 4 gave the poorest fit. Although the assumption that the second and third nearest neighbor oxygen atoms interact with the same energy as the first nearest neighbors may be somewhat in error, it is concluded that the second and possibly third nearest neighbor interactions are of sufficient magnitude to significantly affect the oxygen activity. This may be a result of the geometry of the b.c.c. lattice or it could be an inherent property of oxygen in solution. Second nearest neighbor interactions have also been found to be significant in the hexagonal lattice of Ti-O solid solutions.[94]

It should also be noted that the interaction energies in Table VIII for z = 12 have a notable temperature dependence. This implies that E_{22} is in reality a free energy and is temperature dependent due to a $T\Delta S$ term. This term would result if the vibrational entropies of two isolated oxygen atoms differ from those for two neighboring oxygen atoms.

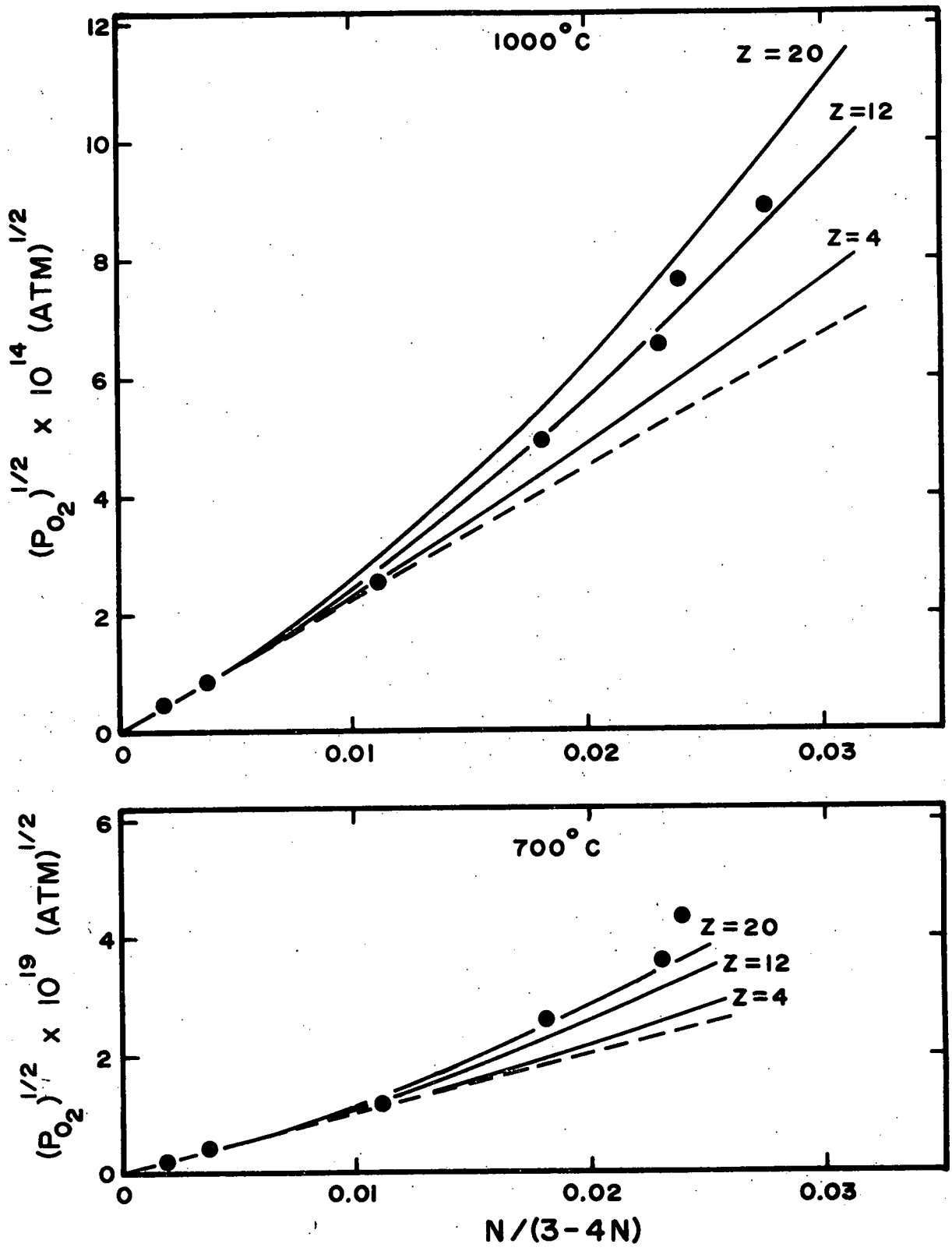

Figure 34: Comparison of the activity calculated by the quasi-chemical model for z = 4, 12, and 20 with the oxygen activity in vanadium at 700 and 1000°C.

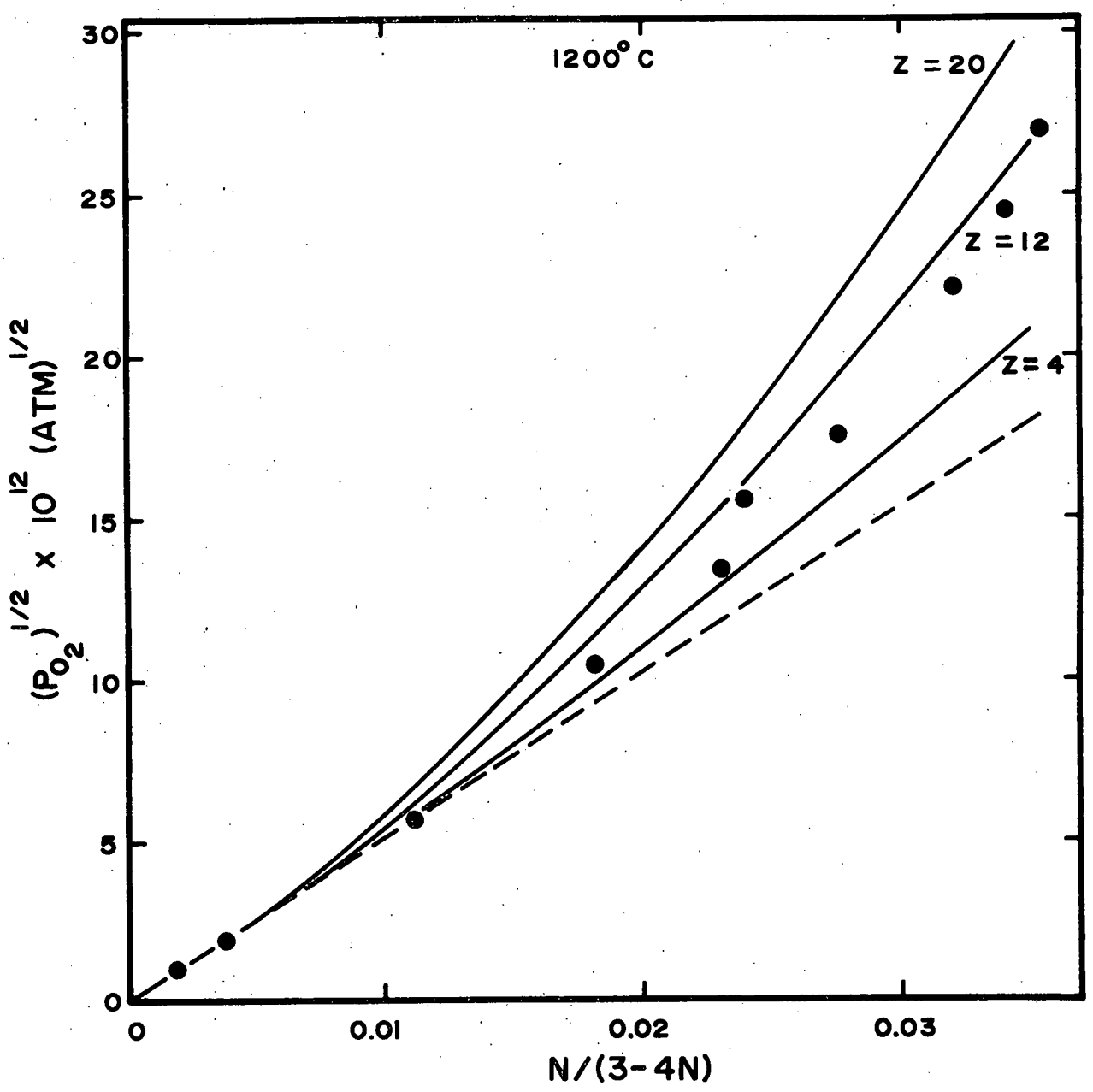

Figure 35: Comparison of the activity calculated by the quasi-chemical model for z = 4, 12, and 20 with the oxygen activity in vanadium at 1200°C.

4.1.4 Central Atoms Model

The central atoms model was tested by calculating the activity using equation (29) and the values of $\Delta\bar{H}^{\infty}$ and $\Delta\bar{S}^{\infty}$ given in the previous section. For repulsive interactions between oxygen atoms $\Delta g_2^{(2)}$ is positive. For values of $\Delta g_2^{(2)}$ greater than approximately 3 equation (29) reduces to

$$\ln a_{2,B} = \ln y_2 + \Delta\bar{H}_2^{\infty}/RT - \Delta\bar{S}_2^{\infty}/R - 2z \ln (1-y_2). \qquad (78)$$

Thus, for $\Delta g_2^{(2)} \geq 3$ the activity no longer depends upon $\Delta g_2^{(2)}$. The maximum deviation from Henry's law accounted for by the model is that given by this equation. Figure 36 shows plots of the activity calculated from equation (78) with z = 4 relative to that for oxygen in vanadium at 700 and 1000°C (973 & 1273 K). As was the case for the quasi-chemical model, the central atoms model could not account for the large deviations from Henry's law when only nearest neighbor oxygen interactions were considered. However, the model was found to describe the experimental data quite well when the second nearest neighbors were included. This is shown by the curves in the figure for z = 12. The values of $\Delta g_2^{(2)}$ which best fit the activity data at 700, 1000, and 1200°C (973, 1273, & 1473 K) were 1.70, 0.65, and 0.45, respectively. Thus, it may also be concluded from the central atoms model that oxygen atom interactions outside the nearest neighbor shell must be taken into consideration in order to describe the oxygen activity.

The temperature dependence of $\Delta g_2^{(2)}$ would appear to be the opposite of that for the interaction energies of the quasi-chemical model for z = 12 given in Table VIII. However, $\Delta g_2^{(2)}$ is a unitless quantity, whereas E_{22} has the units cal/mole. Therefore, when comparisons between $\Delta g_2^{(2)}$ and E_{22} are made, E_{22} must be divided by RT. When this is done $\Delta g_2^{(2)}$ and E_{22} both decrease as the temperature is increased. Thus, the two treatments are qualitatively consistent.

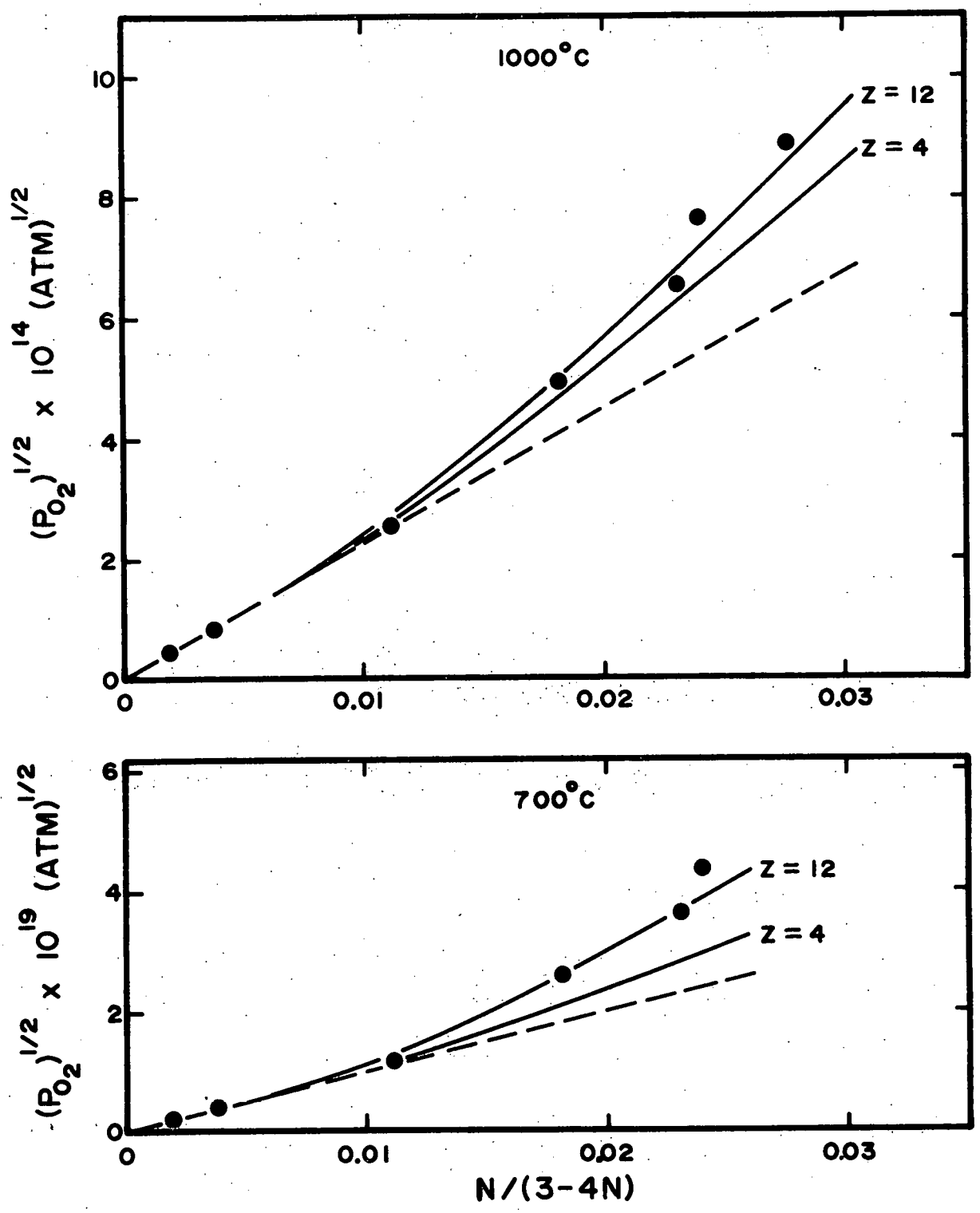

Figure 36: Comparison of the activity calculated by the central atoms model for z = 4 and 12 with the oxygen activity in vanadium at 700 and 1000°C.

The quasi-chemical and central atoms models can also be applied to ternary systems. Unfortunately, the ternary treatments are not believed to be applicable to the Nb-V-O system. Small additions of V to Nb-rich alloys caused decreases in the oxygen enthalpy, entropy, and activity too large to be described by these models. For V-rich alloys the decreases in the thermodynamic properties when Nb was added were small enough to be accounted for by the models, but their application to these alloys would indicate that the bonding between Nb & O is stronger than that between V & O. These decreases in the oxygen activity are believed to be due to volume effects rather than bond energy differences. Therefore, bond energies deduced from the ternary models would not be considered relevant and no attempt was made to fit the data for the V-rich alloys to these models.

4.2 Vanadium-Oxygen System

For dilute solutions, $X \leq 3.2$ at. % oxygen, our results agree very well with the electrochemical results of Fromm and Kirchheim.[21] For more concentrated solutions our oxygen activities show positive deviations from Henry's law while Fromm and Kirchheim indicate that Henry's law is obeyed up to the terminal solubility limit. The two studies gave similar values for the solubility, but the activity of oxygen at that composition was higher for our results. This difference in the activity arises from our higher values of the EMF of cell I than for Fromm and Kirchheim's results. The difference is approximately 30 mV at any given temperature for single phase electrodes containing less that about 3 at. % oxygen. The difference diminishes as the single phase electrodes become more concentrated, in accord with the fact that the studies indicate similar maximum solubilities. One possible explanation for these discrepancies in the reported oxygen activity might be that the two stocks of vanadium had different impurity contents. But this seems

unlikely since the two studies found similar oxygen activities for dilute solutions, for which the effect of impurities on the activity would be expected to be the greatest. To further elucidate solute effects, experiments performed on higher purity vanadium gave substantially the same results as reported above.* The EMF for cell I using the higher purity vanadium with a single phase electrode containing 1.01 at. % oxygen was within 3 mV of the calculated values of E° for the lower purity vanadium, regardless of the temperature. Experiments for cell II using the higher purity vanadium resulted in values of $\Delta\overline{H}^{\circ}$ and $\Delta\overline{S}^{\circ}$ within the reported precision of the values given earlier. Therefore, it seems unlikely that the differences between our results and those of Fromm and Kirchheim are due to the purity of the vanadium and the discrepancies are left unexplained.

It is interesting to compare the solubility of oxygen in vanadium with the solubilities in the other cubic metals. Figure 37 indicates that of the group V metals vanadium has a considerably higher solubility for oxygen than do niobium[3] and tantalum.[4] A brief sampling of the literature[95-100] indicates that for many cubic metal-oxygen systems the solid solubilities range downward from 200 atomic ppm. Group IV metals (Ti, Zr, and Hf), however, can contain several atomic percent of oxygen in the high temperature, cubic phases.[101-103] The group V metals, and in particular vanadium, are very desirable for studies of interstitial solute behavior, since a broad range of composition may be investigated down to relatively low temperatures. This has been demonstrated by the application of the interstitial solution models to the oxygen activity data. The importance of considering oxygen-oxygen interactions outside the nearest neighbor shell could not have been determined were it not for the high oxygen solubility in vanadium.

*The higher purity vanadium was from the same stock as that used for the ternary study. See Table I.

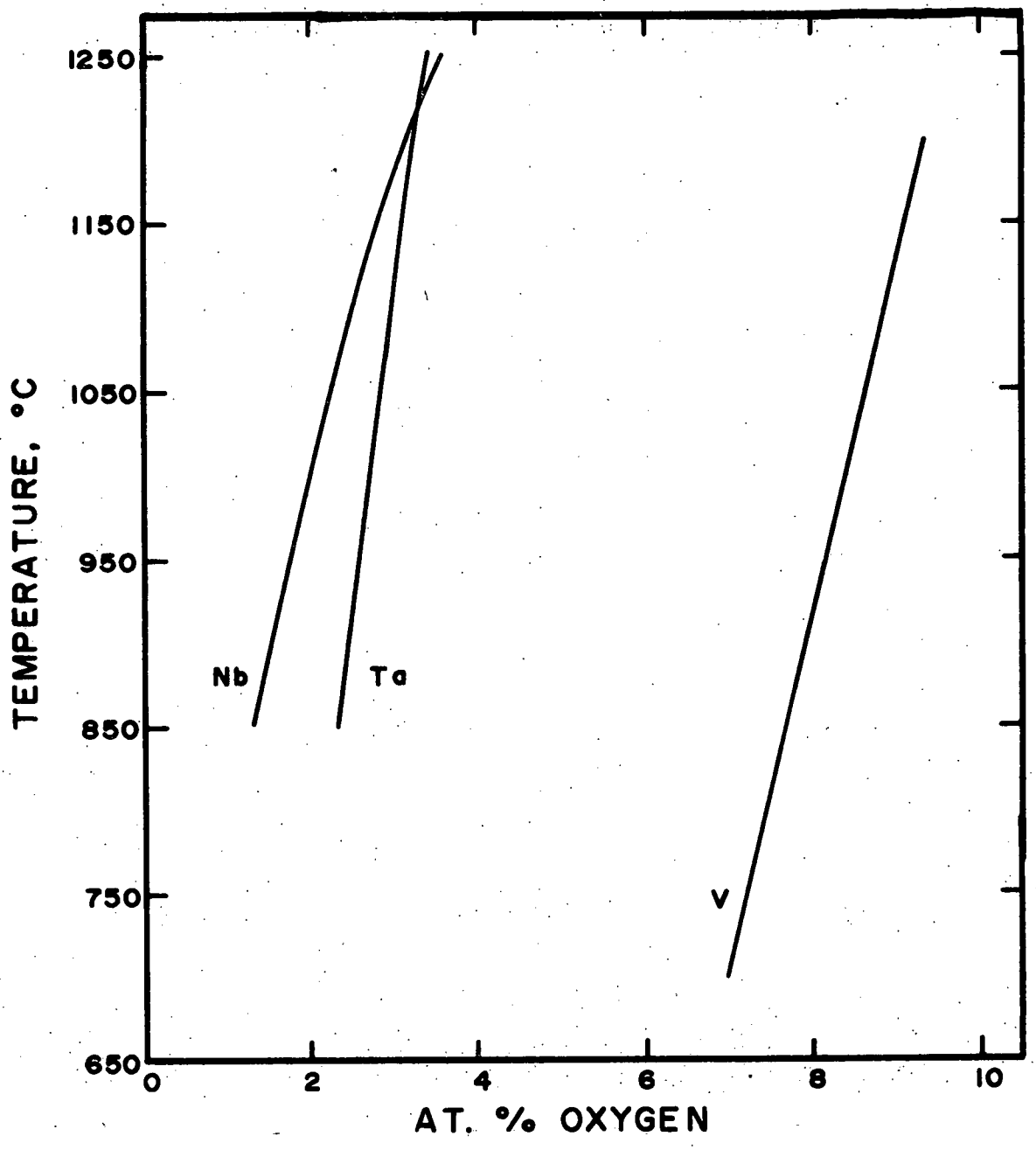

Figure 37: Oxygen solubility in the group V metals.

From a practical standpoint the strong chemical affinity of vanadium for oxygen has implications for its use as a structural material and its degradation in oxygen-containing environments. There is a lower equilibrium oxygen pressure for the V-O terminal solid solution in spite of the fact that it contains roughly a factor of ten greater amount of oxygen than do Nb or Ta at saturation. For example, at 1000°C (1273 K) the equilibrium oxygen partial pressures for the Nb-O, Ta-O, and V-O saturated solutions are 1.13×10^{-20}, 2.99×10^{-20}, and 1.34×10^{-21} Pa., respectively, while the solubilities are 0.24, 0.35, and 2.8 %, respectively, on a weight basis. This means that when comparing vanadium and niobium as possible nuclear reactor materials, tha vanadium must be much better protected from an oxygen-containing environment than niobium--it is a better getter. If, however, only a limited amount of oxygen is available, vanadium could absorb it better than niobium without oxide precipitation at a given temperature.

4.3 Niobium-Vanadium-Oxygen System

The oxygen activity results for the Nb-V-O system are reviewed in Figure 38. The logarithm of the oxygen activity coefficient is plotted as a function of the vanadium content for three different oxygen concentrations and two temperatures. For those alloys in which oxide precipitation was observed the activity coefficient is indicated at the estimated solubility limit. When the temperature was increased from 700 to 1150°C (950 to 1423 K) the effect of the alloying element was diminished. This is evidenced by the observation that the decreases in the activity coefficient plots relative to the binaries were less severe at the higher temperature. The deviations from Henry's law were also diminished at the higher temperature. Solutions are expected to become more random as the temperature is increased. Therefore, these results are not surprising. In view of the fact that vanadium

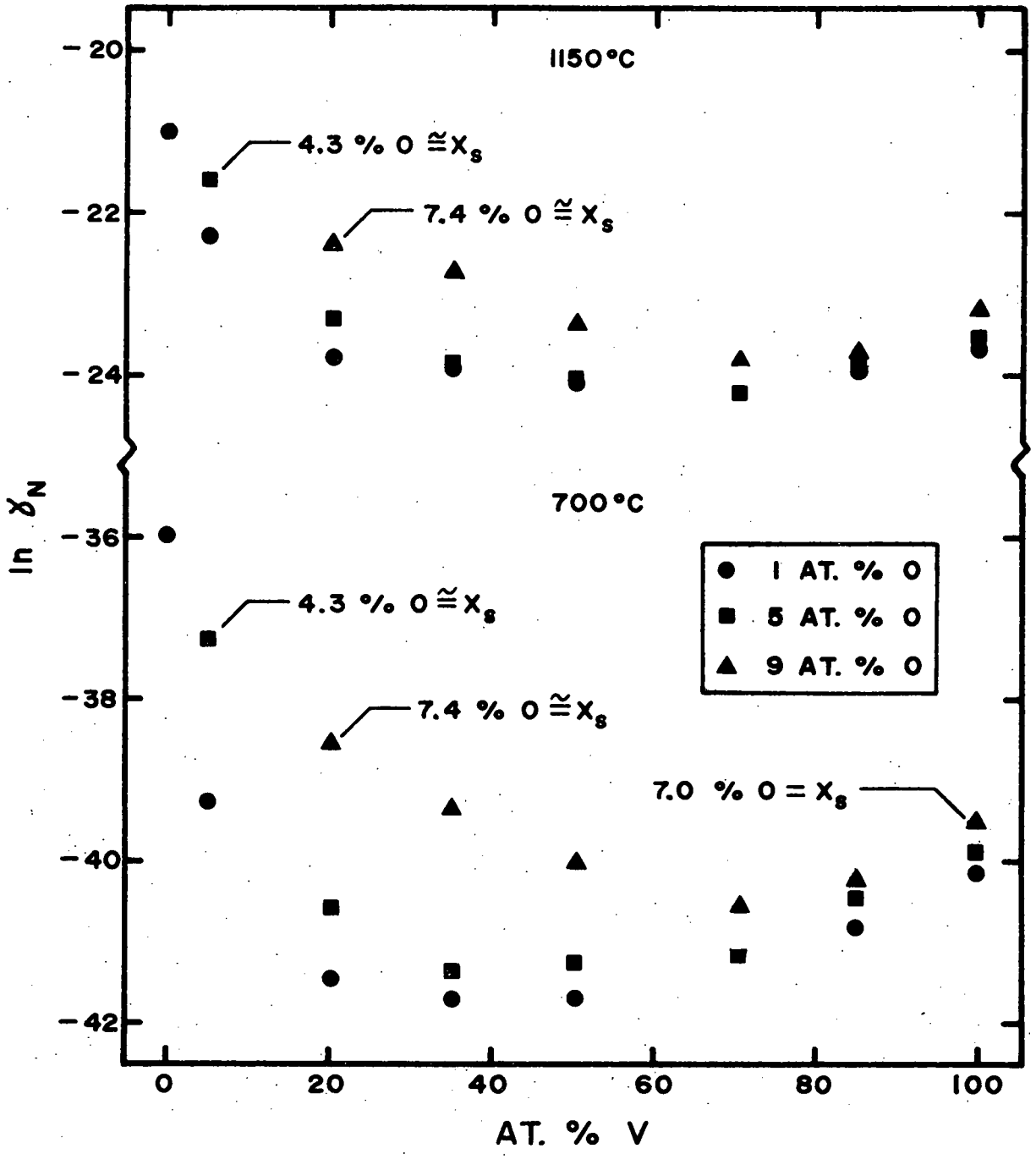

Figure 38: Temperature and vanadium concentration dependence of the oxygen activity coefficient at the oxygen concentrations indicated.

has a somewhat stronger interaction with oxygen than does niobium, the decreases in the activity coefficient in the Nb-rich alloys was also as anticipated. However, the magnitude of the effect was somewhat larger than one might expect, particularly for dilute oxygen solutions in the 20.3 and 35.1 at. % V alloys. The extremely large deviations from Henry's law were also unexpected. For the Nb-rich alloys it is assumed that the oxygen atoms are preferentially attracted to the V atoms. This is supported by the substantial decreases in $\overline{S}^{xs}$ and $\overline{H}^{xs}$ for dilute oxygen compositions in the 5.1 % V alloy as compared to the Nb-O binary (Figure 16). If the oxygen atoms continue to order around the vanadium atoms as more oxygen is added to the solution, significant interactions between the oxygen atoms might result. This would cause the observed large deviations from Henry's law. The slope changes in the EMF curves for the 5.1 % V alloy having 0.29, 0.75, and 2.01 at. % O in solution (Figure 15) and the 20.3 % V alloy having 4.83 and 7.17 at. % O (Figure 14) also suggested ordering of the oxygen. The slope changes indicated that the oxygen entropy is lower at the lower temperatures, implying a more ordered system at these temperatures. However, TEM results indicated solid solution structures over both temperature regions in these alloys. Any ordering must therefore be very localized.

Zirconium and Hafnium additions to Nb have been reported to severely limit the solubility of oxygen in Nb by the formation of ZrO_2 and HfO_2.[27-30] Vanadium might be expected to have the same effect. However, the results have shown that V additions actually increased the oxygen solubility. At 1000°C (1273 K) the oxygen solubility was increased from 2.0 % in Nb to around 4.2 % in the 5.1 % V alloy and to around 7.3 % in the 20.3 % V alloy. Furthermore, the oxide phase was noted to be isostructural with NbO and had the same Nb/V ratio as the matrix. It has been pointed out that the oxide

phase may not be at equilibrium due to the slow redistribution of Nb and V at the temperatures of this study. Thus, although the equilibrium Nb/V ratio may be somewhat different than that of the oxides observed, it is suggested that the oxide is a Nb-rich phase. The increased oxygen solubility limit for the Nb-rich alloys may then be attributed to the decreased activity of the oxygen at infinite dilution due to the vanadium additions. Titanium has been reported to increase the solubility of oxygen in niobium for the same reason.[104] Alternately, the increased solubility in the ternary alloys may be attributed to the oxides phases. The oxide phases which are in equilibrium with the terminal solid solution in the two binaries might be expected to have quite different properties in the ternary system. As mentioned previously, NbO has a cubic NaCl type structure with three molecules per unit cell. Furthermore, NbO is a stoichiometric compound, while the body-centered-tetragonal β phase of the vanadium-oxygen system is an intermediate phase of fairly broad composition range. The vanadium-rich solvus of the β phase is temperature dependent, therefore, the composition of the β phase in equilibrium with the α phase varies with temperature. Thus, the oxide phases present in the respective binaries are quite different from each other and would be expected to have very limited solubility in one another. The presence of vanadium in NbO might increase the free energy of formation of the oxide phase. The same might be said of niobium in the β phase. Increasing the formation energy of the oxide phase would have the observed effect of increasing the oxygen solubility. The fact that the only oxide phase noted in the ternary system was Nb-rich suggests that the formation of the β phase may be suppressed in the ternary system. Although the β phase has a lower free energy of formation than NbO in the binary systems, the opposite may be the case in the ternaries.

The results in Figure 38 for the V-rich alloys indicate that Nb decreased the oxygen activity below that for the V-O system. Furthermore, the deviations from Henry's law were smaller for the 85.2 and 70.7 % V alloys than for the binary system. The negative values for the Wagner interaction coefficients indicate that the Nb decreased both the enthalpy and entropy of the oxygen in solution. All of these factors were somewhat surprising since, in the binaries, Nb does not react with oxygen as strongly as does vanadium. Ofcourse, this reasoning can be overemphasized since the activity of oxygen in niobium is also very low. Nevertheless, this type of behavior is atypical of that demonstrated by numerous systems. For example, in Fe-X-C systems the substitutional elements Co, V, Cr, Mn, Ni, and Si all influence the carbon activity as anticipated from a consideration of the Fe-C and X-C binaries.[40-50] Furthermore, it has been shown that for the Nb-Ta-O system the entropy and enthalpy interaction coefficients are constant across the entire range of the Nb/Ta ratios.[105] With the exception of Si and V in Fe, all the substitutional elements in these alloys have atomic radii within 2.5 % of that of the solvent.* In the alloys of this investigation Nb has an atomic radius approximately 8 % larger than that of V. Similar misfit occurs in the Ta-Mo system. Diffuse x-ray scattering has shown that these alloys form short range ordered solid solutions.[106] Preliminary measurements have indicated that ordering also occurs in the Nb-V system with the maximum ordering occuring around 40 at. % vanadium.[107] In contrast to the Nb-V alloys, Nb-Ta alloys are believed to be completely random.[106] The high degree of misfit and resulting ordering on the Nb-V lattice could therefore be responsible for the unexpected behavior of oxygen in the V-rich alloys. It is interesting to note that the minimum excess enthalpy (Figure 16) and the minimum activity in dilute

*The atomic radii were determined from the lattice parameters of the pure elements.

oxygen solutions (Figure 38) both occur near the Nb/V ratio of maximum ordering. If it is assumed that the oxygen is preferentially attracted to V, then the oxygen might also exhibit short range ordering. The thermodynamic properties would then be quite different from those expected from the binary metal-oxygen systems. Even if the oxygen is not ordered, the misfit on the Nb-V lattice could cause the variations noted due to the strain energy effects noted earlier. It should also be noted that the interstitial solution models can not be expected to apply for such a system due to the large volume changes.

Klueh and Devan[39] reported that Nb increases the activity of oxygen in vanadium at 600°C (873 K), which contradicts the results of this study. However, their alloys also contained several percent of Zr and Fe and substantial quantities of C and N and the effect of Nb could not be completely isolated from those of the other elements present. Therefore, this contradiction is not considered to be significant.

5. CONCLUSIONS

1. Oxygen in solution in vanadium obeys Henry's law for concentrations less than approximately 3.2 at. %. For higher oxygen concentrations there are positive deviations from Henry's law.

2. The positive deviations from Henry's law of the oxygen activity in vanadium are believed to be due to repulsive interactions of several kcal/mole between first and second and possibly third nearest neighbor oxygen atoms.

3. The vibrational entropies of neighboring oxygen atoms are believed to differ from those of isolated oxygen atoms in vanadium.

4. The oxygen solubility in vanadium varies approximately linearly with temperature from 7.0 at. % at 700°C (973 K) to 9.3 at. % at 1200°C (1473 K).

5. Oxygen obeys Henry's law in solution in Nb-V alloys for oxygen concentrations less than approximately 2 at. %. For V-rich alloys within the Henry's law region the oxygen partial pressure can be determined as a function of the niobium and oxygen concentrations and temperature by the relation,

$$P_{O_2} = N_O^2 \times 10^5 \exp -\frac{2}{R}(-23.66 - 7.31N_{Nb}) \exp \frac{2}{RT}(-100,860 - 12,180N_{Nb}) \text{ Pa.},$$

for $N_{Nb} \leq 0.65$.

6. Niobium decreases the activity of oxygen in vanadium and decreases the magnitude of the deviations from Henry's law for $N_{Nb} \leq 0.7$. These effects are believed to be due to the size difference between Nb & V atoms.

7. Vanadium causes large decreases in the activity of oxygen in niobium and causes substantial deviations from Henry's law. These effects are primarily attributed to the stronger bonding between V & O than between Nb & O.

8. Vanadium increases the oxygen solubility in Nb-rich alloys and niobium increases the oxygen solubility in V-rich alloys.

LIST OF REFERENCES

1. E. deLamotte, Y. C. Huang, and C. J. Altstetter, Air Force Materials Laboratory Report ML-TDR-64-134 (1964).

2. E. deLamotte, Y. C. Huang, and C. J. Altstetter, Refractory Metals and Alloys IV, Gordon and Breach Science Publications, Metallurgical Society Conference 41, N. Y., 283 (1967).

3. W. Nickerson and C. Altstetter, Scripta Met. 7, 229 (1973).

4. W. Nickerson and C. Altstetter, Scripta Met. 7, 377 (1973).

5. W. Nickerson, Ph.D. Thesis, University of Illinois (1973).

6. D. Potter and C. Altstetter, Acta Met. 19, 881 (1971).

7. D. M. Shah, Ph.D. Thesis, University of Illinois (1975).

8. K. Kiukkola and C. Wagner, J. Electrochem. Soc. 104, 379 (1957).

9. K. Kiukkola and C. Wagner, J. Electrochem. Soc. 104, 308 (1957).

10. T. H. Etsell and S. N. Flengas, Chem. Rev. 70, 339 (1970).

11. J. W. Patterson, E. C. Bogren, and R. A. Rapp, J. Electrochem. Soc. 114, 752 (1967).

12. A. V. Ramana Rao and V. B. Tare, Scripta Met. 5, 813 (1971).

13. R. A. Rapp, Thermodynamics of Nuclear Materials, IAEC, Vienna, 75 (1967).

14. C. B. Alcock and B. C. H. Steele, Science of Ceramics, The British Ceramic Society, v. II, 397 (1965).

15. B. C. H. Steele and C. B. Alcock, Trans. Met. Soc. AIME 233, 1359 (1965).

16. A. U. Seybolt and H. T. Sumsion, Trans. AIME 197, 292 (1953).

17. W. Rostoker and A. S. Yamamoto, Trans. Amer. Soc. Metals 47, 1002 (1955).

18. J. L. Henry, S. A. O'Hare, R. A. McCune, and M. P. Krug, J. Less-Common Metals 21, 115 (1970).

19. D. G. Alexander and O. N. Carlson, Met. Trans. 2, 2805 (1971).

20. D. L. Smith, J. Less-Common Metals 31, 345 (1973).

21. E. Fromm and R. Kirchheim, J. Less-Common Metals 26, 403 (1972).

22. J. Stringer, J. Less-Common Metals 8, 1 (1965).

23. W. Rostoker and A. Yamamoto, Trans. Amer. Soc. Metals 46, 1136 (1954).

24. H. A. Wilhelm, O. N. Carlson, and J. M. Dickinson, Trans. AIME 200, 915 (1954).

25. D. O. Hobson, ORNL-3212, Oak Ridge National Laboratory (1963).

26. B. R. Rajala and R. J. Van Thyne, High Temperature Materials Conference (1962).

27. A. C. Barber and P. H. Morton, High Temperature Refractory Metals, Gordon and Breach Science Publications, N. Y. 391 (1966).

28. V. C. Marcotte and W. L. Larson, J. Less-Common Metals 10, 229 (1966).

29. A. K. Shurin and V. A. Loktinov, Russian Metallurgy No. 1, 158 (1970).

30. A. K. Shurin and V. A. Loktinov, Russian Metallurgy No. 3, 33 (1970).

31. P. M. Bunn, D. G. Cummings, and H. W. Leavenworth, Jr., J. Appl.Phys. 33, 3009 (1962).

32. D. Mosher, C. Dollins, and C. Wert, Acta Met. 18, 797 (1970).

33. A. Taylor and N. J. Doyle, J. Less-Common Metals 13, 331 (1967).

34. A. Taylor and N. J. Doyle, J. Less-Common Metals 13, 331 (1967).

35. A. Taylor and N. J. Doyle, J. Less-Common Metals 13, 338 (1967).

36. G. Horz and E. Steinheil, J. Less-Common Metals 21, 84 (1970).

37. G. Horz and E. Steinheil, J. Less-Common Metals 27, 243 (1972).

38. R. L. Klueh and J. H. Devan, J. Less-Common Metals 30, 9 (1973).

39. R. L. Klueh and J. H. Devan, J. Less-Common Metals 30, 25 (1973).

40. C. Bodsworth, I. M. Davidson, and D. Atkinson, Trans. Met. Soc. AIME 242, 1135 (1968).

41. P. Chraska and R. B. McLellan, Acta Met. 19, 1219 (1971).

42. T. Wada, H. Wada, J. T. Elliott, and J. Chipman, Met. Trans. 3, 1657 (1972).

43. J. Chipman and E. F. Brush, Trans. Met. Soc. AIME 242, 35 (1968).

44. R. P. Smith, J. Amer. Chem. Soc. 70, 2724 (1948).

45. R. P. Smith, Trans. Met. Soc. AIME 218, 62 (1960).

46. R. P. Smith, Trans. Met. Soc. AIME 233, 397 (1965).

47. A. J. Heckler and P. G. Winchell, Trans. Met. Soc. AIME 227, 732 (1963).

48. L. C. Brown and J. S. Kirkaldy, Trans. Met. Soc. AIME 227, 1461 (1963).

49. R. J. Brigham and J. S. Kirkaldy, Trans. Met. Soc. AIME 227, 538 (1963).

50. R. P. Zupp and D. A. Stevenson, Trans. Met. Soc. AIME 236, 1316 (1966).

51. R. B. McLellan, Mater. Sci. Eng. 9, 121 (1972).

52. M. L. Kapoor, Inter. Met. Revs. 20, 150 (1975).

53. J. H. Hildebrand, J. Amer. Chem. Soc. 59, 66 (1929).

54. R. B. McLellan, in P. S. Rudman, J. Stringer, and R. I. Jaffe, Phase Stability in Metals and Alloys, McGraw-Hill, N. Y., 393 (1967).

55. R. B. McLellan, Trans. Met. Soc. AIME 230, 1468 (1964).

56. R. B. McLellan and P. Chraska, Mater. Sci. Eng. 6, 176 (1970).

57. J. S. Kirkaldy and G. R. Purdy, Can. J. Phys. 40, 202 (1962).

58. M. Hoch, Trans. Met. Soc. AIME 230, 138 (1964).

59. J. Chipman, Trans. Met. Soc. AIME 239, 1332 (1967).

60. D. R. Poirier, Trans. Met. Soc. AIME 242, 685 (1968).

61. R. A. Oriani and C. B. Alcock, Trans. Met. Soc. AIME 224, 1104 (1962).

62. R. Speiser and J. W. Spretnak, Trans. ASM 47, 493 (1955).

63. L. Kaufman, S. V. Radcliffe, and M. Cohen, in V. F. Zackay and H. I. Aaronson (eds.), Decomposition of Austenite by Diffusion-Controlled Processes, Interscience, N. Y., 313 (1962).

64. E. A. Guggenheim, Thermodynamics, North Holland Publishing Co. (1959).

65. R. B. McLellan and W. W. Dunn, J. Phys. Chem. Solids 30, 2631 (1970).

66. R. B. McLellan and W. W. Dunn, Scripta Met. 4, 321 (1970).

67. W. W. Dunn and R. B. McLellan, Met. Trans. 1, 1263 (1970).

68. K. Alex and R. B. McLellan, J. Phys. Chem. Solids 32, 449 (1971).

69. K. Ales and R. B. McLellan, Mater. Sci. Eng. 7, 77 (1971).

70. K. T. Jacob and C. B. Alcock, Acta Met. 20, 221 (1972).

71. C. Wagner, Acta Met. 21, 1297 (1973).

72. K. Schwerdtfeger, Z. Metallk. 66, 139 (1975).

73. H. J. Grabke, S. K. Iyer, and S. R. Srinivasan, Z. Metallk. 66, 286 (1975).

74. C. H. P. Lupis and J. F. Elliott, Acta Met. 15, 265 (1967).

75. P. Hieter, J. C. Mathieu, R. Durand, and E. Bonnier, Advances in Phys. 16, 523 (1967).

76. E. H. Foo and C. H. P. Lupis, Proceedings of the International Conference on the Science and Technology of Iron and Steel, Tokyo (1970), Supplement to Trans. Iron and Steel Inst. of Japan 11, 404 (1971).

77. E. H. Foo and C. H. P. Lupis, Acta Met. 21, 1409 (1973).

78. C. Wagner, Acta Met. 19, 843 (1971).

79. C. H. P. Lupis, Acta Met. 25, 751 (1977).

80. C. Wagner, Thermodynamics of Alloys, Addison-Wesley Press, Inc., Mass. 47 (1952).

81. C. H. P. Lupis and J. F. Elliott, Trans. Met. Soc. AIME 233, 829 (1965).

82. D. Potter, Ph.D. Thesis, University of Illinois (1970).

83. L. S. Darken and R. W. Gurry, Physical Chemistry of Metals, McGraw-Hill, N. Y., 264 (1953).

84. R. P. Elliott, Trans. Amer. Soc. Metals 52, 990 (1960).

85. V. A. Phillips and J. D. Livingston, Phil. Mag. 7, 969 (1962).

86. M. F. Ashby and L. M. Brown, Phil Mag. 8, 1083 (1963).

87. J. S. Snoek, Physica 6, 711 (1941).

88. D. N. Beshers, J. Appl. Phys. 36, 290 (1965).

89. G. A. Shatalov and A. G. Khachaturyan, Phys. Metals and Metallography 25, No. 4, 56 (1968).

90. K. Hiraga, T. Onozuka, and M. Hirabayashi, Mater. Sci. Eng. 27, 35 (1977).

91. B. J. McBride, S. Meimel, J. G. Ehlers, and S. Gordon, Thermodynamic Properties to 6000 K for 210 Substances Involving the First 18 Elements, NASA SP-3001, Washington D.C., 253 (1963).

92. K. Alex and R. B. McLellan, Acta Met. 19, 439 (1971).

93. K. Alex and R. B. McLellan, Acta Met. 20, 11 (1972).

94. R. B. McLellan, Acta Met. 25, 1241 (1977).

95. J. M. Swisher and E. T. Turkdogan, Trans. Met. Soc. AIME 239, 426 (1967).

96. M. T. Hepworth, R. P. Smith, and E. T. Turkdogan, Trans. Met. Soc. AIME 236, 1278 (1966).

97. W. Eichenauer and G. Muller, Z. Metallk. 53, 321 (1962).

98. R. S. Pastorek and R. A. Rapp, Trans. Met. Soc. AIME 245, 1711 (1969).

99. W. R. Kerr and R. A. Rapp, to be published in Met. Trans.

100. E. Fromm and H. Jehn, Met. Trans. 3, 1685 (1972).

101. R. F. Domagala and D. J. McPherson, Trans. AIME 200, 238 (1954).

102. E. S. Bump, M. D. Kessler and M. Mansen, Trans. ASM 45, 1008 (1953).

103. R. F. Domagala and R. Ruh, Trans. ASM 58, 164 (1965).

104. R. T. Bryant, J. Less-Common Metals 4, 62 (1962).

105. R. Lauf and C. Altstetter, Scripta Met. 11, No. 11, 983 (1977).

106. R. E. Predmore and R. J. Arsenault, in Proceeding of International Conference of Mechanical Behavior of Materials, Kyoto, Japan, 155 (1971).

107. C. J. Sparks, Jr., private communication.

VITA

Gary Lee Steckel was born in [redacted]

He graduated from Greenfield High School, Greenfield, Illinois, in May, 1967. In September of the same year he entered the University of Missouri-Rolla. In May of 1971 he received the degree of Bachelor of Science in Metallurgical Engineering from that institution. He entered the Metallurgy Department of the Graduate College of the University of Illinois as a Research Assistant in September, 1972. He received the degree of Master of Science in Metallurgical Engineering from the University of Illinois in June, 1974.

He is a member of the student branch of the American Society For Metals and The Metallurgical Society of AIME. He has co-authored two articles. An article which included his Master's Thesis research was published in Metallurgical Transactions A in March, 1976 and was entitled "Phase Transformation of Stainless Steel During Fatigue". The paper, "Solubility and Thermodynamic Properties of Vanadium-Oxygen Solid Solutions", was published in Acta Metallurgica, December, 1976.